Titre: Title:	Simulations of fluidized fine powders
Auteur: Author:	Deiva Venkatesh Ramachandran
Date:	1999
Type:	Mémoire ou thèse / Dissertation or Thesis
Référence: Citation:	Ramachandran, D. V. (1999). Simulations of fluidized fine powders [Thèse de doctorat, École Polytechnique de Montréal]. PolyPublie. https://publications.polymtl.ca/8601/

UNIVERSITÉ DE MONTRÉAL

SIMULATIONS OF FLUIDIZED FINE POWDERS

DEIVA VENKATESH RAMACHANDRAN

DÉPARTEMENT DE GENIE CHIMIQUE

ÉCOLE POLYTECHNIQUE DE MONTRÉAL

THÈSE PRÉSENTÉE EN VUE DE L'OBTENTION

DU DIPLÔME DE PHILOSOPHIAE DOCTOR (Ph.D.)

(GÉNIE CHIMIQUE)

SEPTEMBRE 1999

UNIVERSITÉ DE MONTRÉAL

ÉCOLE POLYTECHNIQUE DE MONTRÉAL

Cette thèse intitulée:

SIMULATIONS OF FLUIDIZED FINE POWDERS

présentée par: RAMACHANDRAN Deiva Venkatesh

en vue de l'obtention du diplôme de : Philosophiae Doctor

a été dûment acceptée par le jury d'examen constitué de:

M. KLVANA Danilo Ph.D., président

M. CHAOUKI Jamal, Ph.D., membre et directeur de recherche

M. GRMELA Miroslav, Ph.D., membre et co-directeur de recherche

M. TANGUY Philippe, Ph.D., membre

M. TADRIST Lounès, D.D'etat, membre

ACKNOWLEDGEMENT

I would like to thank my supervisors Dr. Jamal Chaouki and Dr. Miroslav Grmela for their encouragement and support throughout my doctoral program. Dr. Chaouki has been very receptive to new ideas and we share a common interest in fundamental research in powder science. Dr. Grmela has always been open to discussions at any time of the day and constantly helpful and supportive.

I am grateful to Dr. Kengo Ichiki for patiently explaining the details of the Stokesian Dynamics technique and for sharing his ideas on the subject.

My thanks go to Mr. Karl Ekindi for his brief but productive time in code translation and Mr. Ramin Mortazavi for his 'bubble' program. I would like to thank my friend and fellow-researcher Mr. Navid Mostoufi especially for his help in the radioactive particle tracking experiment. Dr. Cui Heping has helped me at a crucial juncture with the fiber-optic experiments.

Others whom I would like to thank are Mr. Jean Huard for helping us out in setting up the experimental unit and Mr. Muthukumaran, Mechanical Engineering department at Concordia University for his interesting discussions.

RÉSUMÉ

Durant les dernières années, plusieurs études ont été réalisées dans le but de comprendre le comportement des poudres fines dans les lits vibrants ainsi que dans les lits fluidisés gaz/solides. En effet, la vibration et la fluidisation de ces poudres posent des défis à cause de la complexité des processus microscopiques comme, par exemple, celui de l'agglomération. Cette thèse introduit une technique innovatrice d'incorporation des phénomènes d'agglomération et de désagglomération dans la simulation du comportement des particules fines. Plus précisemment, pour prédire le comportement des poudres cohésives dans les lits vibrants ou fluidisés, les processus d'agglomération et de désagglomération sont modélisés comme la formation et destruction de liaisons interparticulaires durant leurs collisions. Les deux paramètres qui caractérisent ces phénomènes sont *la barrière d'énergie de cohésion* et *la cohésivité*.

Pour cette simulation, la dynamique moléculaire est utilisée pour les lits vibrants, alors que la dynamique stokesienne est employée pour décrire les lits fluidisés gaz/solides.

Des simulations directes sont faites à deux dimensions utilisant 300 sphères ayant un diamètre uniforme de 2.99 mm dans un recipient trapézoïdale sous vibration verticale avec une amplitude de 2.5 mm et une fréquence de 20 Hz sans introduction de gaz. Dans des conditions non-cohésives, les résultats de la simulation sont en accord avec

ceux dans la littérature. Les résultats de la simulation ont aussi montré deux populations d'aggrégats, l'une avec une taille uniforme et l'autre avec une distribution granulométrique étendue. La première situation se trouve dans le cas des poudres faiblement cohésives, alors que l'autre cas est celui des poudres très cohésives. De plus, on a observé certains comportements macroscopiques intéressants comme la présence de cycles alternés d'agglomération et de désagglomération.

Les simulations des lits fluidisés gaz/solides sont réalisées par la dynamique stokesienne en deux dimensions. Afin de valider expérimentalement ce mode de simulation, les caractéristiques du lit et le mouvement des particules obtenus par la simulation de dynamique stokesienne dans le cas de la poudre FCC ('Fluid Cracking Catalyst') sont comparés aux résultats expérimentaux obtenus par la méthode de la poursuite d'une particule radioactive, par fibres optiques ainsi que ceux obtenus directement de la littérature.

Le modèle d'agglomération et de désagglomération est ensuite utilisé avec la méthode de dynamique stokesienne pour simuler le comportement des poudres faiblement et fortement cohésives dans les lits fluidisés. Encore ici, la simulation des poudres faiblement cohésives indique une formation d'aggrégats de taille petite et uniforme qui sont liés par des liaisons faibles. Par contre, celle des poudres cohésives cause l'agglomération complète des particules fines amenant à la formation des gros agglomérats qui défluidisent complètement ou partiellement le lit dépendamment des

deux paramètres que nous avons introduits. Des simulations complémentaires indiquent que des valeurs supérieures d'énergie de collision et des valeurs inférieures de la cohésivité améliorent la fluidisabilité de ce type de poudres.

Pour améliorer la fluidisabilité des poudres fortement cohésives, on a utilisé les trois techniques suivantes (déjà utilisées expérimentalement dans la littérature): (a) vitesses de gaz largement supérieures à la vitesse minimum de fluidisation des particules initiales (b) fluidisation couplée à la vibration du lit et (c) lit fluidisé de forme conique. L'influence de ces techniques sur la microscopie du lit tels que le mouvement des particules et la formation et la destruction des agglomérats durant les collisions a été étudiée d'une manière qualitative. Conformément à la littérature, les trois techniques ont amélioré la fluidisabilité d'une poudre très cohésive. De plus, pour améliorer la fluidisation tout en diminuant l'emportement des particules, une combinaison de la fluidisation à vitesse de gaz supérieure à la vitesse minimum de fluidisation couplée à une vibration externe du lit est suggérée. Enfin, un diagramme des poudres cohésives est fourni pour expliquer les interactions des paramètres du modèle d'agglomération et de désagglomération.

ABSTRACT

During the past few decades, several studies have been conducted to understand the behaviour of powders in vibrated and gas-solid fluidized beds. In fact, vibration and fluidization of these powders pose various challenges due to the complexity of the microscopic processes such as agglomeration. This thesis introduces an innovative technique of incorporating the agglomeration and deagglomeration phenomena in the simulation of the behaviour of fine powders. More precisely, in order to predict the behaviour of cohesive powders in vibrated or gas fluidized beds, the agglomeration and deagglomeration processes are modelled as the formation and destruction of interparticle bonds during particle collisions. The two parameters which characterize these phenomena are the *cohesive energy barrier* and the *cohesivity* of the powder.

For this simulation, Molecular Dynamics is used for vibrated beds while Stokesian Dynamics est employed to describe gas-solid fluidized beds.

Two-dimensional direct simulations are performed using 300 spheres 2.99 mm in diameter in a trapezoidal container vibrated vertically at an amplitude of 2.5 mm and 20 Hz frequency as preliminary conditions. Under non-cohesive conditions, the results are in agreement with those found in the literature. Simulation results reveal two aggregate populations, one with uniform size aggregates and another population with multi-sized aggregates. The former aggregates were more prevalent in weakly cohesive powders

while the latter in highly cohesive powders. Interesting macroscopic bed behaviour such as alternating cycles of agglomeration and deagglomeration were also observed.

Simulations of gas-solid fluidized beds are carried out using the Stokesian Dynamics method in two dimensions. In order to experimentally validate the use of this simulation type, the bed characteristics and the motion of particles obtained by Stokesian Dynamics in the case of FCC powder (Fluid Cracking Catalyst) are compared with experimental results obtained by the radioactive particle tracking method, fiber-optic method and those found directly in the literature.

The agglomeration-deagglomeration model is used in conjunction with the Stokesian Dynamics method to simulate weakly and strongly cohesive powders. Here again, simulation of weakly cohesive powders indicate the formation of small, uniform size aggregates which are held together by weak bonds. Fluidization of strongly cohesive powders causes the complete agglomeration of the fine particles to form of strong, large size agglomerates which caused complete or partial defluidization of the bed depending on the parameters that are introduced. Additional simulation results indicate that higher values of the minimum collisional energy and lower cohesivity of the powder aids in improving the fluidizability of cohesive powders.

To improve the gas fluidizability of strongly cohesive powders, the following three techniques (already used in experiments reported in the literature) are used: (a) gas

velocity much higher than the minimum fluidization velocity (b) vibration-assisted fluidization and (c) tapered fluidizer. The influence of these techniques on the bed microscopy such as particle motion and the formation and destruction of agglomerates during collisions are studied qualitatively. In accordance with the literature, the three techniques improve the fluidizability of a highly cohesive powder. Moreover, for a simultaneous improvement of the fluidizability and restrained particle entrainment, a combination of the fluidization at gas velocity higher than the minimum fluidization condition coupled with an external vibration of the bed is suggested. Finally, a cohesive powder diagram is provided to explain the interactions of the parameters of the agglomeration-deagglomeration model with the operating conditions.

CONDENSÉ EN FRANÇAIS

Les poudres se trouvent partout dans la nature et elles possèdent des comportements uniques et très complexes. En effet, elles peuvent se comprimer comme des gaz, s'écouler comme des liquides et subir des contraintes sans se déformer comme des solides. De plus, les poudres fines appartiennent à une catégorie spéciale des poudres à cause de leurs forces interparticulaires non négligeables par rapport à leur poids. Les poudres fines bien representées par les poudres de Groupe C de la classification de Geldart sont souvent utilisées dans les industries de procédé tels que dans les réactions catalytiques, la production de céramique, le séchage ... Particulièrement, leur fluidisation est un processus très important dans plusieurs types d'industries. Cependant, leur fluidisation est très difficile à atteindre à cause de la présence des forces interparticulaires telles que les forces de Van der Waals, les forces capillaires et les forces électrostatiques.

Les résultats de plusieurs études experimentales indiquent un renardage à basses vitesses du gaz et l'agglomération à hautes vitesses. Pour contrecarrer les effets de ces forces, certaines techniques expérimentales sont développées pour améliorer la fluidisabilité des poudres fines: fluidisation à des vitesses superficielles largement supérieures à la vitesse minimale de fluidisation des particules initiales, la diminution des forces interparticulaires (par exemple le remplacement d'un métal déposé sur une silice par son

oxyde), la vibration du lit et une configuration plus adéquate du lit (exemple du lit conique).

À cause de la difficulté de mesurer directement ces forces particulaires et de leur nature microscopique, très peu d'études existent dans la littérature pour comprendre tous les phénomènes engendrés par ces poudres. Pour la première fois, un travail de recherche complet a été planifié pour simuler et par conséquent pour comprendre le comportement des poudres fines sous des conditions de vibration ou de fluidisation du lit.

Dans un premier temps, cette thèse s'est attaquée à simuler, par la méthode de la dynamique moléculaire, le comportement sans gaz d'un lit vibrant de particules fines en introduisant un processus nouveau d'agglomération et de désagglomération (AGEDE). Au préalable, cette simulation a été partiellement validée par des résultats expérimentaux de la littérature avec des particules ayant des forces interparticulaires négligeables. Ensuite, un lit fluidisé vibrant ou non, mettant en oeuvre des particules C a été simulé en utilisant la dynamique stokesienne couplée au modèle déjà introduit AGEDE. Cette simulation a été aussi partiellement validée par des données obtenues par des techniques de traçage d'une particule radioactive et fibres optiques en fluidisant des particules A (de la classification de Geldart). Grâce à cette simulation, un nouveau pont vient d'être érigé entre les propriétés micoscopiques des poudres fines et leurs comportements macroscopiques.

Vibration des poudres fines:

Des simulations directes ont été réalisées à deux dimensions utilisant 300 sphères ayant un diamètre uniforme de 2.99 mm dans un recipient trapézoïdale sous vibration verticale avec une amplitude de 2.5 mm et une fréquence de 20 Hz et sans gaz. Les trois types de forces qui agissent sur les particules sont les forces des sphères dures (pour éviter le chevauchement des particules), la force de friction et la force de gravité. Dans des conditions non-cohésives, les résultats de la simulation sont en accord avec ceux dans la littérature. Pour prédire le comportement des poudres cohésives, les processus d'agglomération et de désagglomération sont modélisés comme la formation et destruction des liaisons interparticulaires durant les collisions (modèle AGEDE). Les deux paramètres que nous avons définis et qui ont servi à modéliser l'agglomération et la désagglomération des poudres sont *la barrière d'énergie de cohésion* et *la cohésivité* des poudres. Le modèle propose que l'agglomération de plusieurs particules est le fruit d'une collision spéciale entre deux particules (particule initiale ou agglomérat) qui transforment une partie de leur énergie de collision en énergie de liaison. Le rapport de ces énergies est défini comme étant la cohésivité d'une poudre. La désagglomération d'un agglomérat se fait lors d'une collision quand l'énergie de collision peut casser des liaisons internes plus faibles. Le minimum d'énergie capable de détruire un agglomérat est défini comme étant la barrière d'énergie de cohésion.

Les résultats de la simulation montrent deux populations d'aggrégats. Dans le cas d'une poudre faiblement cohésive, une taille uniforme d'aggrégats est obtenue alors que si elle

est fortement cohésive, une large distribution granulométrique caractérise le lit. De plus, certains comportements macroscopiques intéressants peuvent être observés: comme par exemple l'existence de cycles alternés d'agglomération et de désagglomération.

Fluidisation des poudres cohésives par l'air:

Les simulations du lit fluidisés à gaz ont été réalisées en utilisant la dynamique stokesienne en deux dimensions. Dans cette méthode, on estime les interactions hydrodynamiques à travers ses deux composantes: (i) les forces longues-portées qui répresentent les interactions multiples entre toutes les particules et (ii) les forces de lubrication qui représentent les forces répulsives qui agissent entre les particules voisines. Dans la simulation sans cohésion (ou négligeable), les seules interactions interparticulaires sont des collisions élastiques.

Les caractéristiques du lit et le mouvement des particules qui sont obtenues par cette simulation dans le cas des poudres FCC ('Fluid Cracking Catalyst') s'accordent bien avec les résultats expérimentaux obtenus par les méthodes de traçage d'une particule radioactive (TPR) et des fibres optiques, ainsi qu'avec les modèles de bullage qui existent dans la littérature. Dans cette comparaison, la taille et la vitesse des bulles, la porosité du lit et le mouvement des particules ont été considérés.

Le modèle d'agglomération et de désagglomération (AGEDE) est ensuite couplé à la dynamique stokesienne pour simuler des poudres faiblement et aussi fortement cohésives. Encore ici, la simulation des poudres faiblement cohésives indique la formation des aggrégats de taille petite et uniforme qui sont liés par des liaisons faibles. alors que la fluidisation des poudres cohésives cause l'agglomération complète des particules fines qui défluidise le lit. Des simulations complémentaires indiquent que des valeurs supérieures d'énergie de cohésion et des valeurs inférieures de la cohésivité améliorent la fluidisabilité de ces poudres.

La fluidisation des poudres faiblement cohésives cause la formation d'aggrégats de taille uniforme de 3.0 (la longeur caractéristique est 1.0. le rayon des particules) qui occupent 30% de la masse du lit. Environ 10% du lit est formé de gros aggrégats avec une distribution de taille plus que 3.0. Les énergies instantanées des liaisons indiquent que les petits aggrégats sont tenus par les liaisons faibles.

La simulation des poudres fortement cohésives indique une augmentation graduelle de l'énergie des liaisons dans le système. Le diamètre effectif des agglomérats atteint un maximum de 6.0. Dans ce cas, plus que 90% du lit est composé d'agglomérats qui défluidisent complétement le lit. Ce comportement est souvent observé expérimentalement pour des poudres cohésives telles les cryogels.

L'intégration de la dynamique stokesienne au modèle AGEDE a permis de tirer des propriétés macroscopiques des poudres cohésives à partir de données microscopiques telles l'énergie de liaison et la cohésivité.

Pour améliorer la fluidisabilité des poudres fortement cohésives, on a utilisé les trois techniques suivantes (déjà utilisées expérimentalement dans la littérature): (a) vitesses de gaz largement supérieures à la vitesse minimum de fluidisation des particules initiales (b) fluidisation couplée à la vibration du lit et (c) lit fluidisé de forme conique. L'influence de ces techniques sur la microscopie du lit tels que le mouvement des particules et la formation et la destruction des agglomérats durant les collisions a été étudiée d'une manière qualitative. Conformément à la littérature, les trois techniques ont amélioré la fluidisabilité d'une poudre très cohésive. De plus, pour une amélioration de la fluidisation tout en diminuant l'emportement des particules, une combinaison de la fluidisation à vitesse de gaz supérieure à la vitesse minimum de fluidisation couplée à une vibration externe du lit est suggérée.

Enfin, un diagramme des poudres cohésives est fourni pour expliquer les interactions des paramètres du AGEDE. Ce diagramme est un outil qualitatif qui explique la relation du comportement des poudres cohésives et les meilleures conditions opératoires de leur fluidisation.

Pour la continuation de la recherche sur les poudres fines, on suggère quelques recommandations qui incluent l'accélération du code de la dynamique stokesienne, la modification de cette méthode pour simuler la fluidisation d'une poudre hétérogène (distribution non-uniforme de la taille des particules) et la possibilité de simuler de grands systèmes (nombre de particules élevé) afin d'avoir des comportements plus représentatifs.

TABLE OF CONTENTS

LIST OF FIGURES

LIST OF TABLES

LIST OF APPENDICES

CHAPTER 1: INTRODUCTION

1.1 Introduction

Powders form a unique class of solids exhibiting both solid and fluid-like behaviours. Like solids they can withstand deformation, like liquids, they can flow, and like gases, they can be compressed. Fine powders that are of relevance to this paper are best represented by the Group C powders of Geldart's classification. Several industrial processes such as catalytic reactions, drying operations or just simple transportation involve gas fluidization of such fine powders. The presence of interparticle forces such as the Van der Waals, the capillary and the electrostatic forces as well as other direct particle-particle interactions (e.g. interlocking, deformation etc.) make them difficult to be gas fluidized. Experimental observations of gas fluidized fine powders here at the Chemical Engineering Department reveal phenomena such as plug-rise, channelling and particle agglomeration. Certain experimental techniques have been conceived to improve gas fluidizability of such powders including the subjection of cohesive powders to vertical vibration in addition to gas flow in the bed. Several studies are available in the literature on vibrated powders which include reports on behaviours such as bunkering (heaping) and Faraday circulation. The rheology of fine powders is influenced during vibration or gas fluidization by the prevalent interparticle forces that are either direct (attractive, repulsive and frictional forces) or indirect (mediated by the

fluid medium). A detailed experimental study of the effects of such interparticle forces is however quite difficult due to the complexity of the microscopic processes involved.

The current work is a first step in trying to simulate the behaviour of cohesive fine powders in gas fluidized and vibration-assisted gas fluidized beds which are of engineering interest.

In order to gain an understanding of the microscopic processes that are involved in the vibration of Group C powders we turn in this paper to direct simulations. First, we suggest a model of single grains and of interactions among them. Then, using computers, we calculate trajectories of all grains. Finally, we extract from the trajectories the macroscopic properties of interest. In this way, we bridge the microscopic properties of grains with the macroscopic properties characterizing vibrated beds and gas fluidized beds.

The vibrated bed experiments reported in the literature and explained in Chapter 2 were carried out using 300 beads of 2.99 mm diameter in a trapezoidal cell whose thickness was 3 mm, whose walls were inclined at 30° to the vertical axes and whose bottom was 62 mm long. Vertical vibrations were generated sinusoidally using a loudspeaker. Density field and velocity distributions were simultaneously measured at an amplitude A=2.5 mm and frequency f=20 Hz.

In this paper, we follow the simulation studies of Gallas *et al* (refer Chapter 2) and adapt them to fine powders. The adaptation is completely original. The principal new feature that we phenomenologically introduce is the agglomeration-deagglomeration interactions among grains.

To simulate non-cohesive fluidization, we employ the Stokesian dynamics method. The only empirical parameters that have to be introduced are those needed to characterize the Stokesian particle-fluid interactions (Chapter 3). Recent simulations using the Stokesian Dynamics method have reproduced realistic particle motion in gas fluidized granular systems (Chapter 3).

In these simulations, the Stokesian Dynamics method is used to simulate the air fluidization of a two-dimensional bed composed of 128 spherical glass particles with 10 particles forming the fixed bottom of the bed with an uniform air velocity at a value 30% of the single particle terminal velocity.

Chapter 4 describes the simulation of gas fluidized powders mainly the Fluid Cracking Catalyst (FCC) and the discussion of the macroscopic bed properties such as density distribution and characteristics of the bubbling bed from particle positions and motion. The objective here is to compare the results of Stokesian Dynamics with experimental observation using Radioactive Particle Tracking and Fiber-optic methods.

In Chapter 4, we continue our investigation. We extend the Stokesian dynamics simulation method to cohesive fine powders. The principal new feature that we are introducing into the simulation of fluidized beds is the agglomeration-deagglomeration interactions among the particles.

To counteract the effect of the cohesive interparticle forces. certain experimental techniques described in Chapter 5 have been developed in an effort to improve the gas fluidizability of fine powders. Two main categories of techniques used to improve the fluidizability of fine powders are (i) addition of an external force such as vibration, magnetic field or acoustic field and (ii) alteration of the intrinsic properties of the powder such as modifying the surface characteristics and mixing of a dissimilar powder.

In the fifth chapter. we intend to investigate the effects of (i) an external vibratory force (ii) high gas velocity and (iii) tapered bed geometry on the fluidizability of cohesive powders.

In these simulations, the Stokesian Dynamics method is used to simulate the air fluidization of a two-dimensional bed composed of 100 spherical glass particles with 10 particles forming the fixed bottom of the bed and 24 other fixed particles forming the bed wall with an uniform air velocity at a value 30% of the single particle terminal velocity.

1.2 Objectives

1. Develop a phenomenological model to simulate the fluidization of cohesive fine powders.
2. Explain the formation and destruction of agglomerates during the fluidization of fine particles.
3. Explain the macroscopic behaviour of fine powders using microscopic models and theories.

1.3 Thesis structure

This thesis is mainly divided into five parts:

(i) Chapter 2 introduces the proposed agglomeration-deagglomeration model explaining the behaviour of cohesive powders. The area of application in this context is the vibration of fine powders.

(ii) Chapter 3 introduces the Stokesian Dynamics method for the simulation of the gas fluidization of powders without interparticle forces. Results of Radioactive Particle Tracking and Fiber-optic methods on the bed characteristics are reported and compared with the Stokesian Dynamics results.

(iii) Chapter 4 describes the simulation of the gas fluidization of cohesive powders using the Stokesian Dynamics method introduced in Chapter 3 and the agglomeration-deagglomeration model introduced in Chapter 2.

(iv) Chapter 5 throws light on the simulation of certain techniques used to improve the fluidizability of cohesive powders and puts forward a cohesive powder diagram.

(v) Closure of the thesis with conclusions on the work and recommendations for future investigations.

CHAPTER 2: SIMULATIONS OF VIBRATED FINE POWDERS

Reference:

R. Deiva Venkatesh, J. Chaouki and M. Grmela (1998), "SIMULATIONS OF VIBRATED FINE POWDERS", *Powder Technology* (1998).

Keywords:

Powders, Dynamic simulation; Vibrated beds; Agglomeration

SIMULATIONS OF VIBRATED FINE POWDERS

R. Deiva Venkatesh, M. Grmela, J. Chaouki*
BIOPRO Centre, Chemical Engineering Department, Ecole Polytechnique de Montréal, P.O. Box 6079, Montréal, Qué. H3C 3A7, Canada

Abstract

During the past few decades several studies have been conducted to understand the behaviour of powders in vibrated beds. This paper introduces a technique of incorporating the agglomeration and deagglomeration phenomena in the simulation of vibrated fine powders. Two-dimensional direct simulations are performed using 300 spheres 2.99 mm in diameter in a trapezoidal container vibrated vertically at an amplitude of 2.5 mm and 20 Hz frequency as preliminary conditions. Under non-cohesive conditions, the results are in agreement with those found in the literature. As a preliminary effort to predict the behaviour of cohesive fine powders under vibrated conditions, agglomeration and deagglomeration processes are modelled as the formation and destruction respectively of interparticle bonds during particle collisions. Two parameters used to model agglomeration and deagglomeration are *the ease of cohesion* and *cohesivity* of the powder. Dependencies of these parameters on certain physical properties of cohesive powders have been suggested. Simulation results reveal two aggregate populations, one with uniform size aggregates and another population with multi-sized aggregates. The former aggregates were more prevalent in weakly cohesive powders while the latter in highly cohesive powders. Interesting macroscopic bed behaviour such as alternating cycles of agglomeration and deagglomeration were also

observed. Further work is needed in which the aerodynamic forces are taken into account and cohesion mechanisms at the particle surface are modelled.

Keywords : Powders, dynamic simulation, vibrated beds, agglomeration

---

* Corresponding author

1. Introduction

Powders form a unique class of solids exhibiting both solid and fluid-like behaviours. Like solids they can withstand deformation, like liquids, they can flow, and like gases, they can be compressed [1]. Fine powders that are of relevance to this paper are best represented by the Group C powders of Geldart's classification [2]. Several industrial processes such as catalytic reactions, drying operations or just simple transportation involve gas fluidization of such fine powders [3,4]. The presence of interparticle forces such as the Van der Waals, the capillary and the electrostatic forces as well as other direct particle-particle interactions (e.g. interlocking, deformation etc.) make them difficult to be gas fluidized [5]. Experimental observations of gas fluidized fine powders reveal phenomena such as plug-rise, channelling and particle agglomeration [6,7]. Certain experimental techniques [6,8-11] have been conceived to improve gas fluidizability of such powders including the subjection of cohesive powders to vertical vibration in addition to gas flow in the bed [8]. Several studies are available in the literature on vibrated powders which include reports on behaviours such as bunkering (heaping) and Faraday circulation [12,13]. The rheology of fine powders is influenced during vibration by the prevalent interparticle forces that are either direct (attractive, repulsive and frictional forces) or indirect (mediated by the fluid medium). A detailed experimental study of the effects of such interparticle forces is however quite difficult due to the complexity of the microscopic processes involved.

The current work is a first step in trying to simulate the behaviour of cohesive fine powders in gas fluidized and vibration-assisted gas fluidized beds which are of engineering interest. For the moment, we attempt to simply simulate the behaviour of cohesive powders in vibrated beds under vacuum.

In order to gain an understanding of the microscopic processes that are involved in the vibration of Group C powders we turn in this paper to direct simulations. First, we suggest a model of single grains and of interactions among them. Then, using computers, we calculate trajectories of all grains. Finally, we extract from the trajectories the macroscopic properties of interest. In this way, we bridge the microscopic properties of grains with the macroscopic properties characterizing vibrated beds. Direct simulations have long been used to study vibration of granular beds [14-18].

The vibrated bed experiments of Clement and Rajchenbach [19] were carried out using 300 beads of 2.99 mm diameter in a trapezoidal cell whose thickness was 3 mm, whose walls were inclined at 30° to the vertical axes and whose bottom was 62 mm long. Vertical vibrations were generated sinusoidally using a loudspeaker. Density field and velocity distributions were simultaneously measured at an amplitude A=2.5 mm and frequency f=20 Hz. Gallas *et al* [14] have then performed direct simulations of the

vibrated bed described above at the same conditions and have compared their density profiles and velocity distributions with those of the experiments [19].

In this paper, we follow the studies of Gallas *et al* [14] and adapt them to fine powders. The adaptation is completely original. The principal new feature that we phenomenologically introduce is the agglomeration-deagglomeration interactions among grains.

2. Microscopic Model of Group C Powders

Following Gallas *et al* [14], the powder is considered only in two dimensions. The grains are discs of 2.99 mm diameter, placed in a trapezoidal container (3 mm deep) whose movements are restricted to the vertical plane (see Figure 2.1). The grains are subjected to the following four forces :

(i) Hooke's repulsive interparticle force generated by the potential :

$$u(r) = \begin{cases} 0.5\,Y(d-r)^2, \text{if } r \le d \\ 0, \text{if } r > d \end{cases} \tag{1}$$

where Y is the Young's Modulus of the spheres, d is their diameter and r, their centre-centre separation. The repulsive force is given by the gradient of u(r).

(ii) Interparticle frictional force acting on a particle 'P' in contact with another particle 'Q' given by :

$$\mathbf{a}_{PQ} = -Cm\begin{bmatrix} (U_{Px} - U_{Qx})\text{sign}(U_{Px}) \\ (U_{Py} - U_{Qy})\text{sign}(U_{Py}) \end{bmatrix} \tag{2}$$

where C is the coefficient of friction, m is the mass of each sphere, $\mathbf{U}_P$ and $\mathbf{U}_Q$ are the 2D velocity vectors of particles 'P' and 'Q' respectively.

(iii) Gravity force, mg $\mathbf{e}_z$, where g is the acceleration due to gravity, 10 m/s^2 and $\mathbf{e}_z$ is the unit gravitational vector in the downward direction.

(iv) Forces that bring about agglomeration and deagglomeration

The model that we have developed to describe the agglomeration-deagglomeration processes will be described later in this paper.

The first three forces are the same as in Gallas *et al* [14]. The fourth force will be newly introduced. It represents in our modelling the fact that our interest is focussed on Group C powders. The role of agglomeration-deagglomeration processes in the dynamics of vibrated Group C powders can then be studied.

The interaction of grains with the wall is chosen to be the same as in Gallas *et al* [14]. The walls are composed of closely packed grains. In this way, the grain-wall interactions become grain-grain interactions. The external force (in addition to the gravitational force) to which the grains are subjected is the force transmitted to the particles by periodically shaking the container at an amplitude A=2.5 mm and frequency f=20 Hz. Density profiles and z-velocity profiles for this particular set of amplitude and frequency are available from experiments [19] and previous simulation [14] to check the validity of our simulation code in the case of non-cohesive vibrated beds. The effect of

the parameters entering the proposed agglomeration-deagglomeration model is studied without varying the conditions of vibration (see Section 7).

With the first three forces, (i)-(iii), the equations governing the motion of the grains are :

$$\frac{d\mathbf{U}_P}{dt} = g\mathbf{e}_z + (-\frac{1}{m}\nabla_P u(|\mathbf{x}_P - \mathbf{x}_Q|) + \mathbf{a}_{PQ}) \qquad (3)$$

3. Simulations without the agglomeration-deagglomeration process

We fill the container with 300 grains and solve eq.(3) for all particles. The periodic displacement of the container is modelled sinusoidally as, $x_j(t) = A \sin(2\pi ft)$. The parameter values used were, $Yd/m=20{,}000$ m/s^2 and $C=300$ s^{-1} for the spheres and the time step for integration was $(4000f)^{-1}$ [14]. After each quarter period, the particle positions and velocities were recorded. Our C language codes were executed at 130 Mflops on an IBM SP2 processor. The results were then compared with the experiments of Clement and Rajchenbach [19] and with the respective cohesionless simulations of Gallas *et al* [14] and Bloise [20]. The results of our non-cohesive simulations are discussed in Section 7. We then introduce the influence of direct interparticle forces to the above scheme. The agglomeration-deagglomeration model developed for this purpose is explained in the following section.

4. Simulation with agglomeration-deagglomeration

We have a two-fold perspective of particle cohesion based on particle motion in the vibrated bed :

(a) *Natural cohesion* due to interparticle forces such as van der Waals and electrostatic forces which are prevalent even in the absence of particle motion and

(b) *Induced cohesion* due to dynamic contact mechanisms, such as interlocking, surface deformation, etc. achieved by applied forces, which could well be coupled with interparticle attraction thereby enhancing cohesivity.

In the following sub-section, we describe a micromechanical model of agglomeration as well as deagglomeration (similar to the 'hard-sphere chemistry' used in the molecular dynamics simulation of chemical systems [21]) for simulating the behaviour of fine powders. The mechanisms are treated energetically.

Powder Chemistry

Analogous to the simulations of chemical reactions using molecular dynamics [21], where molecular collision is a primary factor for the reaction to occur, we develop a *powder chemistry model* to represent direct interparticle interactions under the influence of an applied force such as vibration. The model has been named *powder chemistry*

since we treat agglomeration and deagglomeration of powder beds as reversible processes similar to reversible chemical reactions.

The model assumptions are as follows :

Assumptions :

1. We assume that both agglomeration and deagglomeration are binary collisional processes.
2. There exists a minimum collisional energy level (Ec_{MIN}) beyond which agglomeration/ deagglomeration is considered possible. This minimum is analogous to the activation energy of chemical reactions.
3. The vibrated bed is not composed of dead zones and particles have individual movements.

The proposed model enunciates the detailed mechanisms of the agglomeration and deagglomeration phenomena in the following manner :

Agglomeration

Agglomeration is effected by a partial transformation of the total kinetic energy of the impacting bodies into a cohesive bond energy (BE) that causes cohesion of the colliding bodies. This is explained by Figure 2.2. The rest of the available kinetic energy is attributed to the resultant aggregate as explained in the energy balance below.

The two model parameters for agglomeration are :

(i) the minimum collisional energy (Ec_{min}) and

(ii) the fraction (e) of kinetic energy to be transformed to cohesive bond energy (BE), representing the inelasticity of agglomerative collisions.

Both model parameters are supposed to be interfacial properties, ε being close to zero for large, dense, spherical grains (eg. Group A powders [2]), while having a value close to unity for flat, light, very fine particles (eg. Group C powders [2]). Low net values of ε may be achieved by various methods such as addition of a dissimilar coarse powder (having lower ε value) to the fine powder or passing a viscous gas through the powder bed [6,9]. Ec_{MIN} supposedly represents particle rearrangement which is necessary for cohesion as well as deformation of colliding grains caused by the external/applied force (in this case, the force of vibration). Low values of Ec_{MIN} represent highly deformable structures leading to larger contact areas which enhance cohesion. In the physical sense, Ec_{MIN} can be referred to as the *ease of cohesion* and ε as the *cohesivity* of the fine powder. Powders with low value of Ec_{MIN} are expected to have high Hausner ratios, HR (HR=tapped bulk density/loose bulk density of the powder) while those with large ε would demonstrate cohesive forces much larger than the gravity force and would require considerable vibrational force to improve gas fluidizability of the powder.

Deagglomeration

Dissociation of particles in an aggregate occurs due to cleavage of all weak cohesive bonds as shown in Figure 2.2. These 'weak bonds' are those bonds whose cumulative sum of bond energies (Σ BE_{WEAK}) is lesser than or equal to the collisional energy (E_{coll}) of the impacting bodies. The collisional energy is given by :

$$E_{coll} = \frac{1}{2}\left(m_P U_P^2 + m_Q U_Q^2\right) \tag{4}$$

Energy balances :

Let two aggregates M and N have initial masses m_M and m_N respectively and intial velocities U_M and U_N respectively prior to a deagglomerative collision. Let they be MD and ND after deagglomeration, their final masses be m_{MD} and m_{ND} respectively and their final velocities be U_{MD} and U_{ND} respectively. The energy balance for deagglomeration is given as follows :

$$m_{MD}U^2_{MD}+m_{ND}U^2_{ND} = m_MU^2_M+m_NU^2_N-(m_M-m_{MD})U^2_M-(m_N-m_{ND})U^2_N-2\Sigma BE_{WEAK}$$

The final mass of M is in general m_{MD} and its final velocity U_{MD}, since the collision may cause the birth of 'child' aggregates/particles from either 'parent' aggregates M and N. In such a case,

$(m_M - m_{MD})$ and $(m_N - m_{ND})$ are the total masses of child particles issuing from M and N respectively and their kinetic energies are conserved during the deagglomerative

collision. BE_{WEAK} represents the sum of the energies of the weak bonds in M and N which have been destroyed.

For redistribution of kinetic energy between MD and ND, we assume that the fraction of the total kinetic energy available for motion of M before deagglomeration is equal to the fraction of the total kinetic energy available to it (i.e.,MD) after deagglomeration. Accordingly,

$$\frac{m_M U_M^2}{m_M U_M^2 + m_N U_N^2} = \frac{m_{MD} U_{MD}^2}{m_{MD} U_{MD}^2 + m_{ND} U_{ND}^2}$$

We now have the velocity of MD as follows:

$$m_{MD} U_{MD}^2 = \left(\frac{m_M U_M^2}{m_M U_M^2 + m_N U_N^2} \right) \left(\begin{array}{l} m_M U_M^2 + m_N U_N^2 \\ -[m_M - m_{MD}] U_M^2 - [m_N - m_{ND}] U_N^2 - 2 \sum_i BE_{WEAK} \end{array} \right) \quad (5)$$

The energy balance for agglomeration is given by :

$$(m_M + m_N) U_{MN}^2 = m_M U_M^2 + m_N U_N^2 - 2\varepsilon E_{coll} \quad (6)$$

Here, U_{MN} is the velocity of the M- and N- combined aggregate and εE_{coll} is the energy of the bond joining M and N.

5. Formation and destruction of aggregates as a reversible chemical reaction

Microscopic simulation of chemically reacting systems have been carried out originally using the Boltzmann and later using the molecular dynamic schemes [21]. We follow these schemes to powder systems. The phenomena of agglomeration and deagglomeration can be regarded as three sets of reversible reactions. The mechanisms are given below :

Particle-particle interactions

$$2A_1 \underset{k_{-1}}{\overset{k_1}{\rightleftharpoons}} A_2 \qquad \text{(R1)}$$

Particle-aggregate interactions

$$A_1 + A_M \underset{k_{-2}}{\overset{k_2}{\rightleftharpoons}} A_{M+1} \qquad \text{(R2)}$$

Aggregate-aggregate interactions

$$A_P + A_Q \underset{k_{-3}}{\overset{k_3}{\rightleftharpoons}} A_{P+Q} \qquad \text{(R3)}$$

Here A_1 represents a single elementary particle used in the simulation, A_2, A_M, A_P, A_Q, A_{M+1} and A_{P+Q} are 'representative' aggregates of various sizes, form and cohesive bond energies involved in the above three reactions.

The reaction rates for the three types of interactions are as follows:

$$\frac{dn_{A_2}}{dt} = k_1 n_{A_1}^2 - k_{-1} n_{A_2} \tag{7}$$

$$\frac{dn_{A_{M+1}}}{dt} = k_2 n_{A_1} n_{A_M} - k_{-2} n_{A_{M+1}} \tag{8}$$

$$\frac{dn_{A_{P+Q}}}{dt} = k_3 n_{A_P} n_{A_Q} - k_{-3} n_{A_{P+Q}} \tag{9}$$

The macroscopic results of the simulations of vibrated powders provide the number concentrations of A_2, A_M, A_P, A_Q, A_{M+1} and A_{P+Q} as well the reaction rates wherefrom the rate constants have been evaluated. The effect of the model parameters ε, Ec_{MIN} on bed characteristics have been studied.

6. Simulation and Analysis Techniques

The simulation of vibrated cohesive powders proceeds as follows :

1. Aggregates constitute several original particles (having diameter d=2.99 mm) called 'members' which are bonded to each other in a pairwise fashion. The identity of each particle is maintained at all times.

2. As mentioned in Section 2, equation (3) is solved to get the particle positions and velocities. The only difference is that all forces acting on the member particles of an aggregate are averaged and the average is then assigned to each of its members.

3. For every time step, at the end of the integration procedure, the interparticle interactions are treated. The steps involved are shown in Figure 2.3 and explained below:

   3.1 Finding out the collisions caused during the current time step.

   3.2 Checking for the occurrence of deagglomeration/agglomeration based on the conditions of Section 4, i.e., energy of collision (E_{coll}) greater than the minimum collisional energy (Ec_{MIN}). If the collisional energy is lesser than the weakest bond in the vicinity of contact, agglomeration occurs. Otherwise, as described in Section 4, all 'weak bonds' of the aggregate are destroyed thereby possibly producing 'child' aggregates or particles.

Besides the primary information about positions and velocities of the particles in the vibrated bed, the various cohesive bond energies (BE) among particle-pairs are stored at the end of each quarter period of the vibratory cycle in a Bond Energy Matrix (BEM). For instance, the matrix element $BEM_{M,N}$ provides the energy of the bond joining particles M and N. Using BEM, the program constructs an Aggregate Member Matrix (AMM) which denotes for any aggregate member M, all its co-members in the same aggregate. Here, $AMM_{M,N}$ is 1 if particles M and N are members of the same aggregate, the value being nul otherwise. AMM is crucial for the intra-aggregate averaging of forces, aggregate identities and estimation of aggregate characteristics.

Characteristics of aggregates :

Two characteristics of aggregates of practical importance that have been extracted from the microscopic simulation are (i) aggregate size or effective diameter, d_{eff} and (ii) circularity, ψ. Effective diameter d_{eff} refers to the diameter of a circle having area equal to that of the aggregate while circularity represents the ratio of the effective diameter of the aggregate to its largest Martin diameter [22]. Besides, the cohesive energies of aggregates, the effective diameters and circularities of the aggregates at three time instants are discussed in the subsequent section. The evolution of the means of the above characteristics and those of the three equilibrium rate constants are also presented.

7. Results and discussion

7.1 Simulation of a non-cohesive powder

In the simulations, the non-overlapping discs were first generated randomly within the container and allowed to settle under gravity. The first 30 transitory cycles were rejected and averages were performed over the next 30 cycles. Figure 2.4 represents the axial profile of the linear density, ρ (ρ=ratio of bulk density to the solid density) for the phase angle ϕ=0. Comparison with experiments [19] shows that our dense region is looser than in the case of experiments where maximum packing is observed. We compared the averaged x- and z-velocity components for both ϕ=0 and ϕ=π with those of experiments [19] and previous simulations [14,20]. We note that in all cases, the x-components of the velocities are always negligible. The z-component of velocity in our simulations for ϕ=0 exactly match with the simulation results of Bloise [20]. Simulation results differ from the experiments [19] as shown in Figure 2.4. In the case of ϕ=π, all studies are in agreement.

7.2 Simulation of cohesive powders

Four simulation studies were carried out with two values each for the parameters Ec_{MIN} and ε. Table 2.1 summarizes the parameter sets.

To compare with the case of non-cohesive fluidization (Figure 2.4), axial profiles of linear density, ρ and mean velocity components were determined for the cohesive powder I. We observed little difference between a non-cohesive and a slightly cohesive powder. On the other hand, instantaneous bed characteristics at three instants 0.2 s, 0.4 s and 0.6 s, represented in Figure 2.5 indicate that the aggregates formed are quite flat having an uniform effective diameter, d_{eff} of about 4 mm. Hereonwards, we refer to aggregates having an effective diameter of 4 mm as *clusters* and aggregates having effective diameter larger than 4 mm as *agglomerates* (aggregates as such mean either *agglomerates* or *clusters*). In the case of the weakly cohesive powder, the aggregate population was mainly *clusters* with very few *agglomerates* were formed. In this figure, A refers to aggregate number (1,2,3,etc.) and cohesive bond energy of an aggregate (BE_A) is the sum of all cohesive bond energies (BE) within that aggregate.

The evolution of the mean cohesive bond energy of aggregates ($<BE_A>$), mean effective diameter ($<d_{eff}>$), mean circularity ($<\psi>$) of aggregates and mass fractions of *clusters* and *agglomerates* of powder I are shown in the subsequent Figure 2.6. We find that nearly 30% of the bed mass had formed *clusters* and about 7% as *agglomerates*. It is interesting to note from the time variation of these mass fractions that there is an alternating pattern of promoting and inhibiting cohesiveness during the vibratory cycle. During the first half-cycle ($\phi=0$ to $\phi=\pi$), agglomeration is predominant while during the second half-cycle ($\phi=\pi$ to $\phi=2\pi$), break-up of aggregates is more prevalent. In the light

of the *powder chemistry model*, the equilibrium constants from equations (7), (8) and (9) for the three types of interactions were also studied. Figure 2.7 points out that the most dominant interaction during agglomeration of powder I is the particle-particle interaction followed by particle-aggregate whereas we observe no inter-aggregate interactions in powder I.

Analyzing the above results in the case of powder II, we find from Figure 2.8, the order of magnitude of the cohesive bond energies is about 1000 times larger than in the case of the lightly cohesive powder. An interesting observation is that the aggregate population is bimodal. We find uniform *clusters* of 4 mm effective diameter as well as a size distribution of large *agglomerates* throughout the simulation. This heterogeneity has also been reported in experimental studies of gas fluidization of fine powders to be more pronounced in the case of highly cohesive samples [6,11]. The circularities of the aggregates have increased slightly with ε. In Figure 2.9, the mean cohesive bond energies ($<BE_A>$) increase as time proceeds since more and more *agglomerates* form besides the *clusters*. The mean effective diameter of the aggregates is around 7.5 mm. In contrast to the previous case of powder I, Figure 2.9 representing the mass fractions indicate that most of the bed (>80%) has formed *agglomerates* while 10% of the bed mass has formed *clusters*. Gas fluidization of strongly cohesive powders such as 14% Ni/Al_2O_3 cryogel produced several large aggregates which were composed of a large portion of the bed mass [7]. Finally, in Figure 2.7 we observe significantly larger values

of the equilibrium constant K_2 for the particle-aggregate interactions. Here, in contrast to the powder I, the inter-aggregate interactions are also found to occur. Comparing powders I and III as well as II and IV, we find from Table 2.2 that Ec_{MIN} determines the starting time of agglomeration, t_a.

To study the effect of bed geometry and to relate to conventional vibrated beds, vibration of powder I in a rectangular container was simulated. In Figure 2.4, we note the increase in the height of the dense bed. From the z-velocity profile at ϕ=0 and from animations, we observed that particles at the base and surface of the bed were mobilized while the mass inbetween remained nearly immobile. However, higher values of Af^2 could improve particle mobility in the rectangular bed.

8. Conclusions

A foundation for a simulation technique allowing to predict the macroscopic behaviour of vibrated cohesive fine powders has been made. Firstly, following the method of Gallas *et al* [12], we have simulated 300 spheres in a trapezoidal container vibrated vertically at an amplitude of 2.5 mm and a frequency of 20 Hz. Next, we have introduced a microscopic model of cohesion processes in powders (*powder chemistry*) and carried out the simulations involving agglomeration-deagglomeration. In theses simulations, the particles are allowed to form aggregates during collisions. The process is controlled by the energy barrier given by the model parameter Ec_{MIN}. The fraction of the collisional energy transformed into cohesive bond energy during such reactive (agglomerative or deagglomerative) collisions was represented by the second model parameter ε. Break-up of aggregates occurs when the collisional energy exceeds the strengths of 'weak' bonds in the colliding bodies. From the perspective of chemical reactions, the agglomeration-deagglomeration phenomena were considered to be reversible reactions with three types of interactions viz particle-particle (equilibrium constant K_1), particle-aggregate (equilibrium constant K_2), aggregate-aggregate (equilibrium constant K_3).

Simulation of four cohesive powders I,III (weakly cohesive), II and IV (strongly cohesive) were carried out by varying both model parameters. Macroscopic results such

as cohesive bond energies of aggregates, their effective diameters and circularities were extracted from the microscopic simulation results viz positions and velocities of the particles and their various cohesive bond energies.

The macroscopic results indicate that in the case of the weakly cohesive powders, the aggregates are of constant minimum size (4 mm) called *clusters* having weak cohesive bond energies of the order of 10^0J and having no significant effect on the density or velocity distributions in the bed. Also, nearly 30 % of the bed mass had formed *clusters* which were formed mainly due to particle-particle interactions. In the case of strongly cohesive powders, besides 10% of the bed forming uniform-size *clusters*, more than 80% of the bed mass had formed larger *agglomerates* of size in the range 5-30 mm and whose cohesive bond energies were of the order of 10^3 J. Here, the formation of aggregates included all three types of interactions mentioned above. Simulation of powder I in a rectangular container exhibited vibromobilization only at the top and bottom of the bed.

In conclusion, the value of ε had a proportional control on the strength and size of the aggregates and their mass fractions while Ec_{MIN} determined mainly the starting time of agglomeration, t_a. Another interesting feature revealed by the simulation is that the first half of the vibratory cycle promotes agglomeration while the second half causes dominance of break-up of aggregates.

The conditions for satisfactory fluidization of fine powders would be low values of ε and high values of Ec_{MIN}. Larger values of Ec_{MIN} have to be used in simulations to observe significant influence on the cohesivity of the powder. How do we modify a fine powder to increase Ec_{MIN} and diminish ε ? These are questions of considerable practical significance. We intend to study them in subsequent publications.

The results of this work are far from those that are of engineering interest in the sense that several simplifications have been made viz, two-dimensional bed, absence of fluid (air) medium, fewer particles, absence of important mechanisms such as particle deformation and the present unavailability of methods of estimating the model parameters. However, at this stage of the research program, our immediate goal was to develop a simple methodology to simulate the macroscopic characteristics of vibrated beds from proposed models of microscopic processes.

Subsequent works will attempt to incorporate the *powder chemistry model* to gas fluidized fine powders and eventually to vibration-assisted gas fluidized beds taking into account the aerodynamic forces. From the engineering point of interest, future work requires modelling the cohesion process at the particle surface in order to relate the parameters that we have introduced in our *powder chemistry model* of agglomeration-deagglomeration to surface properties, deformability and shape of powder grains.

Acknowledgements

The authors would like to thank Arthur M. Squires, Professor Emeritus, Department of Chemical Engineering, Virginia Polytechnique and State University, USA for his helpful suggestions in bringing this paper to its present form.

Table 2.1 Parameter sets for simulation of cohesive powders

Powder	Ec_{MIN} (J)	ε
I	0	0.25
II	0	0.75
III	$0.5.m_1.(300)^2$	0.25
IV	$0.5.m_1.(300)^2$	0.75

Table 2.2 Effect of Ec_{MIN} (ε=0.25)

Ec_{MIN} (J)	t_a (s)
0	$1.25.10^{-5}$
$0.5.m_1.(300)^2$	8.10^{-4}

9. List of Symbols

A	Amplitude of vibration
A	Aggregate number (1,2,3,etc.)
AMM	Aggregate Member Matrix (Dimension=Total number of particles)
a	Frictional force vector
BE	Cohesive Bond energy
BE_A	Cohesive Bond energy of an aggregate
$<BE_A>$	Mean Cohesive Bond Energy of aggregates at a particular time instant
BEM	Bond Energy Matrix (Dimension=Total number of particles)
C	Coefficient of friction
d	Diameter of particles
d_{eff}	Effective diameter of aggregates (diameter of circle having area equal to that of the aggregate)
$< d_{eff} >$	Mean effective diameter of aggregates (instantaneous average over all aggregates)
E_{coll}	Collisional energy
Ec_{MIN}	Minimum collisional energy (*ease of cohesion*)
e	Unit gravitational vector
f	Frequency of vibration
g	Gravitational acceleration

HR	Hausner ratio (tapped bulk density/loose bulk density)
K	Equilibrium constant
k	Reaction rate
MD,ND	Aggregate label after deagglomeration
MN	Aggregate label after agglomeration
m	Mass of particle
N	Number of simulated particles
n	Number concentration of aggregates
r	Interparticle separation
t	Time
t_a	Starting time of agglomeration
U	Particle velocity vector
u	Hooke's repulsive interparticle force potential
x	Position vector of particles (x_x,x_z)
x,z	horizontal and vertical axes respectively
Y	Young's modulus of particles

Subscripts

A	Aggregate
x,z	2D vector components
M,N	Particle labels

P,Q	Aggregate or particle labels (as the case may be)
MD, ND	Aggregate labels after deagglomeration
MN	Aggregate label after agglomeration
x,z	Horizontal and vertical vector components respectively

Greek alphabets

α	Angle of the bed walls with the vertical
ε	Fraction of kinetic energy transformed into cohesive bond energy (*cohesivity*)
ϕ	Phase angle
ψ	Circularity of aggregate
$\langle\psi\rangle$	Mean circularity of aggregates (instantaneous average over all aggregates)
ρ	Linear density = bulk density/solid density

Italics

A	Aggregate
n	Number concentration

References

[1] B.J.Ennis, J.Green and R.Davies, *Chem. Eng. Prog.* (Apr. 1994) 32.

[2] D.Geldart, *Powder Technol.* 7 (1973) 285.

[3] H.M.Jaeger, S.R.Nagel, *Science* 255 (1992) 1523.

[4] E.R.A.Eccles, K.Erdesz and A.S.Mujumdar, *Fluidization VI* (1989) 219.

[5] J.Visser, *Powder Technol.* 58 (1989) 1.

[6] J.Chaouki, C.Chavarie, D.Klvana and G.Pajonk, *Powder Technol.* 43 (1985) 117.

[7] R.Deiva Venkatesh, *Master's thesis*, Ecole Polytechnique de Montréal, 1995.

[8] S.Mori, A.Yamamoto, T.Haruta, *Int. Chem. Eng.*, 31 (1991) 475.

[9] C.Lauga, J.Chaouki, D.Klvana and C.Chavarie, *Powder Technol.* 65 (1991) 461.

[10] R.Chirone, L.Massimilla and S.Russo, *Chem. Engr. Sci.* 48 (1993) 41.

[11] R.Deiva Venkatesh, J.Chaouki and D.Klvana, *Powder Technol.* 89 (1996) 179.

[12] B. Thomas, M.O. Mason, Y.A. Liu and A.M. Squires, *Powder Technol.* 57 (1989) 267.

[13] B. Thomas, Y.A. Liu, R.Chan and A.M. Squires, *Powder Technol.* 52 (1987) 77.

[14] J.A.C.Gallas, H.J.Herrmann and S.Sokolowski, *Physica A* 189 (1992 a) 437.

[15] J.A.C.Gallas, H.J.Herrmann and S.Sokolowski, *Phys. Rev. Lett.* 69 (1992 b) 1371.

[16] Mehta A., in A.Mehta (ed.), *Granular Matter : an Interdisciplinary Approach*, Springer, New York, 1993.

[17] Y.Lan and A.D.Rosato, *Phys. Fluid A* 7 (1995) 1818.

[18] J. Lee, *Physica A* 238 (1997) 129.

[19] E.Clement and J.Rajchenbach, *Europhys. Lett.* 16 (2) (1991) 133.

[20] Y.Bloise, *Master's degree thesis*, Ecole Polytechnique de Montreal (1995).

[21] M.M.Mansour and F.Baras, *Physica A* 188 (1992) 253.

[22] R.D.Cadle, *Particle Size*, Reinhold Publishing Corporation, NewYork, 1965.

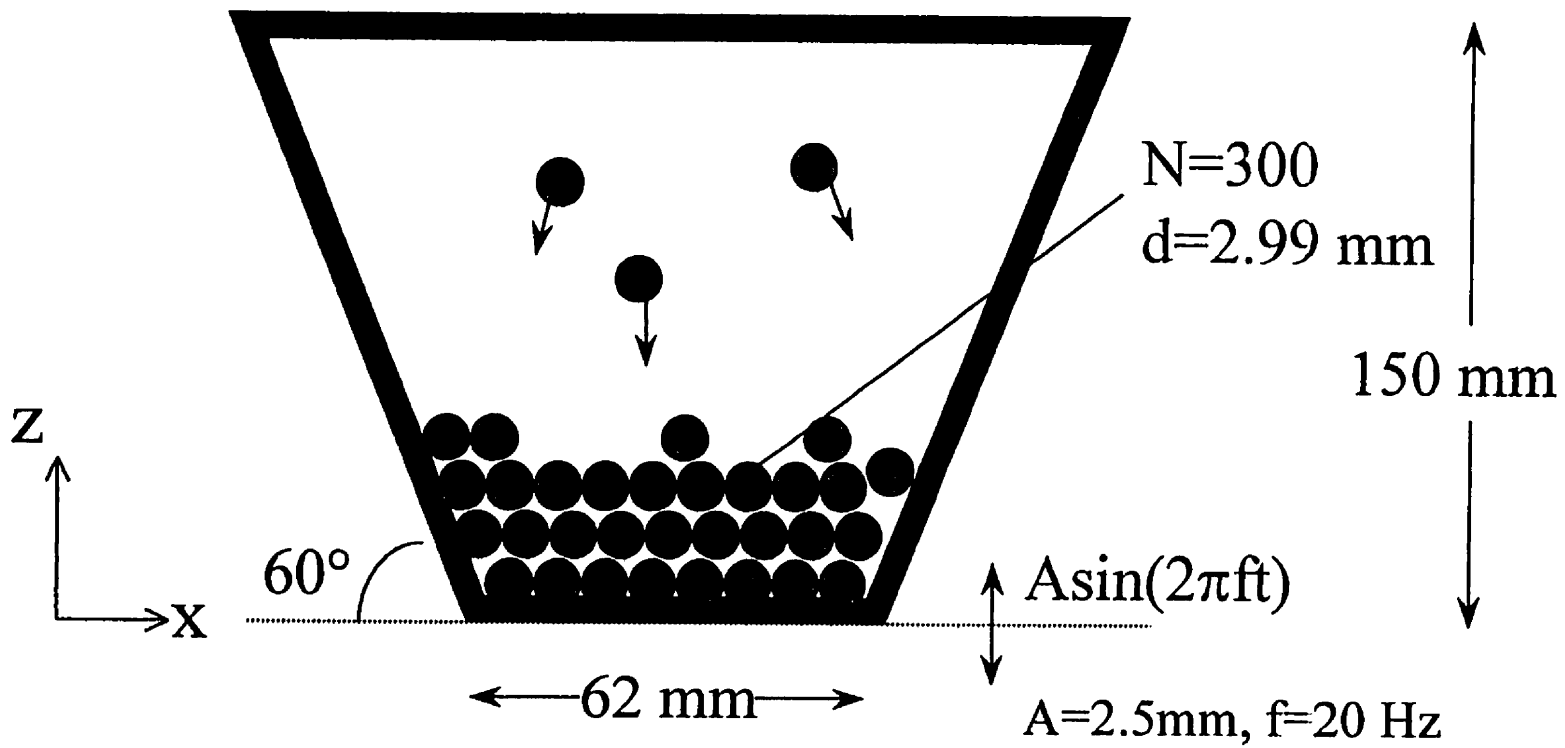

Figure 2.1 Vibrated Bed

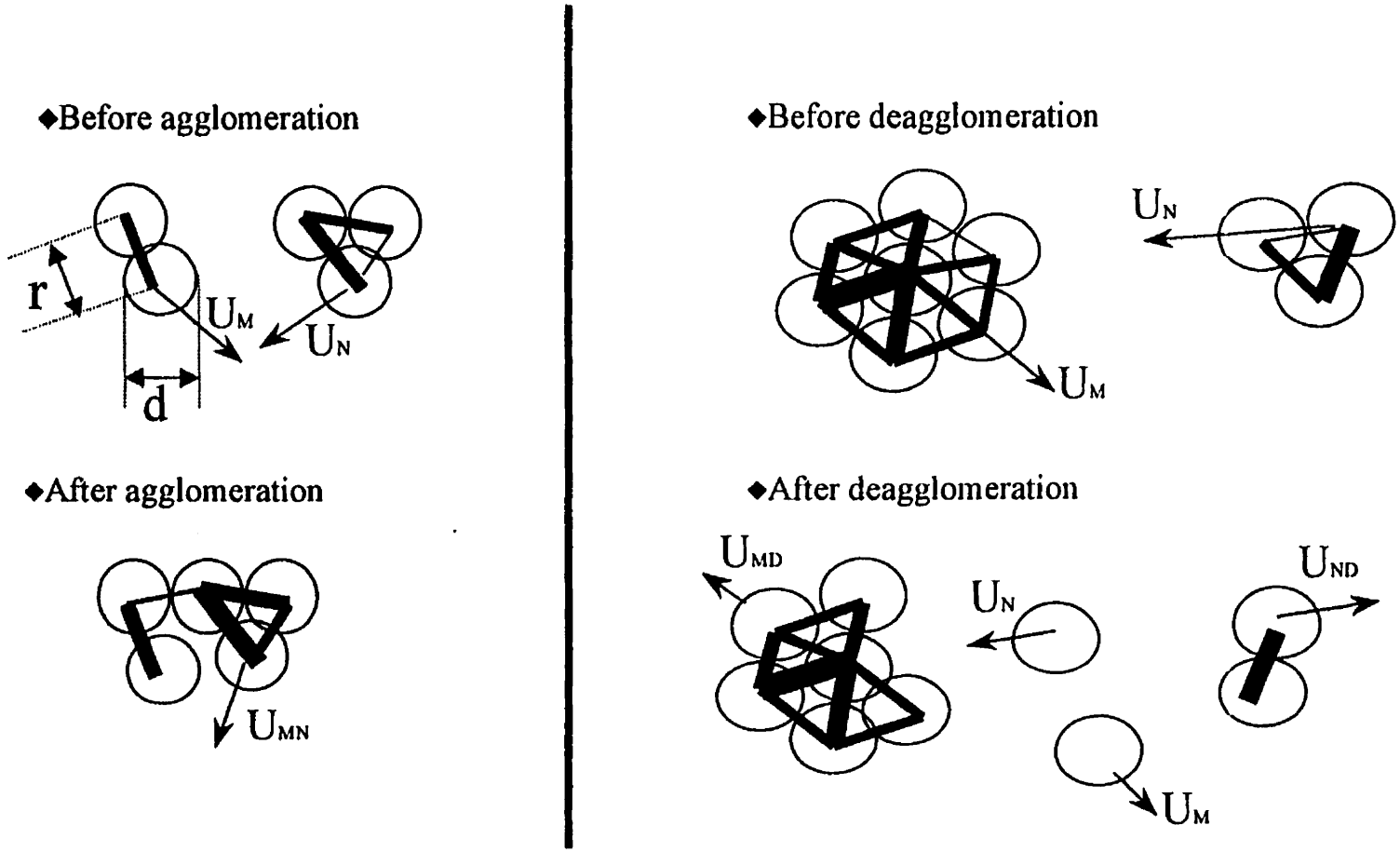

Figure 2.2 Agglomeration and deagglomeration mechanisms

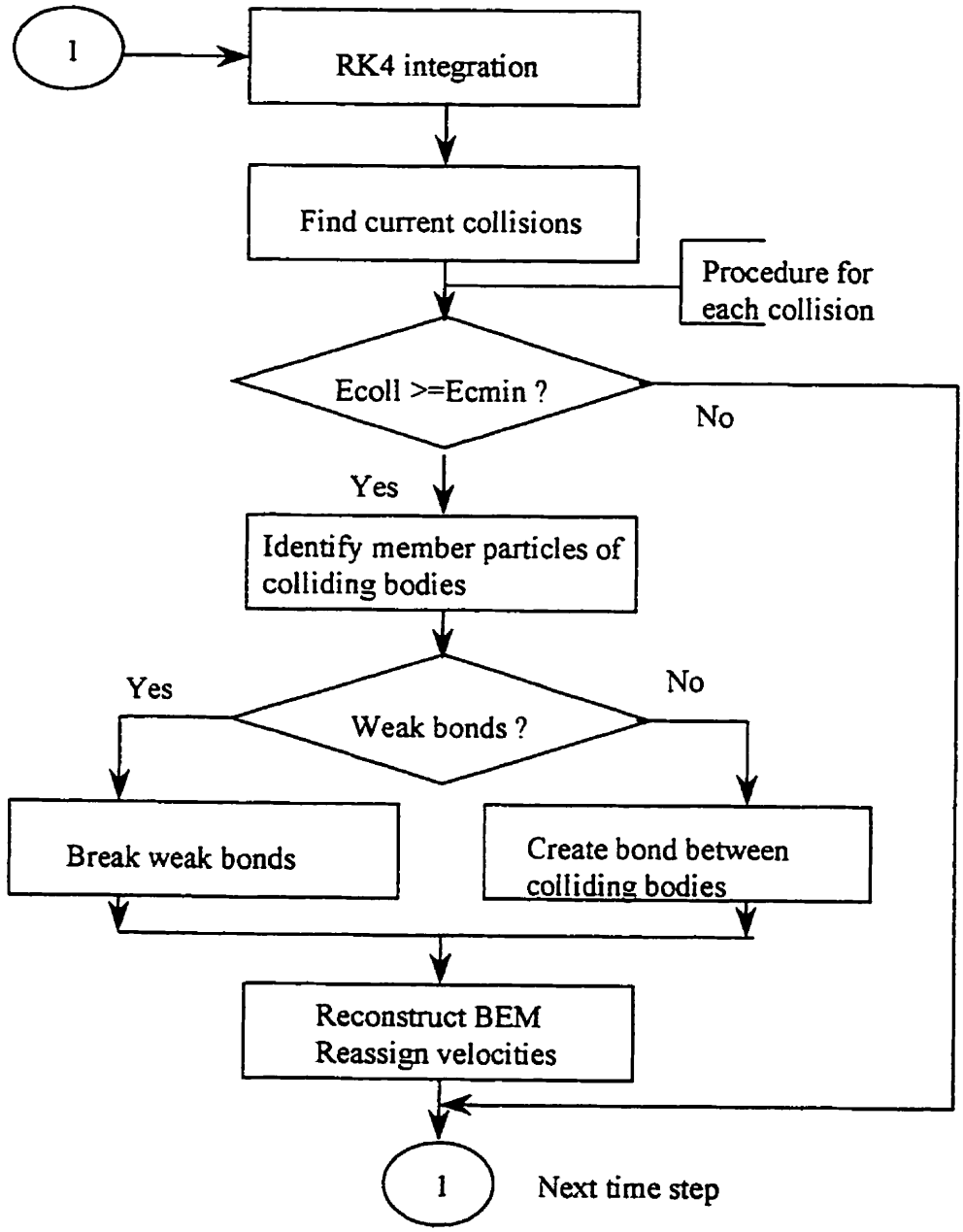

Figure 2.3 Algorithm for formation and break-up of aggregates

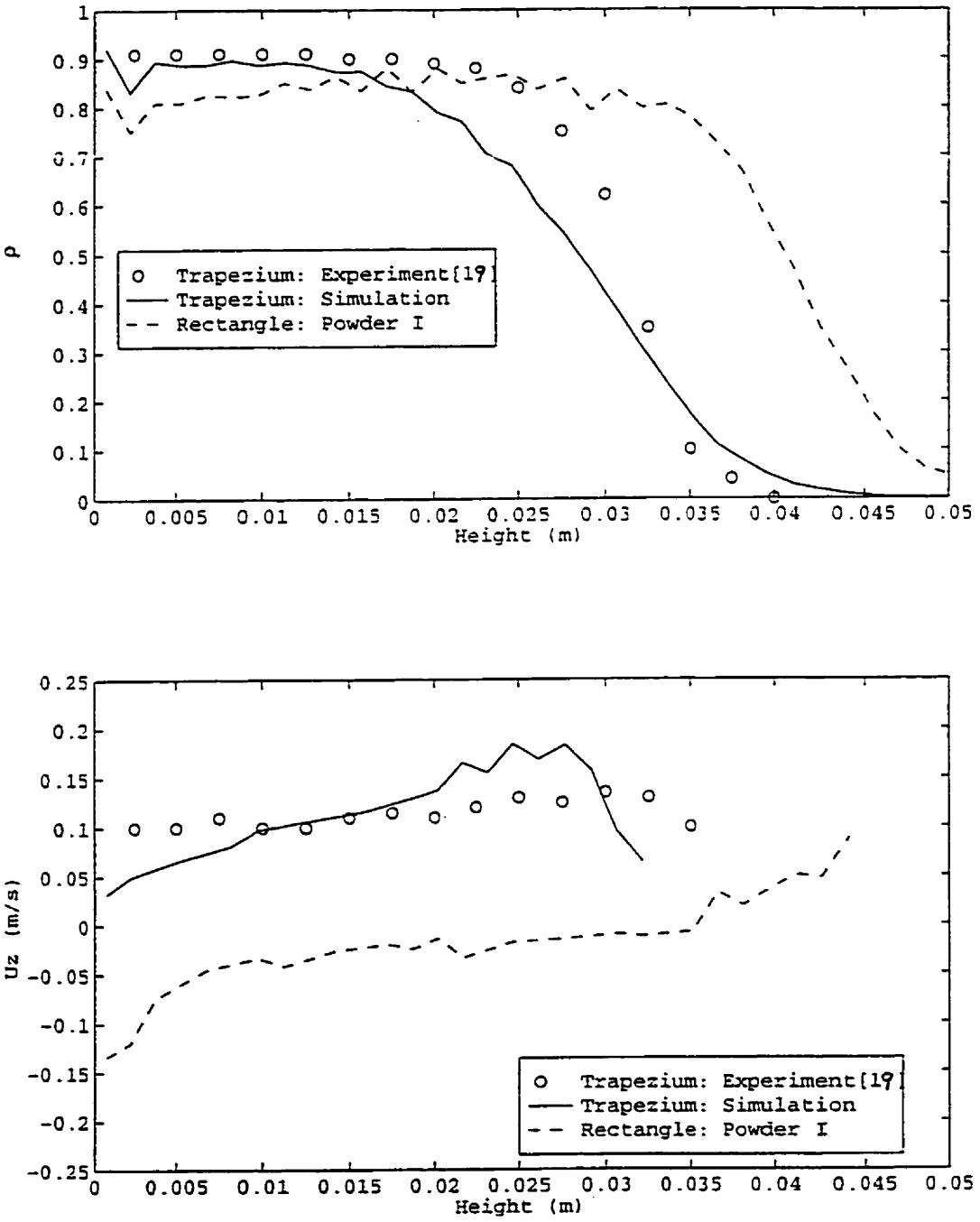

Figure 2.4 Axial profiles of linear density and mean z-velocity (ϕ=0)

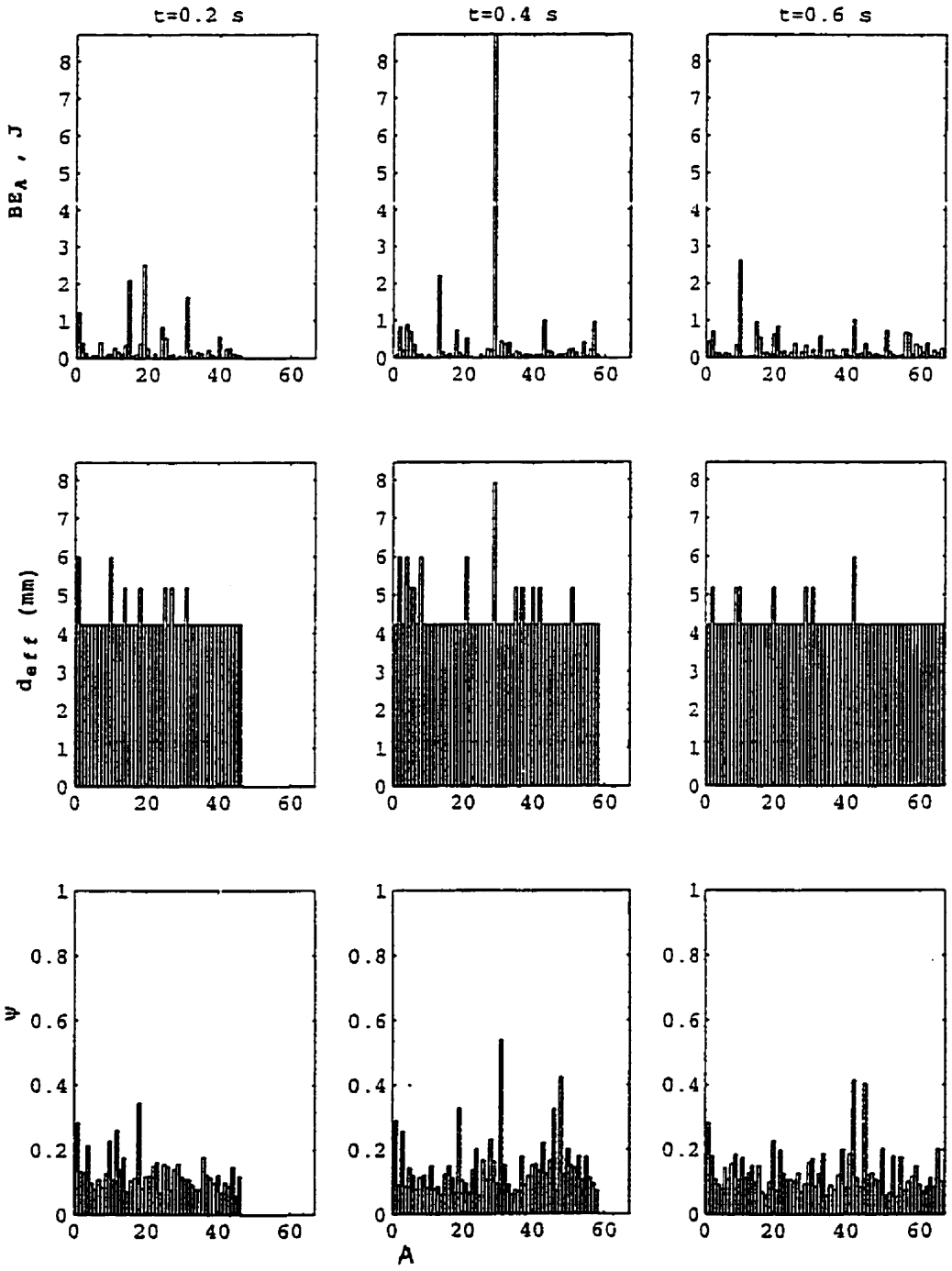

Figure 2.5 Instantaneous bed characteristics (powder I)

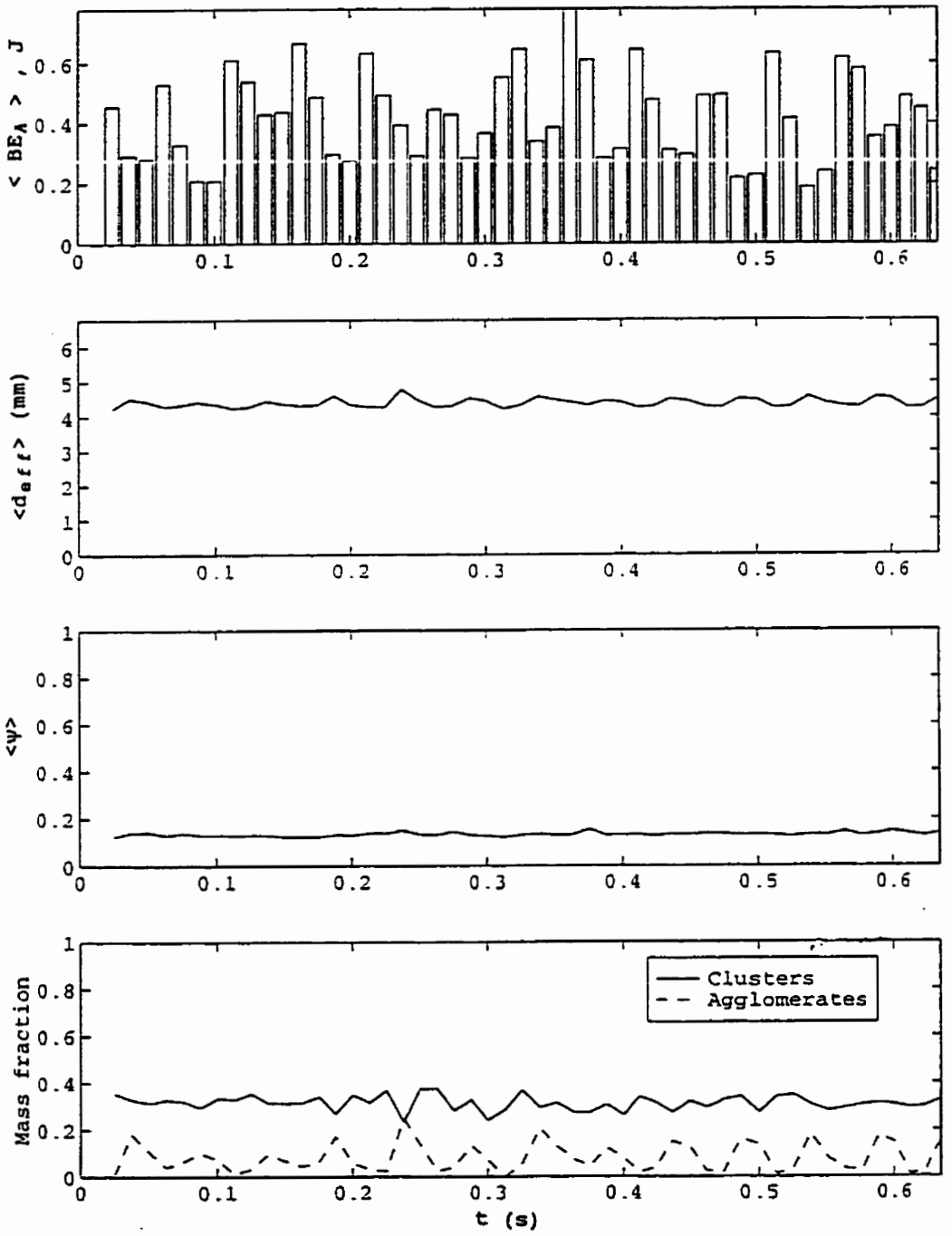

Figure 2.6 Evolution of bed averages (powder I)

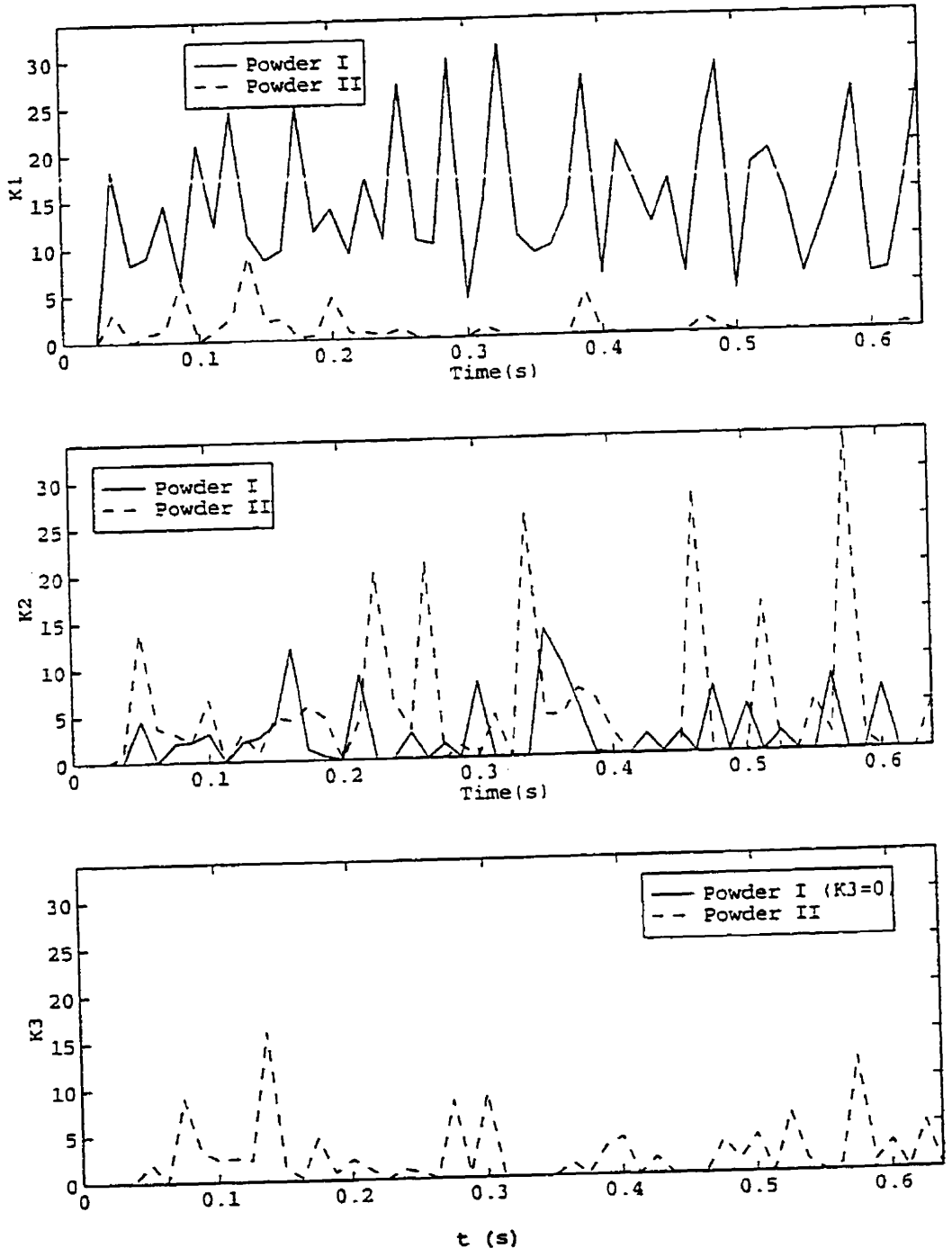

Figure 2.7 Time dependence of equilibrium constants

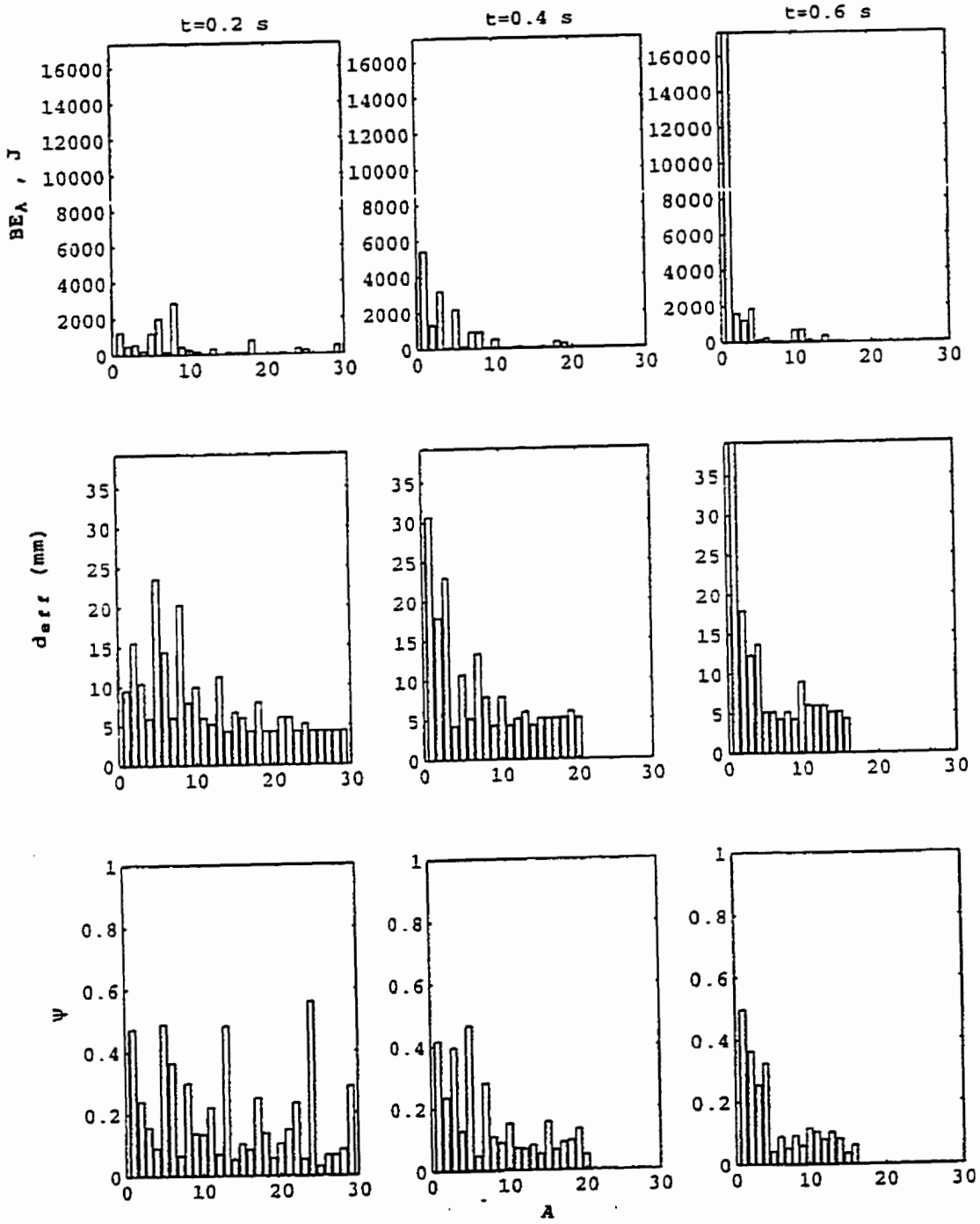

Figure 2.8 Instantaneous bed characteristics (powder II)

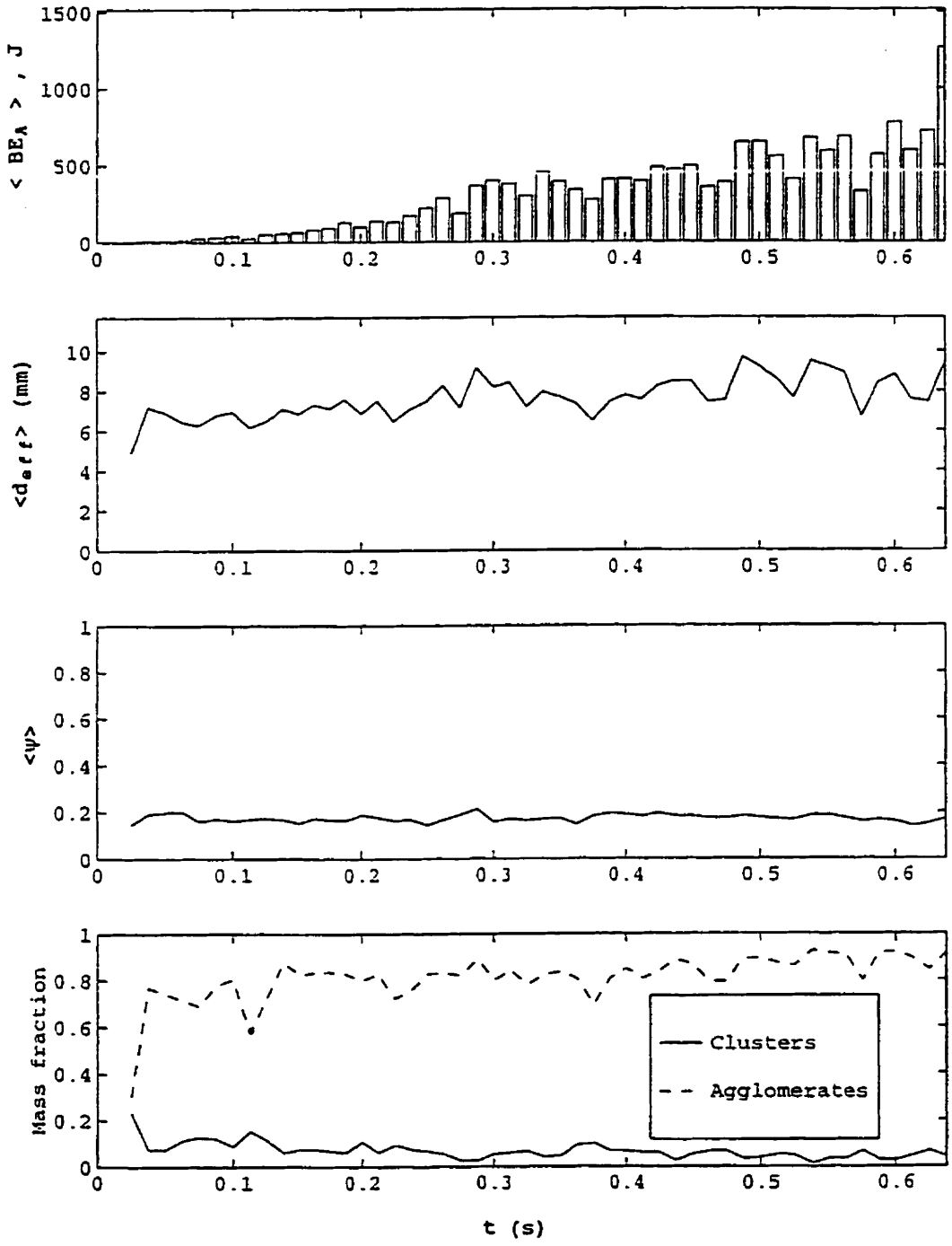

Figure 2.9 Evolution of bed averages (powder II)

CHAPTER 3: SIMULATIONS AND EXPERIMENTS OF POWDER FLUIDIZATION

Reference:

R. Deiva Venkatesh, J. Chaouki, M. Grmela and R. Mortazavi, "SIMULATIONS AND EXPERIMENTS OF POWDER FLUIDIZATION", *Advanced Powder Technology* (submitted for publication).

Keywords:

Fine powders; Fluidized beds; Stokesian Dynamics; Radioactive Particle Tracking

SIMULATIONS AND EXPERIMENTS ON FINE POWDER FLUIDIZATION

R. Deiva Venkatesh[1,2], J. Chaouki[1,2] *,M. Grmela[2] and R. Mortazavi[1,2]
[1]*BIOPRO Centre,* [2]*Chemical Engineering Department, Ecole Polytechnique de Montreal, P.O. Box 6079, Montreal, Qué. H3C 3A7, Canada*

Abstract

The Stokesian Dynamics method is used to simulate the air fluidization of an FCC powder bed. Besides detailed information on the instantaneous motion of the particles in the bed, the characteristics of the bubbling bed were estimated. The particle velocities observed in the simulations are compared to tracer velocities in a radioactive particle tracking experiment conducted at an air velocity of 0.44 m/s in an FCC bed having a diameter of 15 cm. Under equiscale assumptions, the particle velocities in experiment and simulation were in good agreement. Two other simulations on FCC particles at air velocities of 0.09 m/s and 0.06 m/s were compared for bubble characteristics measured with the fiber-optic technique in the experimental fluidized bed. The size and rise velocity of bubbles obtained using the Stokesian Dynamics simulation were in good agreement with predictions by bubbling bed models at the vicinity of the distributor while model predictions differed slightly from experimental measurement at a height of 50 mm from the distributor. The average bed porosity extracted from simulations are close to the experimental measurements.

Within the current assumptions on the quantitative comparison of experimental and simulated fluidization of powders, we conclude that the Stokesian Dynamics method captures the essential behaviour of fluidized beds. The non-definite structure of a fluidized bed has also been differentiated from that of a fixed bed.

Keywords: Powders, fluidized beds, stokesian dynamics, fibre-optic analysis, radioactive particle tracking

---

* Corresponding author

1. Introduction

Powders have widespread applications in the industry ranging from chemical, pharmaceutical, agricultural and food industries. Some of these applications involve the fluidization of fine powders. Powders have been broadly classified as Group C, A, B and D under Geldart's classification of powders [1]. Numerous experimental and theoretical studies can be found in the literature on the gas fluidization of these powders with journals such as Powder Technology dedicated to such studies.

Several interesting phenomena such as channeling and agglomeration are observed in the case of Group C powders. Homogeneous fluidization with bed expansion in Group A powders, bubbling in Group A and B powders and slugging in Group B and D powders are well known with a battery of successful models to predict such phenomena.

These well-established models of fluidized beds serve the purpose of explaining the macroscopic quantities of the bed such as bubble size, bed expansion, bubble velocity and bed porosity but their focus is not on the bed microscopy explaining particle configurations and motion. With the ever-increasing power of computers, progress has been made on both the experimental and modeling routes of studying fluidized beds. Workstations are widely used to process data from radioactive particle tracking, laser velocimetry, optic fiber equipments etc., to study the microscopy of fluidized beds. On the other hand, modeling and simulations of fluidized beds can be performed on

computers for the same reasons. The two categories of fluidized bed models are: (a) the two-fluid model and (b) the discrete-particle model that describe fluidized beds with the latter category having the advantage of effectively describing the particle motion [2].

The focus of this paper is the discrete particle simulation of fluidized powders. To simulate the fluidization of powders, we employ the Stokesian dynamics method. The empirical parameters that have to be introduced in the technique are those needed to characterize the Stokesian particle-fluid interactions [2, 3]. Recent simulations using the Stokesian Dynamics method have reproduced realistic particle motion in gas fluidized granular systems [3, 4].

In these simulations, the Stokesian Dynamics method is used to simulate the air fluidization of a two-dimensional bed composed of 128 spherical glass particles with 10 particles forming the fixed bottom of the bed with an uniform air velocity at a value 30% of the single particle terminal velocity. The bed whose thickness was the same as the size of the particles had width as 35 and height as 50 (dimensionless units).

The purpose of this paper is to compare the bed characteristics such as bubble size, bubble velocity and particle velocities obtained from the Stokesian Dynamics simulation of gas fluidized Fluid Cracking Catalyst with experimental measurements of these quantities using radioactive particle tracking and fiber-optic methods as well as bubbling bed models.

2. Stokesian dynamics method with periodic boundary conditions

We recall the fluidized bed model of Ichiki and Hayakawa [4] (a model to simulate the fluidization of rigid particles). For more details concerning this model refer to the paper of Brady and Bossis [2] describing Stokesian Dynamics and the paper of Ichiki and Hayakawa [4] describing the simulation of fluidized beds using the Stokesian Dynamics method. Ichiki and Hayakawa assume that the bed is composed of monodisperse spheres with no rotational motion. Table 3.1 enlists the characteristics of the fluid and the powder.

The motion of N fluidized particles is given by Newton's equation [4]:

$$St\frac{d\mathbf{u}}{dt} = \exp\left(\frac{t}{St}\right)\mathbf{V} \tag{1}$$

Here, t denotes the time, St is the Stokes number, **x** is the 2D position vector, **u**=U.exp(t/St)

$$\mathbf{U} = \begin{bmatrix} \mathbf{U}_1 \\ \mathbf{U}_2 \\ \cdot \\ \cdot \\ \cdot \\ \mathbf{U}_N \end{bmatrix}$$

where **U** is the 2D velocity vector for the N-particle system.

V, representing the terminal velocity of the particles is given by the following equation:

$$\mathbf{V} - \mathbf{u}^{\infty} = -\underline{\mathbf{R}}^{-1} \cdot \mathbf{E}_Z \tag{2}$$

$\mathbf{u}^{\infty}$ is the superficial fluid velocity vector, $\mathbf{E}_Z$ is the unit vector in the vertical direction and $\underline{\mathbf{R}}$ is the resistance matrix which is estimated from the many-body hydrodynamic interactions and the short-range lubrication forces in the Stokesian Dynamics method with periodic boundary conditions. Position and velocity vectors are dimensionless with the particle radius 'a' as the characteristic length and the single particle terminal velocity v, as the characteristic velocity. The resistance matrix $\underline{\mathbf{R}}$ which is constructed from the particle positions is symmetric, positive-definite and its estimation using periodic boundary conditions is adequately explained by Brady and Bossis [2] and Ichiki and Hayakawa [3]. Using periodic boundary conditions, the hydrodynamic interactions are estimated in all three directions, the long-range forces calculated using the Ewald-summation technique of the mobility matrix [5] and lubrication forces from the lubrication matrix representing the short-range pair-wise repulsive interactions [6].

The instantaneous positions and velocities of the N particles are found out by integrating Eq. (1). For this purpose, we use the fourth-order Runge-Kutta method with a time step of 0.1 and the inversion of the resistance matrix is done using the Cholesky factorization technique. The resistance matrix $\underline{\mathbf{R}}$ and the terminal velocity **V** are estimated for each time step from the position vector **x** at that time. The simulation parameters are listed in

Table 3.1. The particles are allowed to move only in the vertical plane although the hydrodynamic interactions are taken into account in all three dimensions.

The direct interparticle forces during fluidization are treated as elastic collisions where the momenta of colliding particles are exchanged at the end of the time step.

3. Simulation of the gas fluidization of FCC ($u^{\infty} = 0.44$ m/s)

The purpose of this simulation was to compare the particle velocities with the experimental measurements on FCC using the Radioactive Particle Tracking (RPT) technique. We start the simulation with a random configuration of the Fluid Cracking Catalyst (FCC) particles of size 70μm. The dimensions of the unit cell are 17.5x50x2 with periodic boundary conditions in all directions representing a small volume in the central portion of a fluidized bed farthest from the distributor and the walls (see Figure 3.1 for details). Using the Runge-Kutta technique we calculate positions and velocities of all 100 particles for each time step (dt = 0.1) with St = 235 for FCC.

During fluidization, we introduce air with an uniform velocity of 0.44 m/s and track the positions and velocities of all fluidizable particles for each time step. We record every tenth time step upto a maximum of 1000 recorded steps. All simulations were run on an IBM SP2 with a performance of 130 MFlops.

The axial distribution of the time-averaged horizontal and vertical components of the particle velocities obtained from this simulation is compared with those obtained in experiments on radioactive particle tracking of FCC later in Section 7.

4. Simulation of the gas fluidization of FCC (u^{∞} = 0.09 and 0.06 m/s)

In this case, in addition to the 100 fluidizable particles, we have five particles fixed in space at the bottom of the unit cell to represent the distributor where the bubbles would originate. Two gas velocities 0.09 m/s and 0.06 m/s were used in these simulations to compare with the bubble characteristics of a fluidized FCC bed measured experimentally using the fiber-optic method. Here, the unit cell represents a small volume close to the distributor in the experimental bed.

The average bubble size, bubble velocity and area fraction of the bubble phase obtained from the microscopic simulation results are compared with the experimentally measured values in Section 7.

5. Radioactive Particle Tracking Experiment

The experiments were done in a gas-solid fluidized bed as shown in Figure 3.2. The column was made of a Plexiglass pipe with 152 mm internal diameter and 1500 mm height. Air at room temperature was introduced into the bed through a conical section, passing through a stainless steel porous plate and a nozzle type air distributor. Air flow rate was measured by an orifice plate connected to a water manometer. A cyclone placed at the air outlet of the column returns the entrained solids back to the bed.

The solids used in the experiments was the Fluid Cracking Catalyst (FCC) having particle size of 70 μm and a density of 1971 kg/m^3. Initial height of the bed was 0.22 m (1.5 times the column diameter).

The tracer was made of a mixture of gold powder and epoxy resin of size 420 μm to be used in the experiment. It was activated in the SLOWPOKE nuclear reactor of École Polytechnique prior to the experiment. The produced isotope ^{198}Au emits γ-rays which are counted by 16 cylindrical NaI(Tl) scintillation detectors on sliding rails. A typical arrangement of the detectors around the fluidized bed is shown in Figure 3.2. Two personal computers simultaneously register the number of γ-rays detected by each detector in every sampling period of 20 ms. These number of counts are used later to calculate the co-ordinates of the tracer. Details of the system calibration and the inverse reconstruction strategy for tracer position rendition are described by Larachi *et al.* [7, 8].

See Appendix 1. During the experiment the tracer was placed into the bed to move freely with the other particles inside the bed. Movement of the tracer was then monitored for about 5 hours during which the count rate of the tracer at some 820,000 points were acquired. The bed was then made empty and the tracer was recovered from the solids.

6. Fiber-optic experiment

Fiber-optic experiments were carried out in the same column described in Section 4 having 150 mm in diameter at 20°C under different superficial gas velocities in the bubbling regime of fluidization. See Appendix 2. The same FCC powder discussed in the radioactive particle tracking study was used in this case as well.

A cross fiber-optic probe [9] with two cross-fiber bunches of 0.8 mm in diameter composed of several small optic fibers of 40 μm diameter is placed at a position of 50 mm from the distributor to measure the local instantaneous voidage. A PV - 4A Particle Velocity Analyzer made by the Institute of Chemical Metallurgy, Chinese Academy of Sciences is employed to get the time series of dynamic local voidage under different operating conditions. More than 20 runs with 60,000 data each were sampled with a sampling frequency of 16 KHz under the operating conditions. The size of bubbles and their rise velocities at the given height were measured as an average of two radial positions one at the centre of the bed and the other at two-thirds the radius of the bed.

7. Results

7.1 Comparison of Stokesian Dynamics results with Radioactive Particle Tracking (RPT)

As explained in Section 3, the particles are first generated randomly in the unit cell. We introduce uniform air flow in the upward direction with a high velocity of 0.44 m/s. In Figure 3.3 we see a state of the fluidized bed during the 1000 recorded time steps.

Velocity profiles were extracted from the particle trajectories by averaging the 1000 steps for several axial positions. Observe that the entire bed is in a fluidized state in Figure 3.4 which shows the axial distribution of the x- and z- components of the particle velocity along the bed height obtained from FCC simulations at 0.44 m/s.

As mentioned in Section 3, this unit cell having periodic boundary conditions in all directions represents a small area at the centre of a fluidized FCC bed which has the least influence of the wall or distributor. The axial distribution of the average particle velocities computed from the Stokesian Dynamics simulation is therefore representative of a zoom area (dotted box) at the centre of the experimental fluidized bed described in Section 4 which is farthest from the wall, distributor and the bed surface. Using this assumption, we ensure comparison of simulation and experiment at the same dimension scale. It is difficult to simulate conditions near the distributor at the bottom of the bed due to very high velocity of the gas flow. In fact, an attempt to simulate a unit cell with

fixed particles at its bottom to represent a small volume above the distributor proved to be unproductive as particles carried up by the high gas flow (0.44 m/s) were collected against the fixed particles of the periodic image directly above the central cell. The figure also shows experimental results of the x- and z-components of the particle velocities as measured by the radioactive particle tracking technique along the bed height at a radial distance of 1 cm from the axis of the bed. The particle velocities in both cases are rendered dimensionless using the characteristic single particle terminal velocity.

Comparing the x- and z-components of the particle velocities at the central portion of the experimental FCC bed with the simulation results obtained from the Stokesian Dynamics method indicates a good agreement between them. The particles appear in both cases to have a dominant upward motion compared to the lateral movement at the high gas velocity.

7.2 Comparison of Stokesian Dynamics results with Fiber-optic experiments

Comparison of the Stokesian Dynamics simulation results of a bubbling bed were made with measurements of bubble characteristics (bubble size and velocity) based on the fiber-optic technique explained in Section 6. In this case, we need fixed particles at the bottom of the unit cell to act as the distributor where the bubbles would originate. The ratio of the height of the fixed bed that the 100 simulated particles would have formed to the width of the unit cell (17.5) is 1.3. Larger heights of the unit cell would require cell

widths larger than 17.5 to avoid slugging at the top which implies more number of simulated particles and hence longer computational times.

Using the information of instantaneous particle positions and velocities, the void spaces arising in the bed are identified as bubbles and the motion of the bubbles are followed starting from their birth at the distributor to their explosion at the surface of the bed. The history of each bubble viz, their size, velocity can thus be extracted from the simulation data.

In the following discussion where we compare the characteristics of the bubbling bed in the Stokesian Dynamics simulation with the corresponding experimental results, the size and velocity of the bubbles and the bed porosity are calculated as follows from the primary simulation results, the positions and velocities of the particles: Each of the 1000 recorded time steps were snapshot as frames. A 'bubble' program discretizes the area of the fluidized bed (within the unit cell) into an array of squares whose size is of the order of the particle size. The bubble is identified by tracing the border particles which surround the bubble and are characterized by lop-sided neighbors. The sum of the areas of the squares enclosed by such particles gives the two-dimensional area of the bubble. The geometry of the enclosed area specifies the centre of the bubble. From this information, growth rate and rise velocity of bubbles between any two frames is estimated by the program. The porosity of the bed is estimated from the height of the fluidized bed within the unit cell.

Figure 3.5 shows a snapshot of periodic images of the bubbling bed of FCC at 0.09 m/s. Notice that a few particles can be entrained in the rising bubble and the bubble is 'grown' as opposed to its initial size near the distributor where it is comparable to the size of the particle.

Comparing the results of the simulation and experimental measurements of the characteristics of the bubbling bed of FCC particles at an air velocity of 0.09 m/s, in Figure 3.6, we note that the scale of comparison is not the same, i.e., the sizes of the unit cell and the experimental bed differ considerably. Here, we assume that the unit cell represents a small portion of the experimental bed at the proximity of the distributor and far from the wall. An indirect quantitative comparison between the unit cell and the experimental set-up is possible by bridging the experimental results observed at the height of 50 mm along the axis of the bed with simulation results using bubbling bed models as discussed below.

Comparing the results of experiment and simulation, we arrive at the following report: Here bubble sizes have been rendered dimensionless as is usual in Stokesian Dynamics by the particle radius 'a' and the bubble rise velocity by the single particle terminal velocity, v.

Average bed porosity at 0.09 m/s:

The average bed porosity at a height of 50 mm from the distributor is 0.55 in the case of simulation and 0.52 in the case of the experiment. The porosity is averaged radially over two positions, one at the center of the bed and the other at two-thirds the radius of the bed.

Bubble characteristics at 0.09 m/s:

The dimensionless bubble size estimated from simulation results has a value of 18 at a height of 35 (equivalent of 1.2 mm from the distributor) as shown in the inset of the bubble diameter vs height plot in Figure 3.6 for the unit cell. The fiber-optic measurement at this higher velocity at a height of 50 mm from the distributor gave a dimensionless bubble size of 474.86. This is explained by the increase in the size of the rising bubbles as well as due to bubble coalescence. However, the simulation result agrees well with the model for predicting bubble size near the distributor [10], which gives a value of 55 for the given bed depicted in Figure 3.6.

We bridge the simulation results near the distributor with the experimental results at a height of 50 mm using common bubbling bed models. Using the Rowe model for bubble size as a function of the bed height [11], we calculate a bubble size of 19.8 close to our simulation result. The Rowe model shown below and its agreement with the simulation prediction of the bubble size near the distributor is shown in Figure 3.6.

$$d_b = g^{-0.25} z^{0.75} \left(u^{\infty} - u_{mb}\right)^{0.25}$$

(3)

Comparing the bubble rise velocities in both experiment and the bubbling bed model, we find the experimental value to be close to that predicted by the Kunii-Levenspiel model [10] at 50 mm from the distributor. As seen in Figure 3.6, the simulation results (inset) agree well with the model prediction of 0.32.

$$u_b = 1.55\left(u^{\infty} - u_{mf}\right) + 14.1\left(d_b + 0.005\right)\left(d_t^{0.32} + u_{br}\right) \tag{4}$$

$$u_{br} = 0.711\left(g d_b\right)^{0.5} \tag{5}$$

Average bed porosity at 0.06 m/s:

An average bed porosity of 0.49 was estimated from the Stokesian Dynamics results while the radially averaged fiber-optic measurements yielded a value of 0.49 as well.

Bubble characteristics at 0.06 m/s:

At this lower air velocity, we compare the bubble size and their rise velocity obtained in the simulation and the fiber-optic experiment in Figure 3.7. The insets show the bubble characteristics in the unit cell. As in the above case, the unit cell represents an elemental area at the centre of the distributor. The average bubble size obtained by the Stokesian Dynamics method is 12 and the range of the bubble size agrees well with the bubble size of 22.42 predicted by the bubble size model applicable near the distributor [10]. The bubble size obtained by the fiber-optic method is 403.43 which was measured at a height of 50 mm. The Rowe model yields a value of 12.71. Interestingly, the bubble rise

velocity estimated from the simulation is very close to the Kunii-Levenspiel result as shown in the figure. The experimental bubble rise velocity at the height of 50 mm is close to the model prediction.

From the results of comparison with bubbling bed models, we infer that the Stokesian Dynamics method reasonably predicts the bubble size and bubble rise velocities (at the proximity of the distributor).

Comparison between two-dimensional and three-dimensional beds:

It is to be noted that the Stokesian Dynamics simulation of bubbling beds is performed in a pseudo two-dimensional bed while experiments and the Kunii-Levenspiel model are prescribed for three-dimensional bubbles. In two-dimensional beds, the Davidson theory assumes the bubble shape to be cylindrical [12]. It however is reported to overestimate the penetration in actual two-dimensional bubbles (cloud penetration is defined as the ratio of cloud radius to the bubble radius). Using the bubble rise model for two-dimensional bubbles [13] and the bubble size measured in the simulation at the gas velocity of 0.09 m/s, we obtain a bubble rise velocity of 0.403 which is close to both the three-dimensional model as well as the simulation result (Figure 3.6). The same conclusion is reached at the gas velocity of 0.06 m/s where the two-dimensional model yields a bubble rise velocity of 0.3781 again close to simulation results. When the bubble size is as small as obtained in the simulations, we observe little deviation between the two-dimensional and three-dimensional bubble characteristics compared to

simulations. As pointed out in Section 2 that even though the unit cell is pseudo two-dimensional, hydrodynamic interactions are estimated in all three directions. Brady and Bossis [2] have reported that pseudo two-dimensional simulations as well as the Ewald-summation technique are computational conveniences with the physics of the suspension being adequately described by the hydrodynamic interactions even in the absence of particle motion in the third dimension. A recent paper by Morris and Brady [14] justifies the use of pseudo two-dimensional cells in describing the pressure-driven flow of suspensions using Stokesian Dynamics. Here the suspension temperature (mean square of the scalar particle velocity fluctuations) is not affected by the increase in the thickness of the unit cell beyond the particle diameter. The influence of particle motion perpendicular to the plane of flow might cause deviations from the two-dimensional case (both model and simulation) when the system size is large (cell size > $O(10^2)$).

Structure of a fluidized bed

In addition to obtaining the characteristics of the fluidized bed that has been compared with experiments and bubbling bed models, a method of quantifying the structure of the bed using simulations is the estimation of the pair-distribution function.

We compared the structure of the fluidized bed with that of a fixed bed using the pair-distribution function G(r) which is the probability density of finding a particle at a distance r from a given particle [2]. Figure 3.8 compares the pair-distribution function G(r) in the horizontal and vertical directions both in a fixed as well as the fluidized bed

at 0.09 m/s obtained from the instantaneous particle positions of the 100 particles. The marked difference of a fluidized bed (represented in Figure 3.5) from the fixed bed is that G(r) is continuous which indicates a non-definite structure due to the mixing of particles throughout the bed.

8. Conclusions

We simulate the behaviour of gas fluidized FCC using the Stokesian Dynamics method. Initially, we simulate the simulation of FCC powder following the work of Ichiki and Hayakawa [4] using 100 fluidizable particles of 70 μm size. In this case, we considered particle collisions to be elastic and the gas velocity at 0.44 m/s. We observe the finely fluidized state of the bed and computed the x- and z-components of the time-averaged particle velocities along the height of the bed. A radioactive particle tracking experiment was carried out with the air fluidization of FCC under the same conditions and the velocity of the tracer was followed at various positions along the height of the bed. The unit cell of the simulation was assumed to be a small area at the centre of the experimental bed which is least influenced by the extremities of the bed. Comparing the Stokesian Dynamics results of particle velocities and the tracer velocities, we observe a good agreement between the simulation and the radioactive particle tracking method.

Two other simulations were carried out with the FCC powder at 0.09 m/s and 0.06 m/s respectively in the same unit cell. In this case, the characteristics of the bubbling bed such as bubble size, bubble rise velocity and areal fraction of the bubbles were extracted from the instantaneous positions and velocities of the particles. For comparison, two experiments were carried out with FCC at these two velocities and the fiber-optic technique was used to find these characteristics of the bubbling bed at an axial position in the bed.

Assuming the simulated unit cell represents a miniature area at the bottom of the axis of the experimental fluidized bed, comparison of the bubbling bed characteristics indicated that at both the gas velocities, the simulation values of bubble size and velocity are in agreement with the bubbling bed models at the vicinity of the distributor while the experimental measurements of these quantities conform well with model predictions. The bubble characteristics of the simulated bed are in agreement with two-dimensional bubble models and it is argued that for small bubble sizes as obtainable in the simulations, the difference between two-dimensional and three-dimensional models is not significant.

The structure of a fluidized bed was differentiated from that of a fixed bed using the pair-distribution function. This function is continuous for a fluidized bed unlike a fixed bed quantifying the spatial distribution of particles in the fluidized state having a non-definite structure.

Within the current assumptions on the quantitative comparison of experimental and simulated fluidization of powders, we conclude that the Stokesian Dynamics method captures the essential behaviour of fluidized beds. The major challenge/constraint that we face in the experimental comparison of the simulation of fluid-particle systems using the Stokesian Dynamics method described in this paper is the computational time which limits the size of the simulation cell. However, with revolutionary technologies in

computer processing speed expected in the near future, this problem is expected to be 'partially' overcome.

9. List of Symbols

a	Particle radius
d	Diameter
G	Pair-correlation function
g	Gravitational acceleration
m	Mass of particle
N	Total number of simulated particles
Nm	Number of fluidizable particles
Nf	Number of fixed (distributor) particles
r	Interparticle separation
t	Time
U	Particle velocity vector
u^{∞}, uinf	Superficial velocity of fluid
x	Position vector of particles (x_x, x_y, x_z)
x,y,z	Coordinate axes

Subscripts

b	Bubble
br	Single bubble
mb	Minimum bubbling condition
mf	Minimum fluidization condition

p	Particle
t	Tube (bed)
x,y,z	3D vector components

Greek letters

ρ	Linear density (bulk density/solid density)
ν	Single particle terminal velocity (characteristic velocity)
μ	Viscosity of the fluid

Acknowledgements

Deiva Venkatesh is deeply thankful to Navid Mostoufi for his experimental assistance on radioactive particle tracking and Dr. Cui Heping for actively assisting in the fiber-optic studies. He also expresses gratitude to Dr. Kengo Ichiki, Kyoto University, Kyoto, Japan for his continuous help during this work.

References

[1] D.Geldart, *Powder Technol.* 7 (1973) 285.

[2] Brady J.F. and Bossis G., *Annu. Rev. Fluid Mech.*, 20 (1985) 111.

[3] Ichiki K. and Hayakawa H., *Phys. Rev. E*, 52-1 (1995) 658.

[4] Ichiki K. and Hayakawa H., *Phys. Rev. E*, 57-2 (1998) 1990.

[5] Beenakker C.W.J., *J. Chem. Phys.* 50 (1986) 1581.

[6] Jeffrey D.J. and Onishi Y.J., *J. Fluid Mech.*, 139 (1984) 261.

[7] Larachi F., Kennedy G. and Chaouki J., *Nuclear Instruments and Methods in Physics Research A* 338 (1994) 568.

[8] Larachi F., Cassanello M., Chaouki J. and Guy C., *AIChE Journal* 42-9 (1996) 2439.

[9] Reh and Li, Circulating Fluidized Bed Technology III, eds: Basu P., Horio M. and Hasatani M, Pergamon, Oxford (1991) 163.

[10] Kunii D. and Levenspiel O., *Fluidization Engineering*, Second Edition, 1991.

[11] Rowe P.N., *Chem. Eng. Sci.*, 31 (1976) 285.

[12] Davidson J.F. and Harrison D., *Fluidised Particles*, Cambridge Univ. Press (1963).

[13] Cheremisinoff N.P. and Cheremisinoff P.N., *Hydrodynamics of Gas-Solids Fluidization*, Gulf Publishing Co. (1984).

[14] Morris J.F. and Brady J.F., *Int. J. Multiphase Flow*, 24-1 (1998) 105 .

Table 3.1 Fluidized System and Simulation parameters

Powder properties	
d	Particle diameter
a	Particle radius (characteristic length)
ρ_P	Soiid density
v	Single-particle settling velocity
Fluid properties	
ρ_f	Fluid density
μ_f	Fluid viscosity
Bed properties	
L_X	Length
L_Y	Width
L_Z	Thickness
Dimensionless numbers	
Re	Reynolds number
St	Stokes number
Simulation parameters	
dt	Time step
Nr	Number of recordings

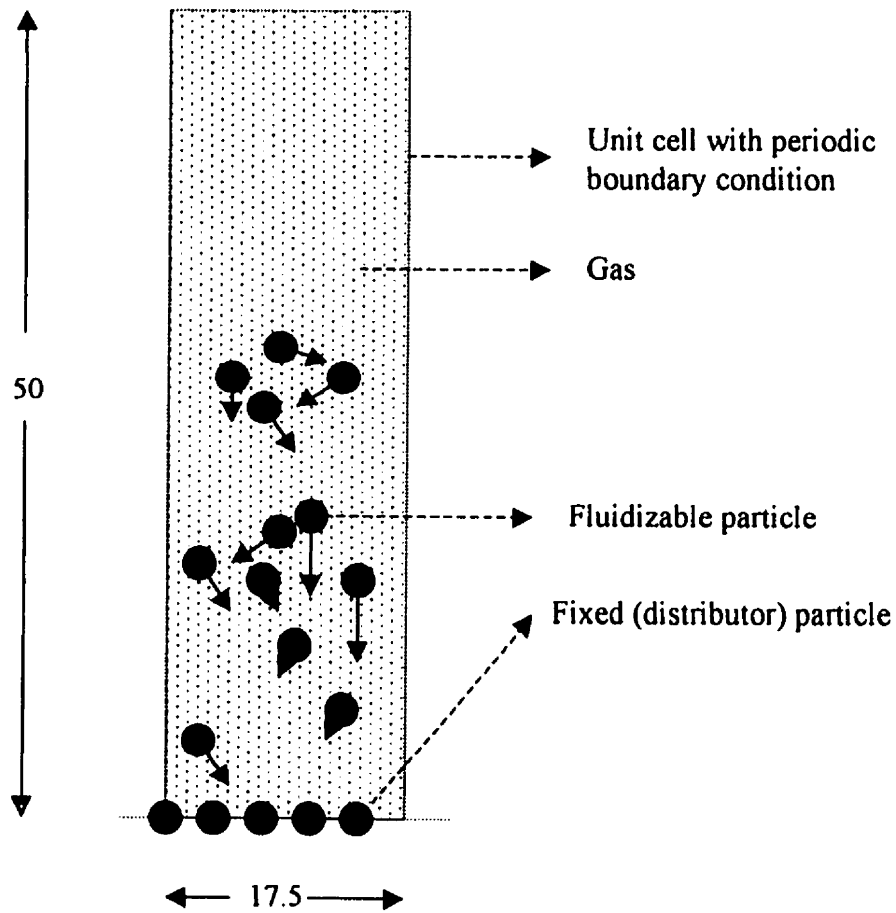

Figure 3.1 Gas fluidized fine powder bed – Unit cell with periodic boundary condition

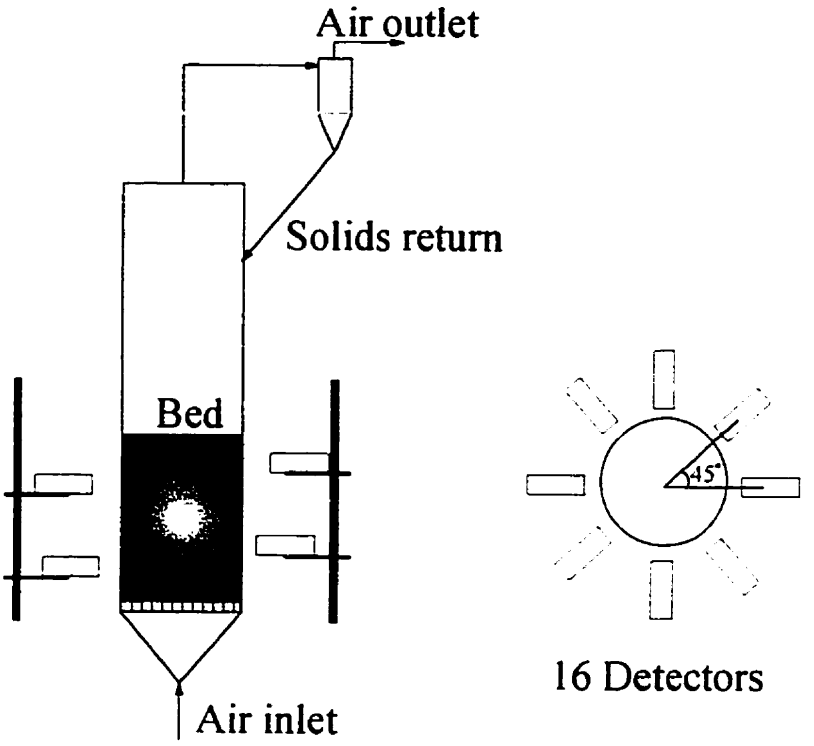

Figure 3.2 Radioactive particle tracking - Experimental set-up and typical configuration of the detectors

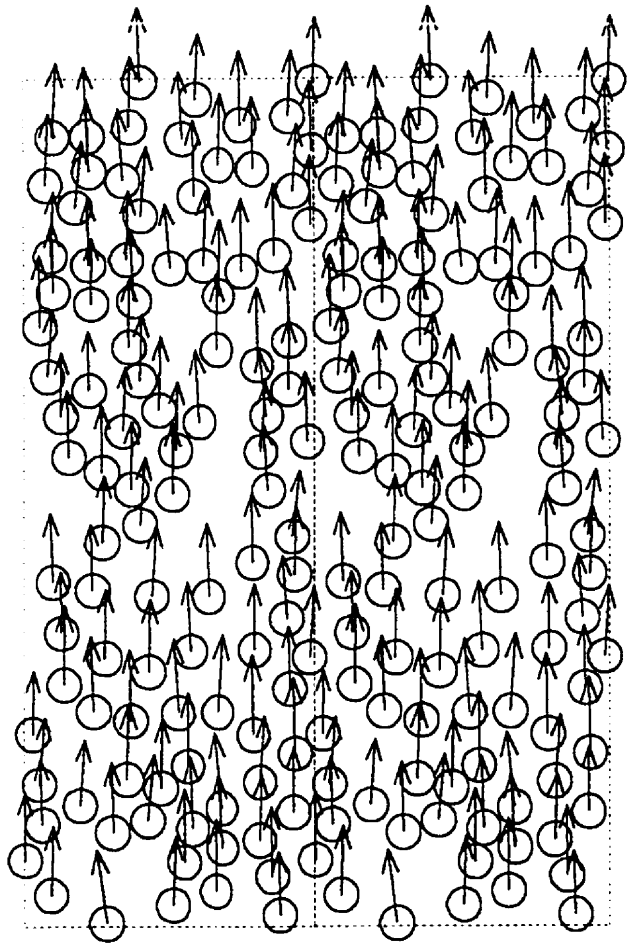

Figure 3.3 Stokesian Dynamics simulation of high-velocity fluidization

($N = Nm = 100$, $u^{\infty} = 0.44$ m/s)

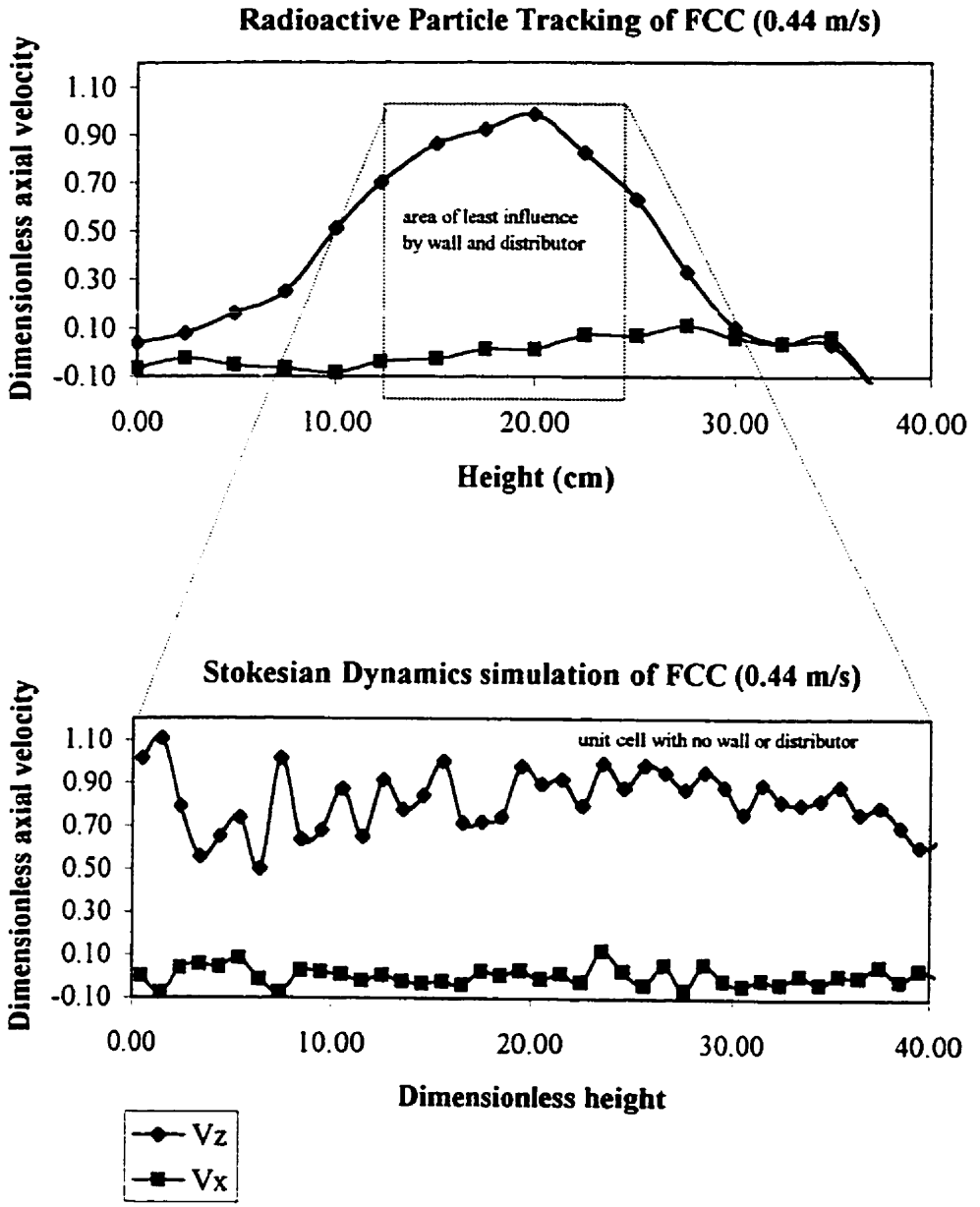

Figure 3.4 Comparison of particle velocities - Stokesian Dynamics vs Radioactive particle tracking (N = Nm = 100, $u^{\infty} = 0.44$ m/s)

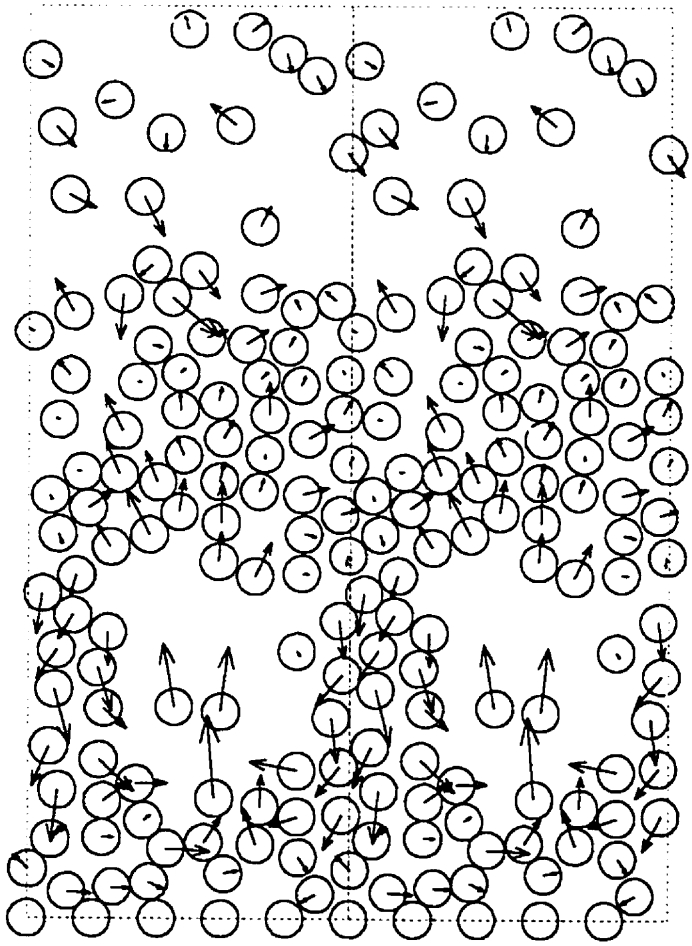

Figure 3.5 Stokesian Dynamics simulation of bubbling beds

(Nm = 100, Nf = 5)

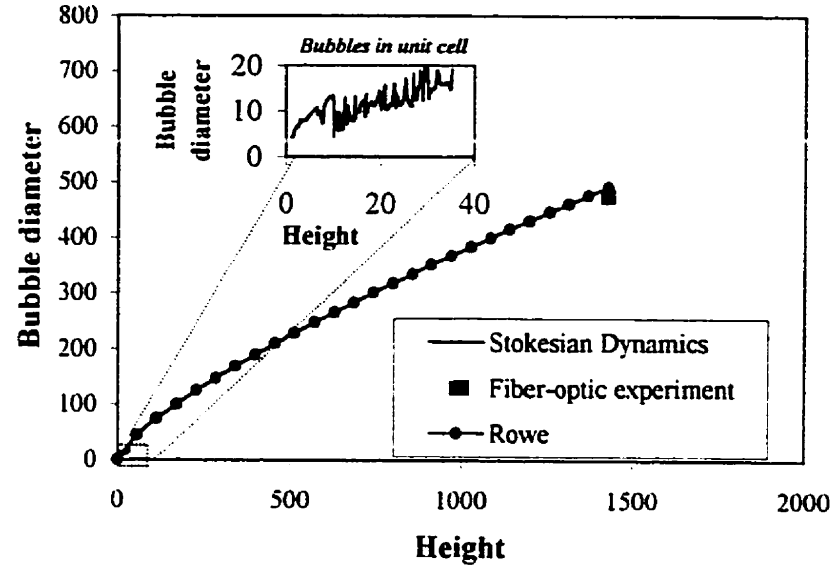

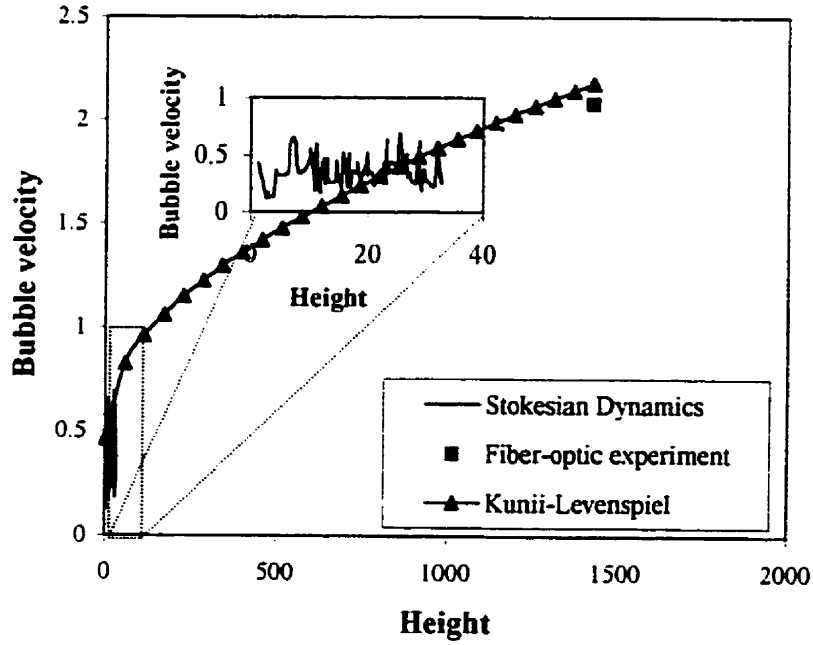

Figure 3.6 Comparison of bubble characteristics - Stokesian Dynamics vs Fiber-optic experiments (Nm = 100, Nf = 5, u^{∞} = 0.09 m/s)

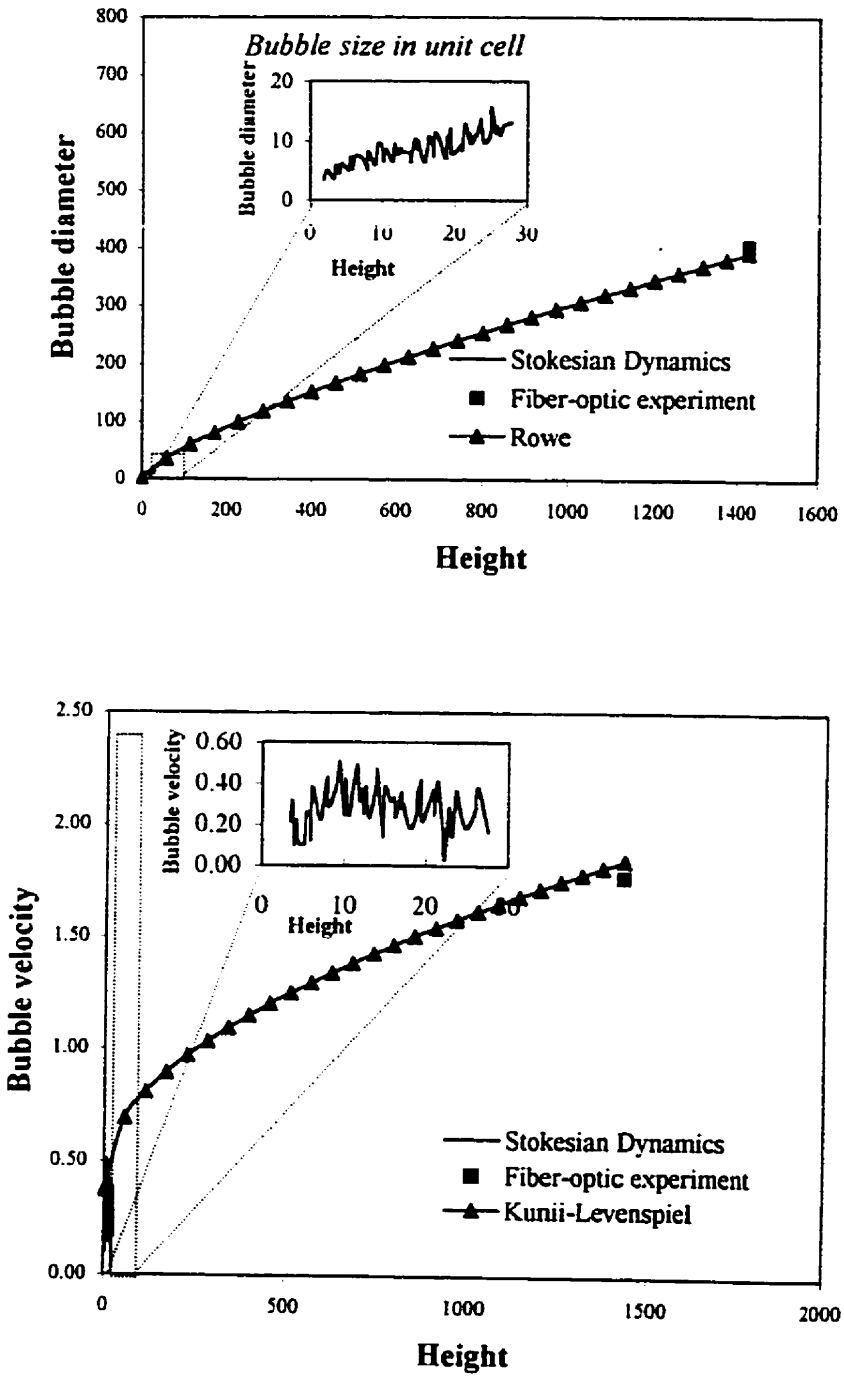

Figure 3.7 Comparison of bubble characteristics - Stokesian Dynamics vs Fiber-optic experiments (Nm = 100, Nf = 5, $u^{\infty} = 0.06$ m/s)

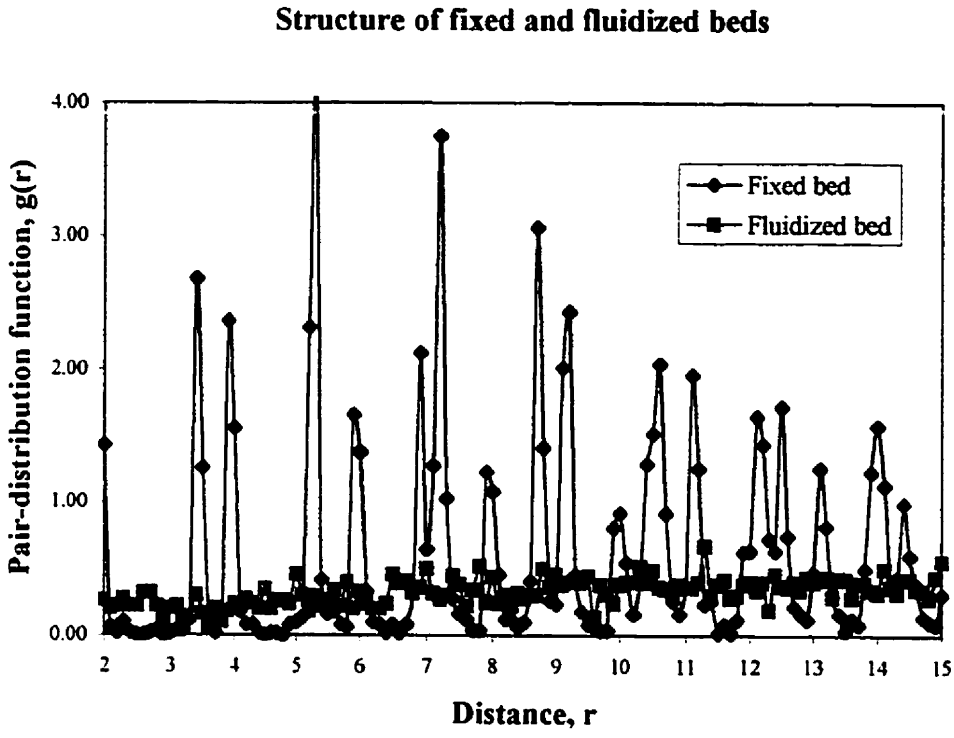

Figure 3.8 Structures of fluidized beds

CHAPTER 4: DYNAMIC SIMULATIONS OF FINE POWDER FLUIDIZATION

Reference:

R. Deiva Venkatesh, M. Grmela and J. Chaouki, "DYNAMIC SIMULATIONS OF FINE POWDER FLUIDIZATION", *Powder Technology* (submitted for publication).

Keywords:

Fine powders; Fluidized beds; Stokesian Dynamics; Agglomeration

DYNAMIC SIMULATIONS OF FINE POWDER FLUIDIZATION

R. Deiva Venkatesh[1,2], M. Grmela[2], J. Chaouki[1,2] *
[1]*BIOPRO Centre,* [2]*Chemical Engineering Department, Ecole Polytechnique de Montreal, P.O. Box 6079, Montreal, Qué. H3C 3A7, Canada*

Abstract

Gas fluidization of fine powders pose various challenges due to the complexity of the microscopic interparticle processes. This work describes the simulation of the behaviour of cohesive fine powders under gas fluidized conditions using the Stokesian Dynamics method for the hydrodynamic interactions and a microscopic model for the formation and destruction of agglomerates. Two-dimensional dynamic simulations are carried out using periodic boundary conditions on weakly and strongly cohesive powders. The agglomeration-deagglomeration model consider agglomeration and deagglomeration processes during particle collisions. The two model parameters are the minimum collisional energy for cohesion and the cohesivity of the powder.

Simulations of weakly cohesive powders indicate the formation of small, uniform size aggregates which are held together by weak bonds. Fluidization of strongly cohesive powders causes the complete agglomeration of the fine particles to form of strong, large size agglomerates which caused defluidization of the bed leading to channelling. Additional simulation results indicate that higher values of the minimum collisional

energy and lower cohesivity of the powder aids in improving the fluidizability of cohesive powders.

Keywords: Fine powders. fluidized beds. stokesian dynamics. agglomeration

* Corresponding author

1. Introduction

Powders are ubiquitous in nature with certain unique behaviours among solid forms. Fine powders are a special category of powders because of their special characteristics due to the small size. Fine powders best represented by Group C powders of Geldart's classification [1] are widely used in process industries in catalytic reactions, simple transportation and other powder handling operations. Some of these processes involve gas fluidization [2, 3]. Gas fluidization of fine powders is difficult to achieve because of the presence of interparticle forces such as van der Waals, capillary and electrostatic forces. Besides these forces, particle deformation and interlocking affect the flow of these powders. Several experimental studies have reported channeling and particle agglomeration, phenomena which are unique to fine powders [4, 5]. To counteract such forces, certain experimental techniques [5, 6, 7, 8, 9] have been developed in an effort to improve the gas fluidizability of fine powders.

Given the difficulty in conducting direct experimental studies of interparticle forces due to their microscopic nature we turn to direct simulations to gain an understanding of the behaviour of Group C powders. This work attempts to simulate the behaviour of fine powder systems under gas fluidized conditions following our earlier work in simulating the behaviour of vibrated fine powders in vacuum [10].

First, we briefly discuss a microscopic model that can be used to simulate the interactions of fine particles with no cohesive forces. We then obtain the trajectories of fluidized particles using computers. Finally, we simulate the cohesive fluidization of fine powders with our proposed model for the formation and destruction of agglomerates. By extracting the macroscopic properties characterizing fluidized beds from particle trajectories, we bridge the microscopic properties of grains with the macroscopic properties of fluidized beds.

To simulate non-cohesive fluidization, we employ the Stokesian dynamics method. The only empirical parameters that have to be introduced are those needed to characterize the Stokesian particle-fluid interactions [11, 12]. Recent simulations using the Stokesian Dynamics method have reproduced realistic particle motion in gas fluidized granular systems [12, 13].

In these simulations, the Stokesian Dynamics method is used to simulate the air fluidization of a two-dimensional bed composed of 128 spherical glass particles with 10 particles forming the fixed bottom of the bed with an uniform air velocity at a value 30% of the single particle terminal velocity. The bed whose thickness was the same as the size of the particles had width as 35 and height as 50 (dimensionless units).

In our earlier paper [10], we introduced a model for the agglomeration and deagglomeration processes in Group C powders. The model treats agglomeration and

deagglomeration as the formation and destruction of interparticle bonds during particle collisions which occur in a vibrated bed of fine powders.

In this paper, we continue our investigation. We follow the studies of Ichiki and Hayakawa [12, 13] and extend their Stokesian dynamics simulation method to cohesive fine powders. The principal new feature that we are introducing into the simulation of fluidized beds in this paper is the agglomeration-deagglomeration interactions among the particles.

2. Stokesian dynamics method with periodic boundary conditions

In this section, we briefly recall the fluidized bed model of Ichiki and Hayakawa [13] (a model to simulate the cohesionless fluidization of rigid particles). For more details concerning this model refer to the paper of Brady and Bossis [11] describing Stokesian Dynamics and the paper of Ichiki and Hayakawa [13] describing the application of Stokesian Dynamics to simulation of fluidization. Ichiki and Hayakawa assume that the bed is composed of monodisperse spheres with no rotational motion.

The motion of N fluidized particles is given by Newton's equation [13]:

$$St\frac{d\mathbf{u}}{dt} = \exp\left(\frac{t}{St}\right)\mathbf{V} \tag{1}$$

Here, t denotes the time, St is the Stokes number, **x** is the 2D position vector, **u**=**U**.exp(t/St)

$$\mathbf{U} = \begin{bmatrix} \mathbf{U}_1 \\ \mathbf{U}_2 \\ \cdot \\ \cdot \\ \cdot \\ \mathbf{U}_N \end{bmatrix}$$

where **U** is the 2D velocity vector for the N-particle system.

V, representing the terminal velocity of the particles is given by the following equation:

$$\mathbf{V} - \mathbf{u}^{\infty} = -\underline{\mathbf{R}}^{-1} \cdot \mathbf{E}_Z \tag{2}$$

$\mathbf{u}^{\infty}$ is the superficial fluid velocity vector, $\mathbf{E}_Z$ is the unit vector in the vertical direction and $\underline{\mathbf{R}}$ is the resistance matrix which is estimated from the many-body hydrodynamic interactions and the short-range lubrication forces in the Stokesian Dynamics method with periodic boundary conditions. The position and velocity vectors are dimensionless with the particle radius 'a' as the characteristic length and the single particle terminal velocity v, as the characteristic velocity [13]. The resistance matrix $\underline{\mathbf{R}}$ which is constructed from the particle positions is symmetric, positive-definite and its estimation using periodic boundary conditions is adequately explained by Brady and Bossis [11] and Ichiki and Hayakawa [12].

The instantaneous positions and velocities of the N particles are found out by integrating Eq. (1). For this purpose, we use the fourth-order Runge-Kutta method with a time step of 0.1. The resistance matrix $\underline{\mathbf{R}}$ and the terminal velocity $\mathbf{V}$ are estimated for each time step from the position vector $\mathbf{x}$ at that time. The particles are allowed to move only in the vertical plane although the hydrodynamic interactions are taken into account in all three dimensions.

The direct interparticle forces in cohesionless fluidization are treated as elastic collisions where the momenta of colliding particles are exchanged at the end of the time step.

3. Simulations without the agglomeration-deagglomeration process

We start the simulation with a fixed powder bed of 20μm rigid particles which was created by a sedimentation run with $\mathbf{V} = \mathbf{0}$. For this initial run, we randomly generate the positions of 128 particles within the unit cell with dimensions 35x50x2. The distributor of the fluidized bed is composed of 10 particles with a constant spacing of 3.5 (see Figure 4.1 for details). Using the Runge-Kutta technique we calculate positions and velocities of all 128 particles for each time step (dt = 0.1) with St = 0 until all particles have settled on top of the distributor. We thus have created the fixed bed initial condition for the fluidization run.

During fluidization, we introduce air with an uniform velocity of 0.3 and track once again the positions and velocities of all fluidizable particles for each time step. We record every tenth time step upto a maximum of 1000 recorded steps. Here we use St = 10 for the rigid particles. All simulations were run on an IBM SP2 with a performance of 130 MFlops. In Section 7.1 we discuss the results of non-cohesive fluidization.

In the next stage, we introduce into the above simulation scheme the influence of direct interparticle forces. The agglomeration-deagglomeration model has been developed for this purpose in Deiva Venkatesh *et al* [10]. We recall it briefly in Section 4.

4. Simulation with agglomeration-deagglomeration

In our earlier work [10], we have proposed a micromechanical model for the agglomeration-deagglomeration processes commonly observed in the fluidization of Group C powders which treats induced powder cohesion resulting from particle collisions under certain operating conditions. According to the proposed model, termed 'powder chemistry model', the agglomeration and deagglomeration observed in powder beds are reversible processes similar to reversible chemical reactions. The powder chemistry model assumes that both agglomeration and deagglomeration are binary collisional in nature and can occur only when the collisional energy of the colliding bodies cross an energy barrier specific to the powder. This minimum collisional energy Ec_{MIN} along with the *'cohesivity'* ε of the powder bed are the two model parameters with which we characterize the agglomeration and deagglomeration processes in our model. The powder cohesivity is explained below.

Agglomeration

Agglomeration is effected by a partial transformation of the total kinetic energy of the impacting bodies into a cohesive bond energy (BE) that causes cohesion of the colliding bodies [10]. The rest of the available kinetic energy is attributed to the resultant aggregate as explained in the energy balance further in this section.

The two model parameters for agglomeration are :

(i) the minimum collisional energy (Ec_{MIN}) and

(ii) the fraction (ε) of kinetic energy to be transformed to cohesive bond energy (BE), representing the inelasticity of agglomerative collisions.

Both model parameters characterize the interfacial properties. The parameter ε is close to zero for large, dense, spherical grains (e.g. Group A powders [1]) and close to unity for flat, light, very fine particles (eg. Group C powders [1]). Low net values of ε may be achieved by various methods such as addition of a dissimilar coarse powder (having lower ε value) to the fine powder or passing a viscous gas through the powder bed [4, 7]. The second parameter Ec_{MIN} supposedly represents particle rearrangement which is necessary for cohesion as well as deformation of colliding grains caused by the external/applied force (in this case, the force of vibration). Low values of Ec_{MIN} represent highly deformable structures leading to larger contact areas which enhance cohesion. In the physical sense, Ec_{MIN} can be referred to as the cohesion energy barrier and ε as the *cohesivity* of the fine powder. Powders with low values of Ec_{MIN} are expected to have high Hausner ratios, HR (HR=tapped bulk density/loose bulk density of the powder) while those with large ε would demonstrate cohesive forces much larger than the gravity force and would require considerable external force to improve gas fluidizability of the powder.

In Figure 4.4, we show the relationship between the model parameters and each of the categories of Geldart's classification of powders. Negligible values of ε are attributed to Group A, B and D types with Group A powders having low values of Ec_{MIN} while Group B and D have very large Ec_{MIN} values. Group AC powders [4] which are slightly cohesive have intermediate values of ε and Ec_{MIN} whereas Group C powders highly cohesive in nature may possess very high Ec_{MIN} and ε closer to unity.

Deagglomeration

Dissociation of particles in an aggregate occurs due to cleavage of all weak cohesive bonds [10]. These 'weak bonds' are those bonds whose cumulative sum of bond energies (Σ BE_{WEAK}) is lesser than or equal to the collisional energy (E_{COLL}) of the impacting bodies.

The collisional energy and the energy balances for agglomeration and deagglomeration are described in our initial paper [10]

5. Formation and destruction of aggregates as a reversible chemical reaction

Microscopic simulation of chemically reacting systems have been carried out originally using the Boltzmann and later using the molecular dynamic schemes [14]. We follow these schemes to powder systems by considering the phenomena of agglomeration and deagglomeration as three sets of reversible reactions. The mechanisms are given below :

Particle-particle interactions

$$2A_1 \underset{k_{-1}}{\overset{k_1}{\rightleftharpoons}} A_2 \qquad \text{(R1)}$$

Particle-aggregate interactions

$$A_1 + A_M \underset{k_{-2}}{\overset{k_2}{\rightleftharpoons}} A_{M+1} \qquad \text{(R2)}$$

Aggregate-aggregate interactions

$$A_P + A_Q \underset{k_{-3}}{\overset{k_3}{\rightleftharpoons}} A_{P+Q} \qquad \text{(R3)}$$

Here A_1 represents a single elementary particle used in the simulation, A_2, A_M, A_P, A_Q, A_{M+1} and A_{P+Q} are 'representative' aggregates of various sizes, form and cohesive bond energies involved in the above three reactions.

The reaction rates for the three types of interactions are as follows:

$$\frac{dn_{A_2}}{dt} = k_1 n_{A_1}^2 - k_{-1} n_{A_2} \tag{8}$$

$$\frac{dn_{A_{M+1}}}{dt} = k_2 n_{A_1} n_{A_M} - k_{-2} n_{A_{M+1}} \tag{9}$$

$$\frac{dn_{A_{P+Q}}}{dt} = k_3 n_{A_P} n_{A_Q} - k_{-3} n_{A_{P+Q}} \tag{10}$$

The macroscopic results of the simulations of fluidized fine powders provide the number concentrations of A_2, A_M, A_P, A_Q, A_{M+1} and A_{P+Q} as well the reaction rates wherefrom the rate constants have been evaluated. The effect of the model parameters ε, Ec_{MIN} on bed characteristics have been studied.

6. Simulation and analysis techniques

The following steps indicate the basic steps of the simulation of gas fluidization of cohesive powders as described in our previous work [10]:

1. Aggregates constitute several original particles (size d=20μm) called 'elements' which are bonded to each other in a pairwise fashion.
2. To obtain the instantaneous positions and velocities of all elements, we solve Eq.(1). For cohesive fluidization, the only difference is that we reassign terminal velocities of elements within an aggregate based on momentum conservation on the aggregate. Since the number of particles in the unit cell is $O(10^2)$, we assume that aggregate sizes are of the same order and we neglect rotational motion of the aggregate.
3. For every time step, the interparticle interactions are treated at the end of the integration procedure if the conditions of agglomeration/deagglomeration are met. If the collisional energy is lesser than the weakest bond in the vicinity of contact, then agglomeration occurs. Otherwise, all 'weak' bonds of the aggregate are destroyed thereby possibly producing 'child' aggregates or particles.

Characteristics of aggregates

Two characteristics of aggregates of practical importance that have been extracted from the microscopic simulation are (i) aggregate size or effective diameters, d_{eff}, and (ii) circularity. Effective diameter d_{eff} refers to the diameter of a circle having area equal to that of the aggregate while circularity represents the ratio of the

effective diameter of the aggregate to its largest Martin diameter [15]. The evolution of the effective size of aggregates and those of the three equilibrium rate constants are also discussed.

7. Results

7.1 Simulation of a gas fluidized non-cohesive powder

As explained in Section 3, the particles are first generated randomly in the unit cell, and allowed to sediment onto the distributor particles. The initial height H_0 of the fixed bed thus formed is 13.93. We then introduce uniform air flow in the upward direction with velocity 0.3. In Figure 4.2 we see four consecutive states of the evolution of the bed during the 1000 recorded time steps. We notice the formation of bubbles at the bottom of the bed and their subsequent destruction at the surface.

Linear density profiles and velocity profiles were extracted from the particle trajectories by discarding the initial 500 recorded steps and averaging the next 500 steps. Figure 4.3 represents the axial profile of the linear density, ρ (ρ=ratio of the bulk density to the solid density) averaged over 500 steps after discarding the initial 500 steps. Observe that the entire bed is in a fluidized state and the dense portion of the bed has a porosity of 0.4 and the expanded bed height of 40. Figure 4.3 also shows the axial distribution of the x- and z- components of the particle velocity. The proximity of the z-component of the average velocity to zero along the bed height indicates that the expanded bed is uniformly fluidized. On the other hand, we observe that the x-component deviates from zero.

In the above simulation, we found the value of the porosity of the expanded bed to be 0.81. The Richardson and Zaki model [16] for this bed parameters yields a value of 0.83 for the porosity of the expanded bed. More detailed comparisons of the Stokesian Dynamics simulation results with experiments on gas fluidized powders (FCC) is dealt by Deiva Venkatesh *et al* [17].

7.2 Simulation of a gas fluidized cohesive powder

We simulate the behaviour of the gas fluidization of cohesive powders by integrating the powder chemistry model with the Stokesian Dynamics technique. Two slightly cohesive powders A,C and two highly cohesive powders B and D listed in Table 4.1 were studied. Powders A,B had $Ec_{MIN} = 0$ while C,D had $Ec_{MIN} = 0.5$. Finally, we simulated the behaviour of a Powder F which had $\varepsilon = 0.75$ and $Ec_{MIN} = 2.0$.

The initial condition for all five cohesive powders was a random configuration of 100 fluidizable particles in the same cell size described in Section 3 with additional fixed particles forming the wall of the fluidized bed. The superficial gas velocity was again 0.3. The system size was limited by the available computing power providing simulation data within reasonable amount of time for all cases that were investigated. The agglomeration and deagglomeration collisions were allowed to occur at the end of each time step and the dimensionless bond energies (characteristic energy is the kinetic energy of a single particle at its terminal velocity) recorded along with the particle positions and velocities as explained in Section 6.

Figure 4.5 shows the evolution of bed characteristics of Powder A. We observe weak bonds that are formed within the first 100 time steps. The effective diameter of this weakly cohesive powder sets at 3.0 and the resultant homogeneous bed is finely fluidized. As in our previous work, we categorize aggregates of particles as a result of cohesion whose effective diameter is less than 3.0 as 'Clusters'. Aggregate sizes beyond this limit are termed 'Agglomerates'. The mass fraction of clusters in the case of powder A was close to 10% of the entire bed while around 30% of the bed mass had formed the large sized agglomerates. The remaining major portion of the bed remained as individual particles which is an experimentally observable characteristic of weakly cohesive powders [10].

Simulation of the strongly cohesive Powder B indicates rapid agglomeration of the bed to form multi-sized agglomerates. Unlike Powder A, Figure 4.6 shows a gradual build-up in the bond energy of the system with the strong bonds one order of magnitude higher than those of Powder A. The particles initially form clusters which in turn form the larger agglomerates which reach a maximum effective diameter of about 6.0. Following the evolution of the mass fractions of the clusters and agglomerates, we note that the initially formed clusters yield to the complete agglomeration of the bed with 90% of the bed mass forming agglomerates of size larger than 3.0 and the rest of the bed remaining as clusters. This is typical of strongly cohesive powders. Note that the sizes of the agglomerates that are formed is proportional to the number of particles in the system. In Figure 4.7 we see the states of the bed in four time instants where we observe rapid

agglomeration when the large agglomerates (shaded particles) settle at the bottom causing defluidization of the bed. The minimum fluidization velocities of the particles, clusters and the agglomerates that are formed were estimated according to Kunii and Levenspiel [16] and are found to be 0.0019 m/s, 0.0044 m/s and 0.0238 m/s respectively. The actual fluid velocity corresponding to the dimensionless value of 0.3 is 0.0090 m/s which is well above the u_{mf} of the particles and clusters, but below that of the agglomerates. This is an interesting phenomenon which has been observed in experiments of strongly cohesive powders such as Ni/Al_2O_3 cryogels [9]. Subsequently, we observe in the animations of Powder B that the gas channels through the agglomerated bed although the channels are unstable.

We also followed the average kinetic energy of the particles in the bed for all the four powders. We note that the weakly cohesive powders A and C attain a finely fluidized state whereas the strongly cohesive Powders B and D are defluidized. Powder D also exhibits unstable fluidization with fluctuating particle velocities.

To study the effect of the minimum collisional energy Ec_{MIN}, we performed simulations of Powder F which differed from Powder B by $Ec_{MIN} = 2.0$ representing particles which are cohesive but require a certain minimum energy which may be utilized to facilitate cohesion, for example, to enable surface deformation which increases surface contacts. Figure 4.8 demonstrates that the magnitudes of the bond energies are reflective of the cohesive energy barrier of the powder though the size of the aggregates is much reduced

compared to Powder B in Figure 4.6. In fact a minimal portion of the bed (<10%) had formed aggregates initially which then are completely destroyed to regain the cohesionless fluidized state. This insinuates that the actual surface characteristics, orientation and geometry of the interacting particles may influence the behaviour of a cohesive powder regardless of the cohesive nature of the powder material.

From the phenomenological perspective of agglomeration and deagglomeration as reversible chemical reactions, we calculate the equilibrium constants for the three particle-interactions during 'reactive' collisions in Powders A and B. In weakly cohesive powders as shown in Figure 4.9 we find that simple particle-particle interactions are dominant. This is similar to the observations made in vibrated beds [10]. In the case of the strongly cohesive Powder B, initially particle-particle interactions dominate followed by rapid interagglomerate interactions until the entire bed is agglomerated (see Figure 4.9). Note that particle-agglomerated interactions do not play a major role in either of these powders. Clearly the figure explains that the interparticle and particle-agglomerate interactions gain importance with increasing cohesivity of the powder. On the other hand, comparing the two powders B and F which differ by $Ec_{MIN} = 2.0$ in Figure 4.10, we find that particle-particle interactions is the only type of interaction that is favoured by a higher cohesive energy barrier. It seems that a better quality of fluidization may be achieved by increasing the Ec_{MIN} value.

Recent theories by Wang *et al* [18] based on experimental observations of cohesive fine powder fluidization support our powder chemistry model proposed in our previous work [10]. They have proposed a relative cohesiveness fraction for cohesive powders which represents the degree of cohesiveness similar to ε which is an important factor in determining the size distribution of the agglomerates that are formed. They also have categorized particles as single particles, natural agglomerates similar to our clusters and fluidized agglomerates. It is evident from their conclusion that the cohesivity of a fine powder controls the size distribution of agglomerates for a given powder material.

8. Conclusions

We simulate the behaviour of cohesive fine powders in gas fluidized conditions by combining our powder chemistry model with the Stokesian Dynamics method. Initially, we simulate the cohesionless simulation of fine powders following the work of Ichiki and Hayakawa [12] using 128 fluidizable particles of 20μm size with 10 fixed particles forming the distributor at the bottom of the bed. In this case, we considered particle collisions to be elastic and the gas velocity at 0.3. We observe the finely fluidized state of the bed as well as the formation and destruction of bubbles as was observed in their work. The expanded bed porosity of this bed was in agreement with the Richardson and Zaki model of homogeneous fluidization.

Following simulations include the agglomeration and deagglomeration mechanims described by the powder chemistry model. The two model parameters were the (a) the minimum energy level Ec_{MIN} for collisions to be 'reactive', i.e., agglomerative or deagglomerative and (b) the cohesivity ε of the powder. Four powders A,C which are weakly cohesive and B,D which are strongly cohesive were studied. Powders A,B had no energy barrier for cohesion whereas C,D had Ec_{MIN} = 0.5. Macroscopic bed characteristics such as bond energies of the aggregates and their effective diameter and circularities were estimated from the microscopic simulation results.

Gas fluidization of weakly cohesive powders caused the formation of aggregates of uniform size of about 3.0 called 'clusters' which formed 30% of the bed mass. Nearly 10% of the bed mass formed the large-sized 'agglomerates'. The instantaneous bond energies indicate aggregates held together by weak bonds characteristic of Group AC particles [4]. Simulations of strongly cohesive powders indicate a gradual increase in the magnitude of the bond energy of the system. The effective diameter of the agglomerates reaches a maximum of 6.0. More than 90% of the bed had formed agglomerates in this case while the rest remained as weak clusters. This behaviour has been commonly observed in strongly cohesive powders such as cryogels [10]. Another interesting relation to experiments observed in the simulation of highly cohesive powders is the de-fluidization of the bed due to agglomeration leading to unstable channeling. The estimated u_{mf} values of the particles and the clusters were well below the fluid velocity unlike the u_{mf} of the agglomerates which was higher.

Considering the formation and destruction of agglomerates as reversible reactions with three types of interactions viz., particle-particle (K_1), particle-agglomerate (K_2) and agglomerate-agglomerate (K_3), we find that particle-particle interactions in the case of weakly cohesive powders and particle-particle, interagglomerate interactions in the case of strongly cohesive powders play a decisive role in determining their behaviour under the given gas flow conditions. For a strongly cohesive powder, higher values of Ec_{MIN} reduces agglomeration and favours homogeneous fluidization of the powder.

Conclusively, low values of the cohesivity and high values of Ec_{MIN} have been found to improve the gas fluidizability of cohesive fine powders.

Our integration of the Stokesian Dynamics method with the powder chemistry model helps to extract the macroscopic properties of cohesive powders from microscopic simulation results. This simulation technique paves a way for further detailed studies on the behaviour of cohesive fine powders under gas fluidized conditions. In our future work, we will investigate the improvement of the fluidizability of cohesive powders which is of engineering interest.

9. List of Symbols

A	Aggregate number (1, 2, 3 etc)
AEM	Aggregate Element Matrix (dimension = total number of particles)
a	Particle radius
BE	Cohesive bond energy
BEM	Bond Energy Matrix (dimension = total number of particles)
d	Diameter of the particles
d_{eff}	Effective diameter of aggregates (diameter of circle having area equal to that of the aggregate)
E_{COLL}	Collisional energy
Ec_{MIN}	Minimum collisional energy (cohesive energy barrier)
g	Gravitational acceleration
HR	Hausner ratio (tapped bulk density/loose bulk density)
K	Equilibrium constant
MD,ND	Aggregate label after deagglomeration
MN	Aggregate label after agglomeration
m	Mass of particle
N	Total number of simulated particles
Nm	Number of fluidizable particles
Nf	Number of fixed (distributor) particles
n	Number concentration of aggregates

r	Interparticle separation
t	Time
U	Particle velocity vector
u^{∞}, uinf	Superficial velocity of the fluid (dimensionless)
x	Position vector of particles (x_x, x_y, x_z)
x,y,z	Coordinate axes

Subscripts

A	Aggregate
x,y,z	3D vector components
M,N	Particle labels
P,Q	Aggregate or particle labels (as the case may be)
MD,ND	Aggregate labels after deagglomeration
MN	Aggregate label after agglomeration

Greek letters

ε	Fraction of kinetic energy transformed into cohesive bond energy (*cohesivity*)
ρ	Linear density (bulk density/solid density)
ν	Single particle terminal velocity (characteristic velocity)
μ	Viscosity of the fluid

Italics

A	Aggregate
n	Number concentration

Acknowledgements

Deiva Venkatesh is deeply thankful to Dr. Kengo Ichiki, Kyoto University, Kyoto, Japan for his continuous help during this work.

References

[1] D.Geldart, *Powder Technol.* 7 (1973) 285.

[2] H.M.Jaeger, S.R.Nagel, *Science* 255 (1992) 1523.

[3] E.R.A.Eccles, K.Erdesz and A.S.Mujumdar, *Fluidization VI* (1989) 219.

[4] J.Chaouki, C.Chavarie, D.Klvana and G.Pajonk, *Powder Technol.* 43 (1985) 117.

[5] R.Deiva Venkatesh, *Master's thesis*, Ecole Polytechnique de Montréal, 1995.

[6] S.Mori, A.Yamamoto, T.Haruta, *Int. Chem. Eng.*, 31 (1991) 475.

[7] C.Lauga, J.Chaouki, D.Klvana and C.Chavarie, *Powder Technol.* 65 (1991) 461.

[8] R.Chirone, L.Massimilla and S.Russo, *Chem. Engr. Sci.* 48 (1993) 41.

[9] R.Deiva Venkatesh, J.Chaouki and D.Klvana, *Powder Technol.* 89 (1996) 179.

[10] Deiva Venkatesh R., Grmela M. and Chaouki J., *Powder Technol.* (1998).

[11] Brady J.F. and Bossis G., *Annu. Rev. Fluid Mech.*, 20 (1985) 111.

[12] Ichiki K. and Hayakawa H., *Phys. Rev. E*, 52-1 (1995) 658.

[13] Ichiki K. and Hayakawa H., *Phys. Rev. E*, 57-2 (1998) 1990.

[14] M.M.Mansour and F.Baras, *Physica A* 188 (1992) 253.

[15] R.D.Cadle, *Particle Size*, Reinhold Publishing Corporation, NewYork, 1965.

[16] Kunii D. and Levenspiel O., *Fluidization Engineering*, Second Edition, 1991.

[17] Deiva Venkatesh R., Chaouki L., Grmela M. and Mortazavi R., *Powder*

Technology (a) (to be published).

[18] Wang Z., Kwauk M. and Li H., *Chem.Eng.Sci.*, 53-3 (1998) 377-395.

Table 4.1 Powders used for simulation

Powder	ε	Ec_{MIN}
A	0.25	0.0
B	0.75	0.0
C	0.25	0.5
D	0.75	0.5
F	0.75	2.0

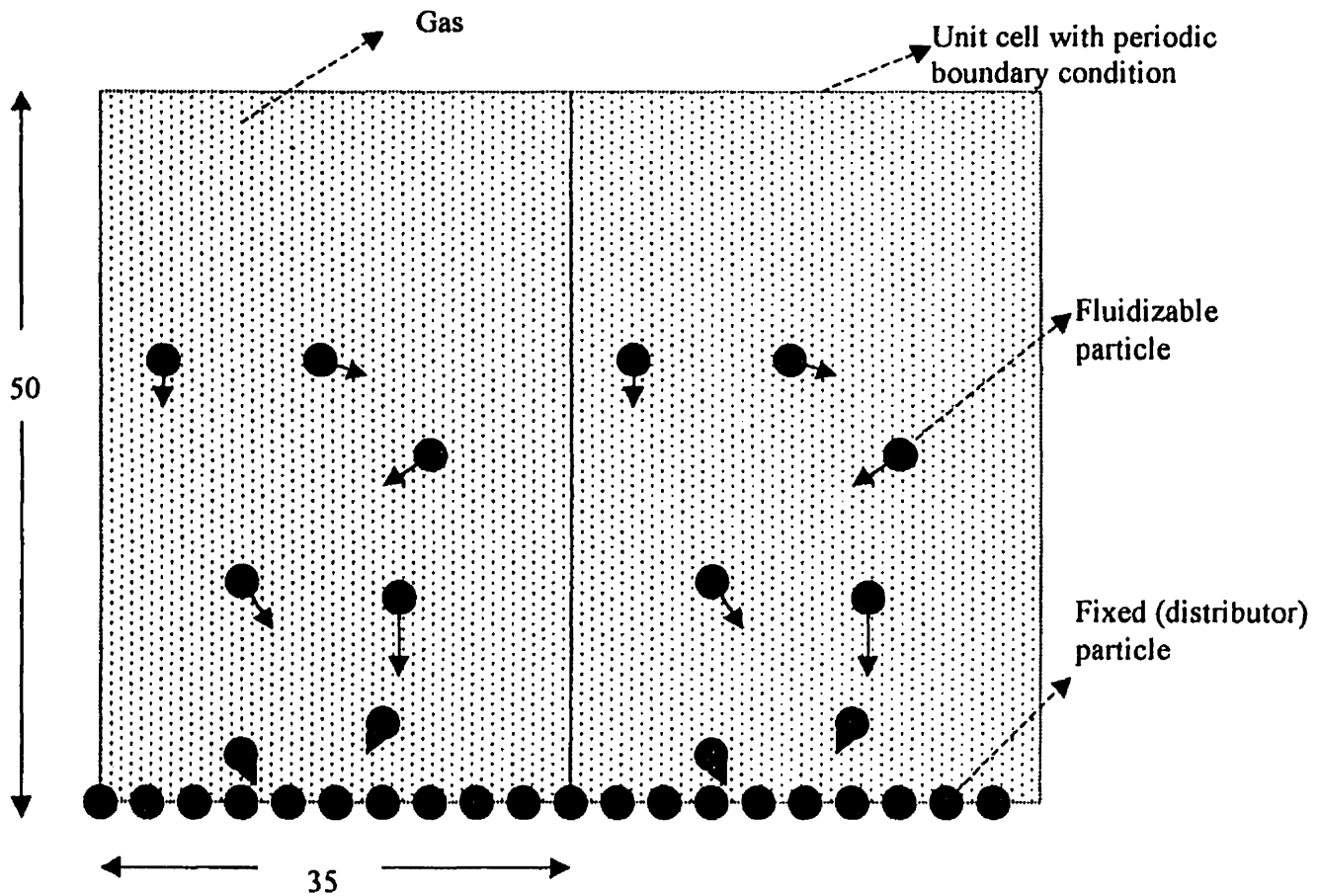

Figure 4.1 Gas fluidized fine powder bed – Unit cell with periodic boundary condition

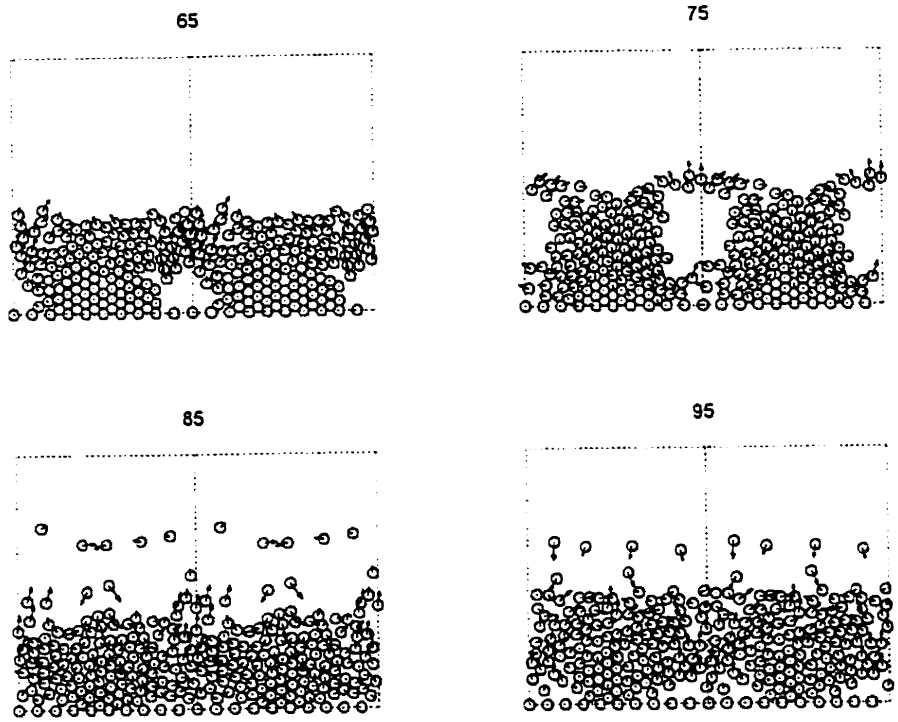

Figure 4.2 Bubbling in a gas fluidized fine particle bed

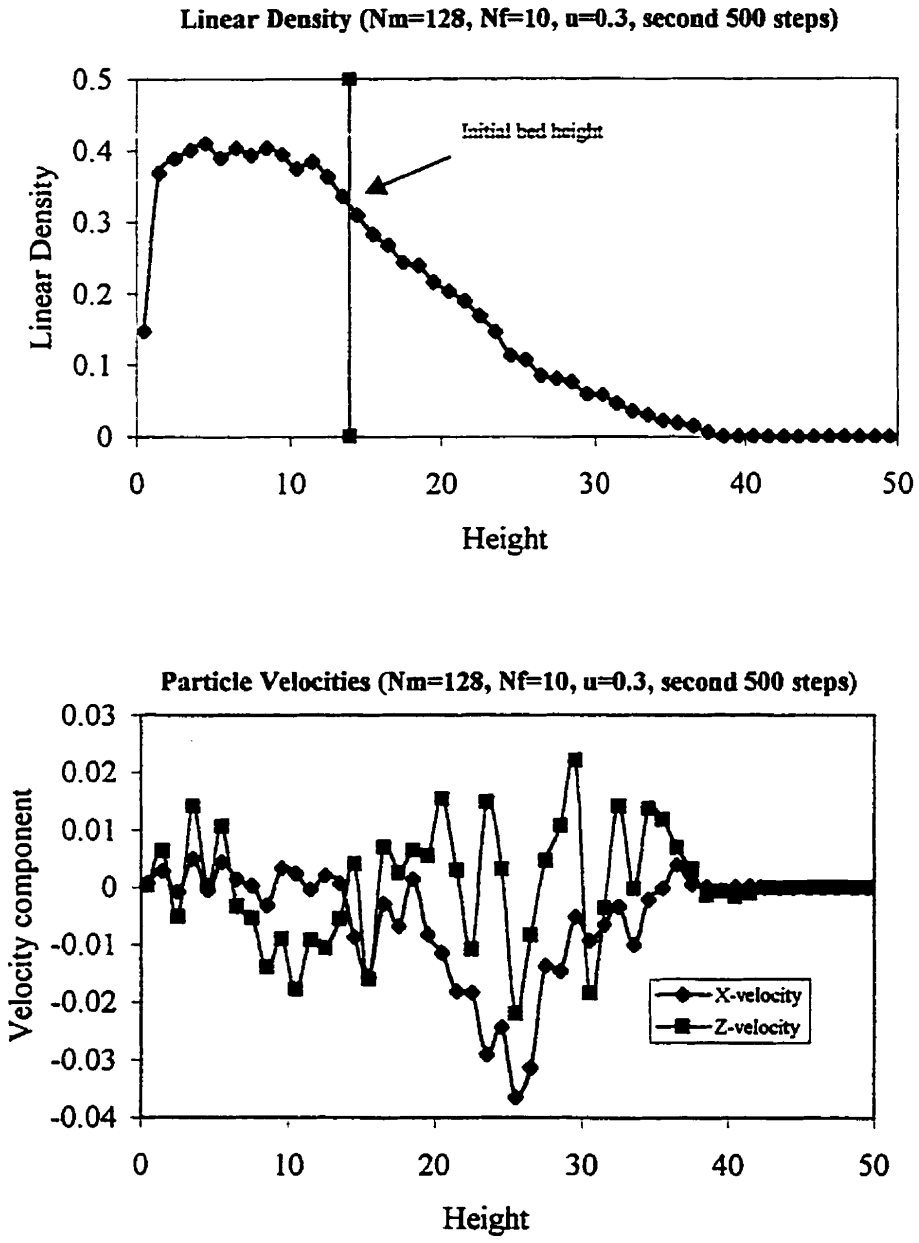

Figure 4.3 Hydrodynamics of non-cohesive fluidization

(Nm=128, Nf=10, uinf=0.3)

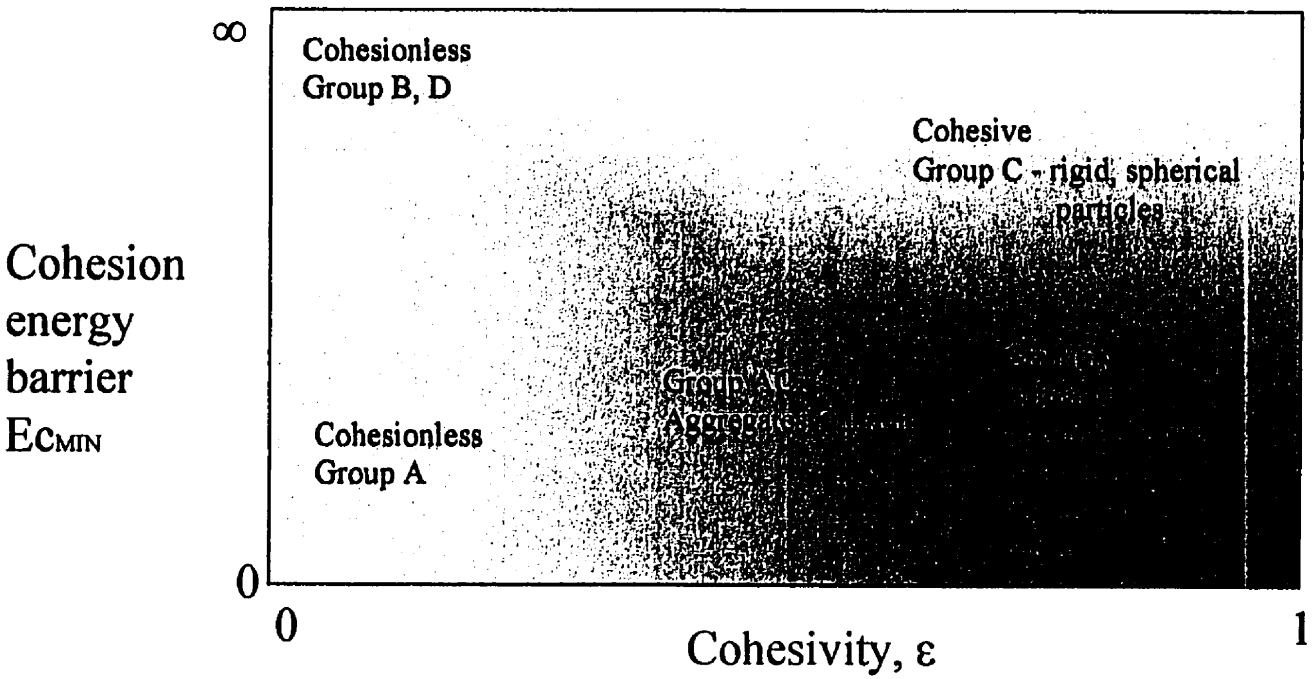

Figure 4.4 Relationship between model parameters and Geldart powders

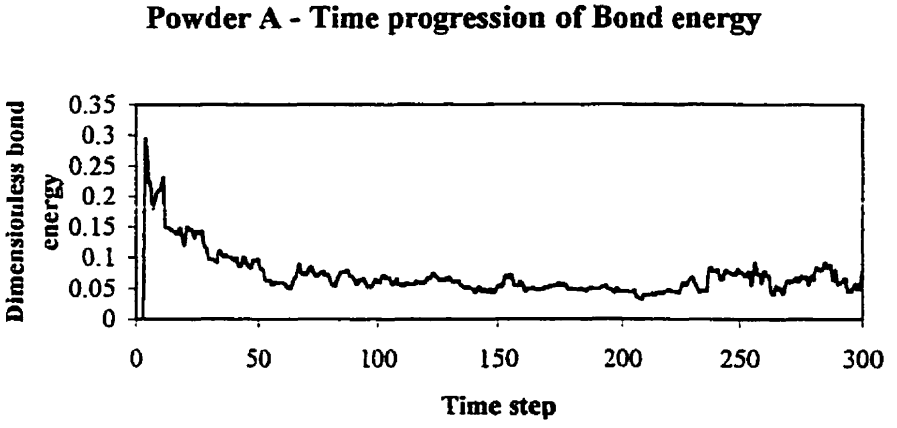

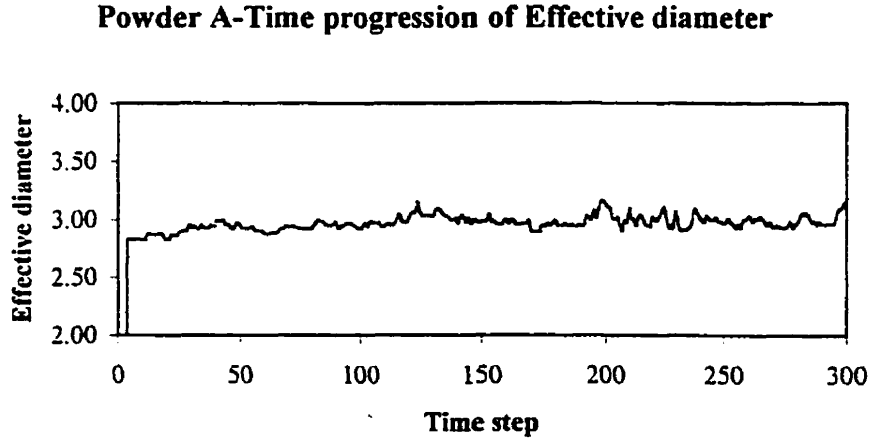

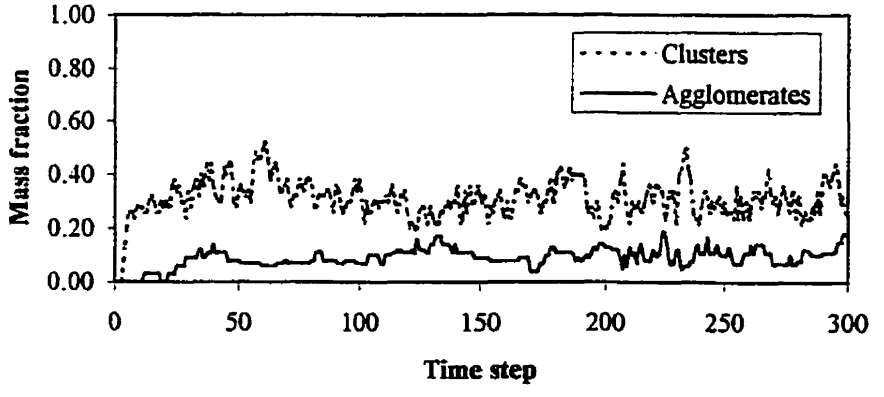

Figure 4.5 Bed characteristics of a weakly cohesive powder

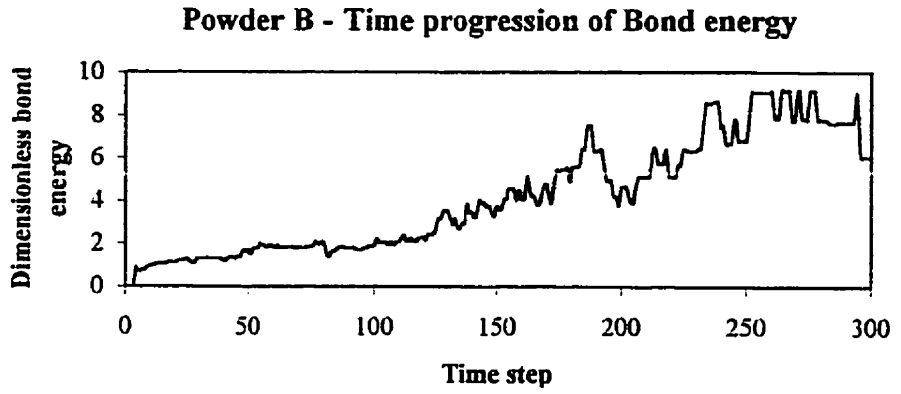

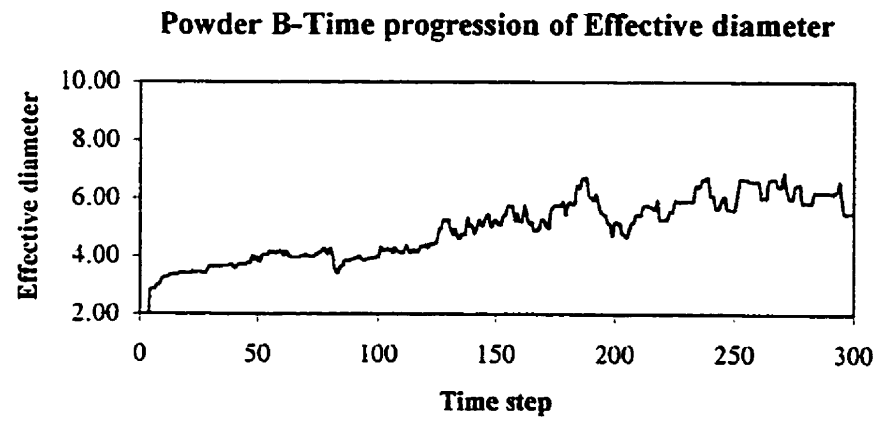

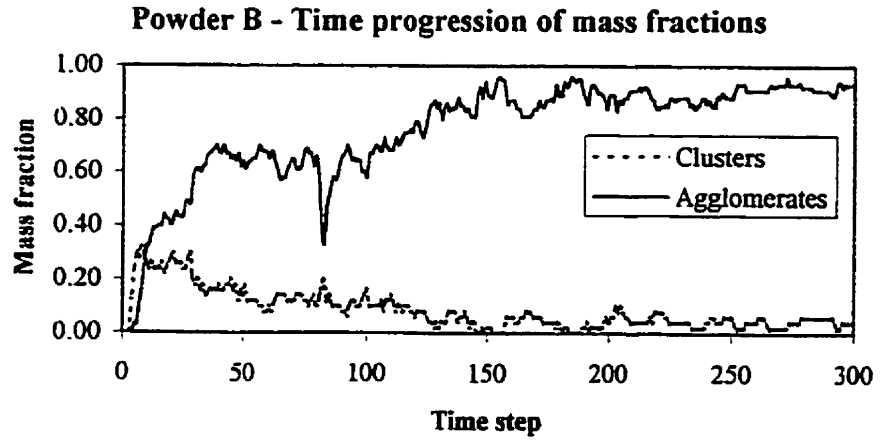

Figure 4.6 Bed characteristics of a strongly cohesive fine powder

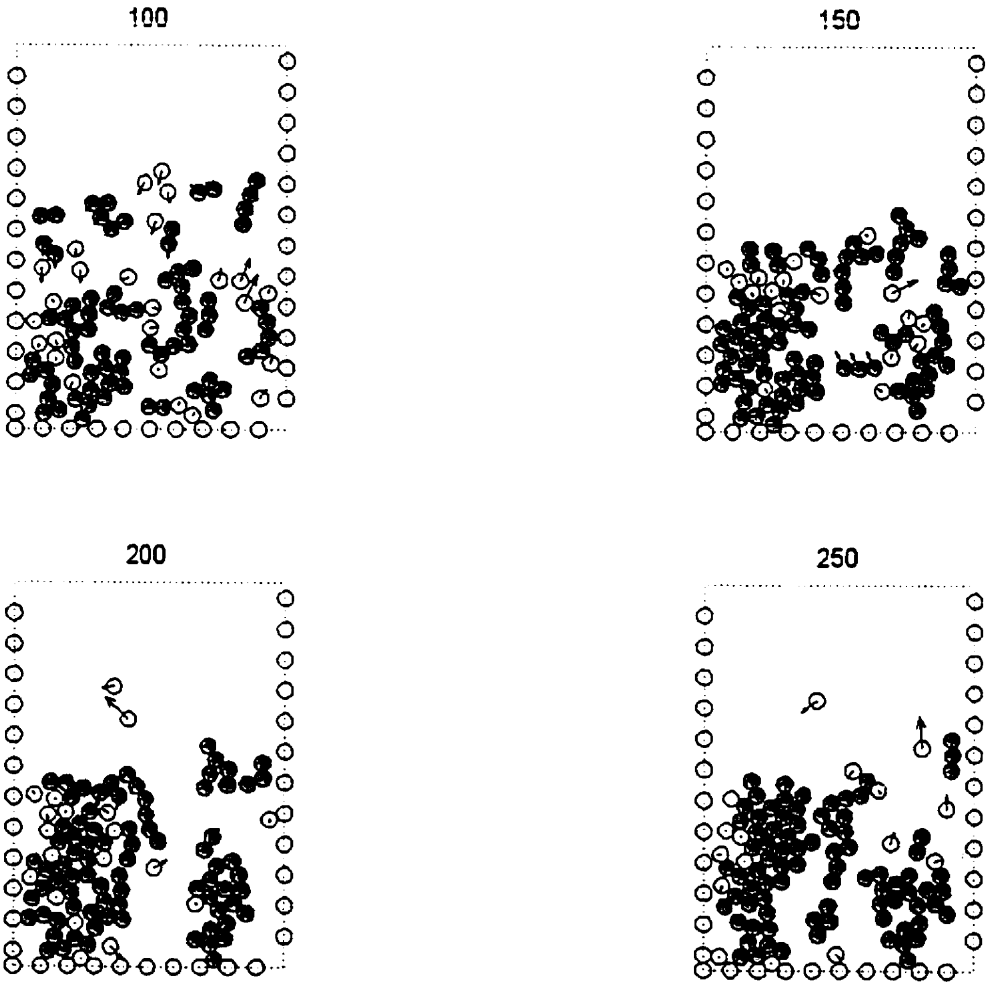

Figure 4.7 Defluidization of a strongly cohesive fine powder

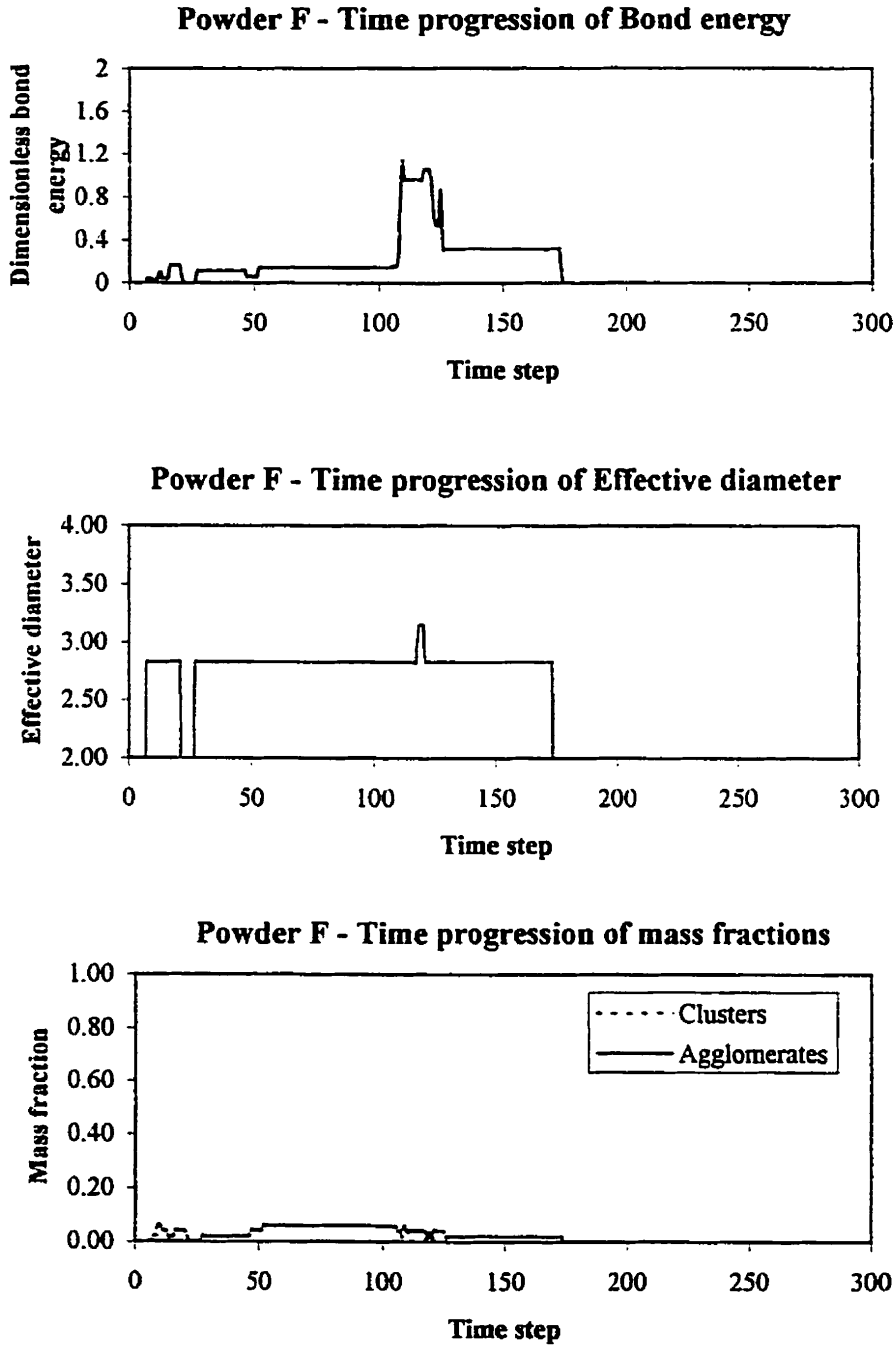

Figure 4.8 Bed characteristics of a powder with inhibited cohesion

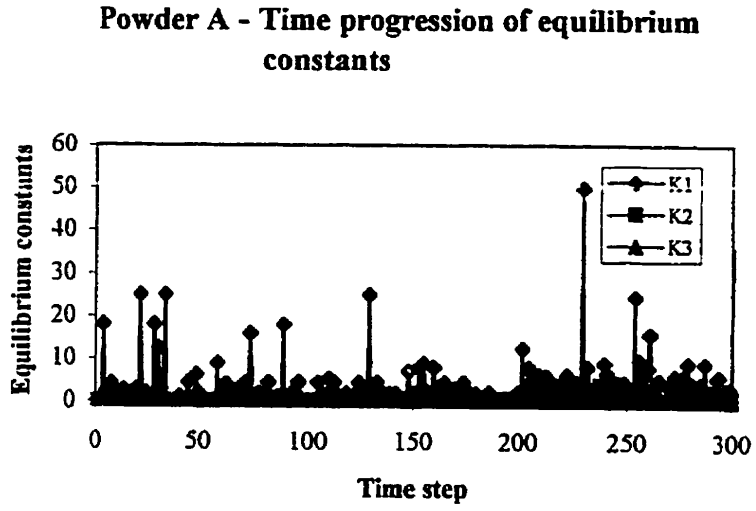

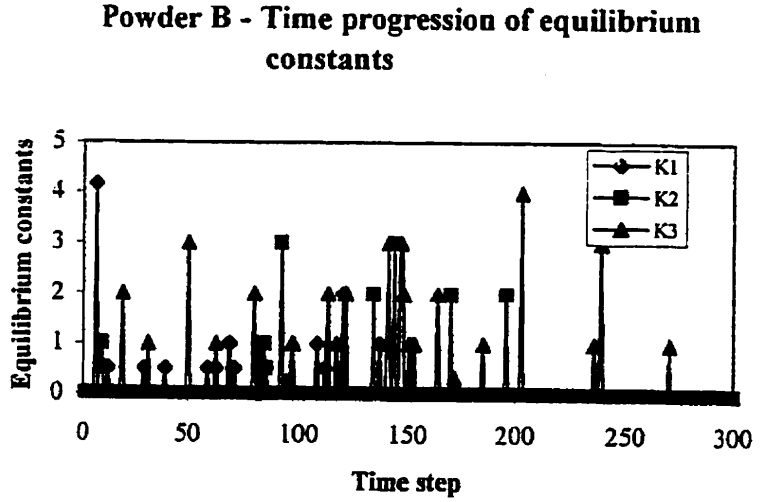

Figure 4.9 Effect of cohesivity on particle interactions

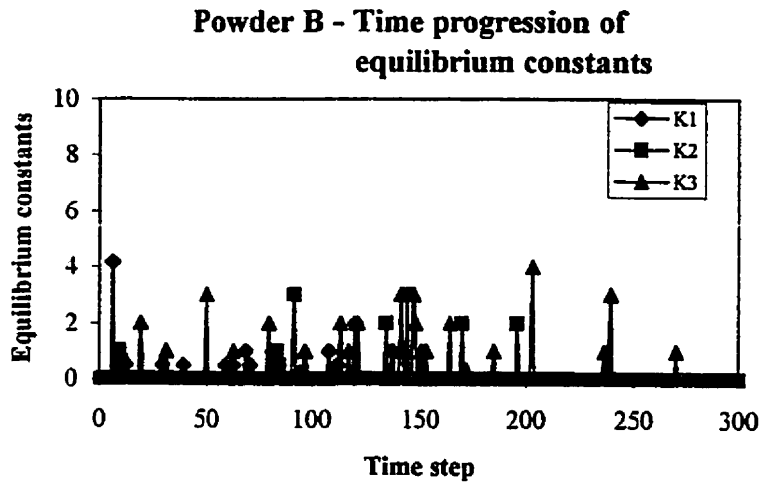

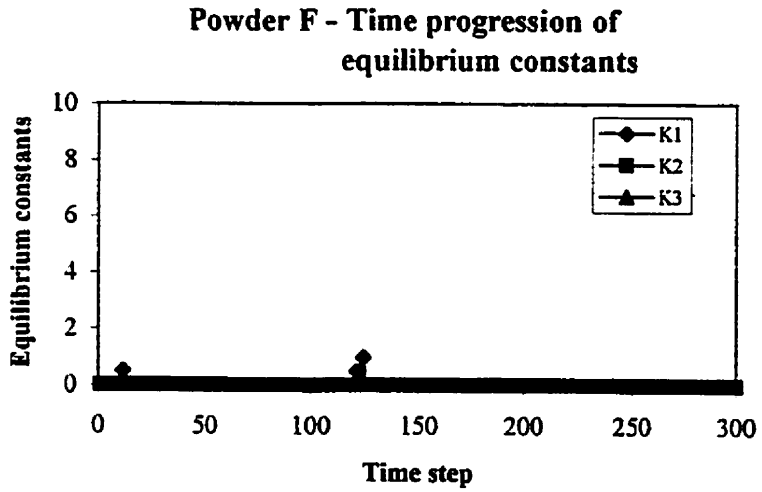

Figure 4.10 Effect of minimum collisional energy on particle interactions

CHAPTER 5: IMPROVEMENT OF THE FLUIDIZABILITY OF COHESIVE FINE POWDERS

Reference:

R. Deiva Venkatesh, J. Chaouki and M. Grmela, "IMPROVEMENT OF THE FLUIDIZABILITY OF COHESIVE FINE POWDERS", *Powder Technology* (submitted for publication).

Keywords:

Fine powder; Improvement of fluidizability; Agglomeration; Deagglomeration

IMPROVEMENT OF FLUIDIZABILITY OF FINE POWDERS

R. Deiva Venkatesh[1,2], M. Grmela[2], J. Chaouki[1,2] *
[1]*BIOPRO Centre,* [2]*Chemical Engineering Department, Ecole Polytechnique de Montreal, P.O. Box 6079, Montreal, Qué. H3C 3A7, Canada*

Abstract

Simulations of the gas fluidization of a cohesive powder are performed using Stokesian Dynamics and an agglomeration-deagglomeration model. Our objective is to investigate methods of improving the fluidizability of fine powders. Three techniques, namely (a) high gas velocity (b) vibration-assisted fluidization and (c) tapered fluidizer are suggested and investigated. While all three techniques are found to effectively improve the fluidizability of a strongly cohesive powder, we suggest a combination of high velocity fluidization assisted by external vibration of the fluidized bed to minimize entrainment of particles. Results of current and previous simulations are summarized in a cohesive powder diagram involving the parameters of the agglomeration-deagglomeration model and the operating conditions.

Keywords: Fine powders, improvement of fluidizability, agglomeration

* Corresponding author

1. Introduction

Fine powders described by Group C powders of Geldart's classification [1] of powders are unique due to their cohesive nature when subject to gas fluidization. The rapidly growing application of ultra-fine particles in industry, fluidization of fine particles has become a significant emerging field [2]. Fine powders best represented by Group C powders of Geldart's classification are widely used in process industries in catalytic reactions, simple transportation and other powder handling operations. Gas fluidization of fine powders is difficult to achieve because of the presence of interparticle forces such as Van der Waals, capillary and electrostatic forces. Besides these forces, particle deformation and interlocking may affect the flow of these powders [3]. Several experimental studies have reported channeling and particle agglomeration, phenomena which are unique to fine powders due to the effect of interparticle forces [4, 5].

To counteract the effect of such forces, certain experimental techniques [4, 6, 7, 8, 9] have been developed in an effort to improve the gas fluidizability of fine powders. Two main categories of techniques used to improve the fluidizability of fine powders are (i) addition of an external force such as vibration, magnetic field or acoustic field and (ii) alteration of the intrinsic properties of the powder such as modifying the surface characteristics and mixing of a dissimilar powder [2]. Our experimental studies also have shown that in the case of highly cohesive Ni/Al_2O_3 cryogels employment of a conical fluidizer improved the fluidizability of such powders [5].

In our earlier work [10], we have simulated the gas fluidization of fine particles which are cohesive in nature using a compound simulation technique which uses the Stokesian Dynamics method [11] to describe the hydrodynamic forces and our microscopic model to explain the agglomeration and deagglomeration mechanisms in fine powders [10]. We have been able to simulate the formation and destruction and agglomerates during gas fluidization of Group C powders. In this paper, we intend to investigate the effects of (i) an external vibratory force (ii) high gas velocity and (iii) tapered bed geometry on the fluidizability of cohesive powders.

In these simulations, Stokesian Dynamics method is used to simulate the air fluidization of a two-dimensional bed composed of 100 spherical glass particles with 10 particles forming the fixed bottom of the bed and 24 other fixed particles forming the bed wall with an uniform air velocity at a value 30% of the single particle terminal velocity. The bed whose thickness was the same as the size of the particles had width as 35 and height as 50 (dimensionless units). Here, the radius of the particles was the characteristic length and the single particle terminal velocity was the characteristic velocity.

In our earlier paper [3], we introduced a model for the agglomeration and deagglomeration processes in Group C powders. The model treats agglomeration and deagglomeration as the formation and destruction of interparticle bonds during particle collisions which occur in a vibrated bed of fine powders.

We follow the studies of Ichiki and Hayakawa [12,13] and extend their Stokesian Dynamics simulation method to cohesive fine powders. The principal new feature that we are introducing into the simulation of fluidized beds in this paper, besides the agglomeration-deagglomeration interactions among the particles, is the effect of the operating conditions, externally applied force and the bed geometry.

2. Stokesian dynamics method with periodic boundary conditions

In this section, we briefly recall the fluidized bed model of Ichiki and Hayakawa [13] (a model to simulate the cohesionless fluidization of rigid particles). For more details concerning this model we refer to the paper of Brady and Bossis [11] describing Stokesian Dynamics and the paper of Ichiki and Hayakawa [13] describing the application of Stokesian Dynamics to simulation of fluidized beds. Following Ichiki and Hayakawa, we assume that the bed is composed of monodisperse spheres with no rotational motion.

The motion of N fluidized particles is given by Newton's equation [13]:

$$St\frac{d\mathbf{u}}{dt} = \exp\left(\frac{t}{St}\right)\mathbf{V} \tag{1}$$

Here, t denotes the time, St is the Stokes number, $\mathbf{x}$ is the 2D position vector, $\mathbf{u}=\mathbf{U}.\exp(t/St)$ where $\mathbf{U}$ is the 2D velocity vector for the N-particle system.

$$\mathbf{U} = \begin{bmatrix} \mathbf{U}_1 \\ \mathbf{U}_2 \\ \cdot \\ \cdot \\ \cdot \\ \mathbf{U}_N \end{bmatrix}$$

$\mathbf{V}$, representing the terminal velocity of the particles is given by the following equation:

$$\mathbf{V} - \mathbf{u}^{\infty} = -\underline{\mathbf{R}}^{-1} \cdot \mathbf{E}_Z \tag{2}$$

$\mathbf{u}^{\infty}$ is the superficial fluid velocity vector, $\mathbf{E}_Z$ is the unit vector in the vertical direction and $\underline{\mathbf{R}}$ is the resistance matrix which is estimated from the many-body hydrodynamic interactions and the short-range lubrication forces in the Stokesian Dynamics method with periodic boundary conditions. Position and velocity vectors are dimensionless with the particle radius 'a' as the characteristic length and the single particle terminal velocity v, as the characteristic velocity. The resistance matrix $\underline{\mathbf{R}}$ which is constructed from the particle positions is symmetric, positive-definite and its estimation using periodic boundary conditions is adequately explained by Brady and Bossis [11] and Ichiki and Hayakawa [12].

The instantaneous positions and velocities of the N particles are found out by integrating Eq. (1) using the fourth-order Runge-Kutta method with a time step of 0.1. The resistance matrix $\underline{\mathbf{R}}$ and the terminal velocity $\mathbf{V}$ are estimated for each time step from the position vector $\mathbf{x}$ at that time. The particles are allowed to move only in the vertical plane although the hydrodynamic interactions are taken into account in all three dimensions.

The direct interparticle forces in cohesionless fluidization were treated as elastic collisions in our earlier work [10] with the superficial air velocity at 0.3. Here, we

combine the microscopic model of cohesive powders with the Stokesian Dynamics method to simulate agglomeration and deagglomeration processes.

3. Cohesive powder model

In our earlier work [3], we have proposed a micromechanical model for the agglomeration-deagglomeration processes commonly observed in the fluidization of Group C powders which treats induced powder cohesion resulting from particle collisions under certain operating conditions. According to the proposed model, termed 'powder chemistry model', the agglomeration and deagglomeration observed in powder beds are reversible processes similar to reversible chemical reactions. The powder chemistry model assumes that both agglomeration and deagglomeration are binary collisional in nature and can occur only when the collisional energy of the colliding bodies cross an energy barrier specific to the solid phase. This minimum collisional energy Ec_{MIN} along with the *'cohesivity'* ε of the powder bed are the two model parameters with which we characterize the agglomeration and deagglomeration processes in our model. The powder cohesivity is explained below.

Agglomeration

Agglomeration is effected by a partial transformation of the total kinetic energy of the impacting bodies into a cohesive bond energy (BE) that causes cohesion of the colliding bodies [3]. The rest of the available kinetic energy is attributed to the resultant aggregate as explained in the energy balance further in this section.

The two model parameters for agglomeration are :

(i) the minimum collisional energy (Ec_{min}) and

(ii) the fraction (ε) of kinetic energy to be transformed to cohesive bond energy (BE), representing the inelasticity of agglomerative collisions.

Both model parameters characterize the interfacial properties. The parameter ε is close to zero for large, dense, spherical grains (e.g. Group A powders [1]) and close to unity for flat, light, very fine particles (eg. Group C powders [1]). The second parameter Ec_{MIN} represents particle rearrangement which is necessary for cohesion as well as deformation of colliding grains caused by the external/applied force (in this case, the force of vibration). In the physical sense, Ec_{MIN} referred to as the minimum collisional energy and ε as the *cohesivity* of the fine powder. The physical significances of the model parameters are discussed in our original paper [3].

In Figure 5.1, we show the relationship between the model parameters and each of the categories of Geldart's classification of powders. Negligible values of ε are attributed to Group A, B and D types with Group A powders having low values of Ec_{MIN} while Group B and D have very large Ec_{MIN} values. Group AC powders [4] which are slightly cohesive have intermediate values of ε and Ec_{MIN} whereas Group C powders highly cohesive in nature possess very high Ec_{MIN} and ε close to unity.

Deagglomeration

Dissociation of particles in an aggregate occurs due to cleavage of all weak cohesive bonds [3]. These 'weak bonds' are those bonds whose cumulative sum of bond energies (Σ BE_{WEAK}) is lesser than or equal to the collisional energy (E_{COLL}) of the impacting bodies. The collisional energy and the energy balances for agglomeration and deagglomeration are discussed in detail in our earlier paper [3].

4. Simulation of a gas fluidized cohesive powder

We start the simulation by randomly generating the positions of 100 rigid particles of 20μm within the unit cell with dimensions 35x50x2. The distributor of the fluidized bed is composed of 10 particles with a constant spacing of 3.5 and the walls formed by 24 particles spaced at a gap of 4.0 (see Figure 5.2 for details). Using the Runge-Kutta technique we integrate Equation (1) to calculate the positions and velocities of all 100 particles.

During fluidization, we introduce air with an uniform velocity and track once again the positions and velocities of all fluidizable particles for each time step. We record every tenth time step upto a maximum of 300 recorded steps. Here we use St = 10 for the rigid particles. All simulations were run on an IBM SP2 with a performance of 130 MFlops.

We introduce into the above simulation scheme the influence of direct interparticle forces. The agglomeration-deagglomeration model explained in Section 3 is used for this purpose. At the end of each time step, the powder chemistry model is applied to the system and the agglomeration and deagglomeration processes are accounted for as explained in Deiva Venkatesh *et al* [10].

5. Formation and destruction of aggregates

Microscopic simulation of chemically reacting systems have been carried out originally using the Boltzmann and later using the molecular dynamic schemes [14]. We follow these schemes to powder systems by considering the phenomena of agglomeration and deagglomeration as three sets of reversible reactions. The mechanisms are given below :

Particle-particle interactions

$$2A_1 \underset{k_{-1}}{\overset{k_1}{\rightleftharpoons}} A_2 \qquad \text{(R1)}$$

Particle-aggregate interactions

$$A_1 + A_M \underset{k_{-2}}{\overset{k_2}{\rightleftharpoons}} A_{M+1} \qquad \text{(R2)}$$

Aggregate-aggregate interactions

$$A_P + A_Q \underset{k_{-3}}{\overset{k_3}{\rightleftharpoons}} A_{P+Q} \qquad \text{(R3)}$$

Here A_1 represents a single elementary particle used in the simulation, A_2, A_M, A_P, A_Q, A_{M+1} and A_{P+Q} are 'representative' aggregates of various sizes, form and cohesive bond energies involved in the above three reactions.

The reaction rates for the three types of interactions are as follows:

$$\frac{dn_{A_2}}{dt} = k_1 n_{A_1}^2 - k_{-1} n_{A_2} \tag{8}$$

$$\frac{dn_{A_{M+1}}}{dt} = k_2 n_{A_1} n_{A_M} - k_{-2} n_{A_{M+1}} \tag{9}$$

$$\frac{dn_{A_{P+Q}}}{dt} = k_3 n_{A_P} n_{A_Q} - k_{-3} n_{A_{P+Q}} \tag{10}$$

The macroscopic results of the simulations of fluidized fine powders provide the number concentrations of A_2, A_M, A_P, A_Q, A_{M+1} and A_{P+Q} as well the reaction rates wherefrom the rate constants have been evaluated. The effect of the model parameters ε, Ec_{MIN} on bed characteristics has been studied.

6. Simulation techniques

The following steps indicate the basic steps of the simulation of gas fluidization of cohesive powders:

1. Aggregates constitute several original particles (size d = 20μm) called 'elements' which are bonded to each other in a pairwise fashion.
2. To obtain the instantaneous positions and velocities of all elements, we solve Eq.(1). For cohesive fluidization, the only difference is that we reassign terminal velocities of elements within an aggregate based on momentum conservation on the aggregate. Since the number of particles in the unit cell is $O(10^2)$, we assume that aggregate sizes are of the same order and we neglect rotational motion of the aggregate.
3. For every time step, the interparticle interactions are treated at the end of the integration procedure if the conditions of agglomeration/deagglomeration [3].

Characteristics of the agglomerated bed such as the effective diameter d_{eff} which refers to the diameter of a circle having area equal to that of the aggregate and the mass fraction of agglomerates in the bed are discussed. The circularity of aggregates represents the ratio of the effective diameter of the aggregate to its largest Martin diameter [15]. The evolution of the above characteristics and those of the three equilibrium rate constants for the particle interactions are also presented.

7. Results

7.1 Simulation of a gas fluidized cohesive powder – basic case

We simulate the behaviour of the gas fluidization of fine powders by integrating the powder chemistry model with the Stokesian Dynamics technique. We investigate the methods of improving the fluidizability of cohesive fine powders using a Powder B with $\varepsilon = 0.75$ and $Ec_{MIN} = 0.0$. The basic simulation of the gas fluidization of this powder is as follows:

The initial condition of Powder B was a random configuration of 100 fluidizable particles in the same cell size indicated in Figure 5.2 with fixed particles forming the wall and bottom of the fluidized bed. The superficial gas velocity was 0.3. As in our earlier studies, the system size was limited by the available computing power providing simulation data within reasonable amount of time for all cases that were investigated. The agglomeration and deagglomeration collisions were allowed to occur at the end of each time step and the dimensionless bond energies (characteristic energy is the kinetic energy of a single particle at its terminal velocity) recorded along with the particle positions and velocities as explained in Section 6.

Figure 5.3 shows the evolution of bed characteristics of Powder B. As in our previous work, we categorize aggregates of particles as a result of cohesion whose effective diameter is less than 3.0 as 'Clusters'. Aggregate sizes beyond this limit are termed

'Agglomerates'. Simulations of the strongly cohesive Powder B indicate rapid agglomeration of the bed to form multi-sized agglomerates. Figure 5.3 shows a build-up in the bond energy of the system with the strong bonds. The particles initially form clusters which in turn form the larger agglomerates which reach a maximum effective diameter of about 6.0. Following the evolution of the mass fractions of the clusters and agglomerates, we note that the initially formed clusters yield to the complete agglomeration of the bed with 90% of the bed mass forming agglomerates of size larger than 3.0 and the rest of the bed remaining as clusters. This is typical of strongly cohesive powders as observed in experiments [9]. In Figure 5.4 we see the states of the bed at four time instants where we observe rapid agglomeration when the large agglomerates (shaded particles) settle at the bottom causing defluidization of the bed. This is an interesting phenomenon which has been observed in experiments of strongly cohesive powders such as Ni/Al_2O_3 cryogels [9]. Subsequently, we observe in the animations of Powder B that the gas channels through the agglomerated bed although the channels are unstable.

From the phenomenological perspective of agglomeration and deagglomeration as reversible chemical reactions, we calculate the equilibrium constants for the three particle-interactions during 'reactive' collisions in Powder B. In weakly cohesive powders we find that simple particle-particle interactions are dominant. In the case of the strongly cohesive Powder B, initially particle-particle interactions dominate followed

by rapid interagglomerate interactions until the entire bed is agglomerated. Note that particle-agglomerated interactions do not play a major role in either of these powders.

Recent theories by Wang *et al* [2] based on experimental observations of cohesive fine powder fluidization support our powder chemistry model proposed in our previous work [3]. They have proposed a relative cohesiveness fraction for cohesive powders which represents the degree of cohesiveness similar to ε which is an important factor in determining the size distribution of the agglomerates that are formed. They also have categorized particles as single particles, natural agglomerates similar to our clusters and fluidized agglomerates. As we observe with Powder B, higher cohesivity values lead to large size agglomerates having a wide size distribution held together by strong bonds.

Note that in this basic case, the size of the agglomerates is limited by the number of particles in the system, a limitation on computing power. In the following sub-sections, we study the effect of three techniques to improve the fluidizability of cohesive powders which show poor gas fluidization otherwise. The three techniques are (a) fluidizing at high operating gas velocity, (b) vibration-aided gas fluidization and (c) employment of a conical fluidizer.

7.2 Simulation of a gas fluidized cohesive powder – high gas velocity

In our experimental studies on aerogels and cryogels containing more than 10% Ni supported on alumina, we observed that at high velocities, pronounced particle

convection causes the agglomerates to break thereby producing smaller agglomerates which fluidize normally [4, 5, 9]. In an effort to study the effect of high gas velocity on the agglomerated bed characteristics and validate our agglomeration-deagglomeration model in such situations, we simulate the gas fluidization of Powder B at a gas velocity of 0.8. All other parameters remain as stated above for the basic case. Figure 5.5 shows that the gradual increase in bond energies in Powder BHV as in Powder B is limited at high velocities to a maximum of about 2.5 when agglomerates reach a stable size of 3.5. The circularity of the agglomerates is not affected by the higher fluidization velocity. The major departure in the behaviour of Powder B fluidized at a gas velocity of 0.8 from its behaviour when fluidized at the air velocity of 0.3 is that the size of the agglomerates is quite reduced by the higher air flow rate along with a remarkable reduction in the portion of the bed that is actually agglomerated. Less than 10% of the bed formed clusters while nearly 20% of the bed was in the form of agglomerates at the higher air velocity. Clearly, higher gas velocities improve the fluidizability of the cohesive Powder B as was observed in certain experiments mentioned earlier [Deiva Venkatesh, 1995].

Comparing the various particle and agglomerate interactions in the case of Powder B fluidized at the two gas flow rates, we note in Figure 5.6 that unlike the heterogeneous nature of the interactions at the lower gas velocity of 0.3 where all three types, particle-particle, particle-agglomerate and interagglomerate interactions play an important role, when the gas velocity was raised to 0.8 merely particle-particle interactions are present

with negligible particle-agglomerate and no agglomerate-agglomerate interactions. This result supports the above conclusion that 'high' gas velocities improve the quality of fluidization. However, high gas velocities pose the problem of particle elutriation especially in the case of fine powders which are the focus of our study.

7.3 Simulation of a gas fluidized cohesive powder – vibration-assisted fluidization

Another method that is suggested in the literature to improve the fluidizability of fine powders is to aid the hydrodynamic forces with external vibration of the fluidizer. A vertical vibration of the fluidized bed vessel with constant amplitude and frequency is normally utilized. In our earlier work, we have simulated the effect of pure vibration on a cohesive powder and observed induced agglomeration and deagglomeration in the absence of air. In experiments of vibrated beds, we do however have air inside the bed even in the absence of flow which we have now taken into account.

Mori *et al* [6] have used an acoustic field at the bottom of the fluidized bed in their experiments which reportedly break the agglomerates and enable homogeneous fluidization of the powder. Eccles *et al* [16] have successfully simulated the gas fluidization of powders in a vertically agitated vessel for drying processes to increase the mass transfer rate. In our simulation run, we study the mechanical effects of vibration on the cohesiveness and hydrodynamics of the powder bed.

In this simulation, we vibrate the wall particles in Figure 5.7 at an amplitude A = 0.5 and a dimensionless frequency f = 0.1 (characteristic frequency = 1/dimensionless time = 1/time taken by a single particle to travel through its radius at its terminal velocity) which corresponds to 3 KHz. Figure 5.8 represents the characteristics of the cohesive bed of Powder B with gas velocity as 0.3 in the presence of external vibration. Powder B under vibration is termed as Powder BV. The agitated container transfers part of its kinetic energy to fluidized particles during collisions. The competition between the hydrodynamic and vibratory forces leads to an effective cohesiveness of the powder. As seen in this figure, agglomeration has been greatly reduced by the supplementary energy provided by the vibration. Merely 10% of the bed had agglomerated to mostly form clusters which are loosely held together after a short initial cohesive behaviour.

Figure 5.9 indicates a clear improvement in the particle interactions i.e., particle interactions restricted to single particles with no aggregates playing a role.

The real advantage of vibration-assisted fluidization in the case of fine powders lies in the fact that although as in the previous sub-section 7.2, high operating velocities help to destabilize the agglomerates, they also lead to elutriation of the fine (especially those with very low densities) powders. Also in the case of catalytic reactions, the reaction rate may limit the superficial gas velocities to lower values to achieve longer residence times. To simultaneously operate at lower gas velocities and still achieve near-

homogeneous fluidization, mechanical vibration can be an effective technique as observed in the simulation of Powder BV.

7.4 Simulation of a gas fluidized cohesive powder – tapered beds

A third technique to possibly improve the fluidizability of cohesive fine powders is to vary the geometry of the fluidized bed itself. In our experimental study carried out earlier [5], we successfully improved the homogeneous fluidization of a strongly cohesive cryogel using a conical fluidized bed at high velocities. The expanding bed area in the upward direction enhanced particle convection and the maximum gas velocity near the distributor caused the agglomerates at the bottom to break into finer particles. Particles were circulated in a cyclic fashion with upward carry-over by the gas at the center of the bed and downward descent near the inclined walls. See Figure 5.10 for the simulation cell of a tapered bed.

Using Stokesian Dynamics and the agglomeration-deagglomeration model, we simulated the behaviour of Powder B in a tapered bed of expanding cross-section. Powder B used in a tapered bed is referred to as Powder BT. The width of the distributor was 14.0 and the walls were at an angle of 14° to the vertical as in our earlier experiments. For comparison with rectangular beds, we used the same dimensionless air flow rate (35 x 0.3) as in Powder B while keeping all parameters same including the size of the unit cell as shown in Figure 5.10. The velocity however reduces as the air rises in the tapered bed. Results showed that there is a slight improvement in the quality of fluidization of

the cohesive powder with nearly 80% of the bed having agglomerated as opposed to the entire bed in the case of Powder B. The size of the large agglomerates is also seen to be slightly reduced. We attribute this slight improvement in the fluidizability to the low flow rate of the air. In our experiments on tapered beds, we observed that at low flow rates close to minimum fluidization conditions, agglomerates are formed even in tapered beds forming a cylindrical core. It was only at high flow rates corresponding to greater than twice the u_{mf} value that particle convection plays a major role in the hydrodynamics eventually leading to more agglomerates being destroyed at the bottom of the conical bed causing homogeneous fluidization.

We observed a pronounced improvement in the fluidizability of Powder BT at a higher flow rate of (35.0 x 0.6) as shown in Figure 5.11 compared to the agglomerated bed characteristics of Powder B (rectangular fluidized bed).

8. Cohesive powder diagram

For ease of understanding of the physical importance of our two model parameters ε and Ec_{MIN}, we represent them in a cohesive powder diagram represented by Figure 5.12 based on our understanding of their behaviour from experiments and simulation. The purpose of this diagram is to elaborate on the influence of the physical properties of fine powders on the formation and destruction of agglomerates through the model parameters. The figure contains two plot types (a) a set of three-dimensional plots of agglomerate size d_{agg} vs superficial gas velocity u^{∞} vs Ec_{MIN} for various ε (two values 0.25 and 0.75 of cohesivity are shown in the figure) and (b) d_{agg} vs minimum fluidization velocity, u_{mf} for a given solid density and fluidizing gas. The origin O represents a fixed bed of a non-cohesive powder while the horizontal axis represents non-cohesive conditions. Weakly cohesive powders A and C and strongly cohesive powder B, D and F reported in our earlier paper [10] are represented on a single vertical plane (marked by dotted lines) for an identical gas velocity of 0.3. Powder B when fluidized at double the velocity (u^{∞} = 0.6) is represented by Powder BHV. The two warped triangular surfaces shown perpendicular to the plane of the paper correspond to ε values of 0.25 and 0.75 respectively for weak and strong cohesivities. Each point on these warped surfaces represent a combination of a given cohesive powder fluidized by a given gas at a particular superficial velocity. If the projection of such a point for any Powder X at a particular operating gas velocity onto the d_{agg} vs u_{mf} plane lies to the right of the d_{agg} vs u_{mf} curve, the agglomerated bed will be fluidized (Powders A,C, F and

BHV), otherwise the agglomerated bed may be partially fluidized or even defluidized (Powders B and D). In effect, the intersections of the projection of d_{agg} vs u_{mf} curve and the warped surfaces give the minimum fluidization condition ($u^{\infty} = u_{mf}$) of the cohesive powders on the triangular surfaces.

9. Conclusions

Following our earlier work on the simulation of fluidization of cohesive powders using the Stokesian Dynamics method and our agglomeration-deagglomeration model, we now have simulated three techniques of improving the fluidizability of fine powders which normally exhibit poor gas fluidization due to the influence of the interparticle forces.

To recapitulate, the two model parameters of our model are the (a) the minimum energy level Ec_{MIN} for collisions to be 'reactive', i.e., agglomerative or deagglomerative and (b) the cohesivity ε of the powder. Macroscopic bed characteristics such as bond energies of the aggregates and their effective diameter and circularities were estimated from the microscopic simulations results.

At first, we simulated as a basic case the cohesive fluidization of a Powder B which had $\varepsilon = 0.75$ and $Ec_{MIN} = 0.0$ without any intention of improving its hydrodynamics. This simulation at a gas velocity of 0.3 was the reference for all other simulations to verify the influence of the various techniques adopted.

Gas fluidization of the strongly cohesive Powder B caused the formation of aggregates of uniform size of about 3.0 called 'clusters' which formed 10% of the bed mass. Nearly 90% of the bed mass formed the large-sized 'agglomerates'. Simulation of

Powder B also indicates a gradual increase in the magnitude of the bond energy of the system. The effective diameter of the agglomerates reaches a maximum of 6.0. This behaviour has been commonly observed in strongly cohesive powders such as cryogels [9]. Another interesting relation to experiments observed in the simulation of highly cohesive powders is the defluidization of the bed due to agglomeration leading to unstable channelling.

Considering the formation and destruction of agglomerates as reversible reactions with three types of interactions viz., particle-particle (K_1), particle-agglomerate (K_2) and agglomerate-agglomerate (K_3), we find that interagglomerate interactions in the case of the strongly cohesive Powder B play a decisive role in determining its behaviour under the given gas flow conditions. For such a strongly cohesive powder, higher values of Ec_{MIN} have already been shown to reduce agglomeration and to favour homogeneous fluidization of the powder [10].

The first technique that we used to improve the fluidization quality of Powder B is to operate the fluidized bed at high gas velocities at values much greater than the minimum fluidization velocity of the particles. The gas velocity used was 0.8. At this velocity we observed that fewer agglomerates were formed at a smaller size range (3.0 – 4.0). Unlike the basic case, the strength of the bonds were much reduced by nearly a factor of 10 and only 25% of the bed had formed agglomerates and clusters as opposed to the entire bed of Powder B which had agglomerated and defluidized at the air velocity of

0.3. At the higher gas velocity we also note that particle-particle interactions is the most dominant type. The disadvantage in this method is that the fine particles would be entrained by the gas at high flow rates which could also be limited by process requirements.

Simulations of Powder B when the 'fixed' particles forming the wall of the fluidized bed were vibrated at an amplitude of 0.5 and frequency of 0.1 revealed interesting results. Not only did the addition of the external vibratory force destroy the agglomerates, but the vibrated powder nearly reached a state of homogeneous fluidization. Only 10% of the bed had formed weak clusters.

Simulations of the cohesive powder B in a tapered bed (wall angle = 14°) whose cross-section increases with height at the same flow rate as in a rectangular bed showed a slight improvement in the fluidizability. However, at a higher air flow rate of 0.6, the powder formed few clusters and showed a better quality of fluidization. Experiments on cryogels in a conical fluidizer at high air velocities (twice the minimum fluidization velocity) markedly improved the fluidizability of the highly cohesive powders with intense particle circulation and homogeneous fluidization. However, the same experiments showed that at lower velocities near incipient fluidization, agglomerates formed at the core of the bed.

From the current simulations we conclude that a combination of high velocity gas fluidization assisted by vibration at the bottom of the bed can greatly improve the fluidizability of cohesive powders by destroying the agglomerates which are usually formed.

We also have presented a cohesive powder diagram which relates our experimental understanding of the behaviour of cohesive powder under fluidized conditions to the proposed model parameters for simulation and operating conditions. The diagram qualitatively allows to find suitable operating conditions for the satisfactory fluidization of a given cohesive powder.

10. List of Symbols

A	Aggregate number (1, 2, 3 etc)
A	Amplitude of vibration (dimensionless)
AEM	Aggregate Element Matrix (dimension = total number of particles)
a	Particle radius
BE	Cohesive bond energy
BE_A	Cohesive bond energy
BEM	Bond Energy Matrix (dimension = total number of particles)
d	Diameter of the particles
d_{eff}	Effective diameter of aggregates (diameter of circle having area equal to that of the aggregate)
E_{COLL}	Collisional energy
Ec_{MIN}	Minimum collisional energy
f	Frequency of vibration (dimensionless)
g	Gravitational acceleration
HR	Hausner ratio (tapped bulk density/loose bulk density)
K	Equilibrium constant
MD,ND	Aggregate label after deagglomeration
MN	Aggregate label after agglomeration
m	Mass of particle
N	Total number of simulated particles

Nm	Number of fluidizable particles
Nf	Number of fixed (distributor) particles
n	Number concentration of aggregates
r	Interparticle separation
t	Time
U	Particle velocity vector
u^{∞}, uinf	Superficial velocity of the fluid
x	Position vector of particles (x_x, x_y, x_z)
x,y,z	Coordinate axes

Subscripts

A	Aggregate
x,y,z	3D vector components
M,N	Particle labels
P,Q	Aggregate or particle labels (as the case may be)
MD,ND	Aggregate labels after deagglomeration
MN	Aggregate label after agglomeration

Greek letters

ε	Fraction of kinetic energy transformed into cohesive bond energy (*cohesivity*)
ρ	Linear density (bulk density/solid density)

v	Single particle terminal velocity (characteristic velocity)
μ	Viscosity of the fluid

Italics

A	Aggregate
n	Number concentration

References

[1] Wang Z., Kwauk M. and Li H., *Chem.Eng.Sci.*, 53-3 (1998) 377-395.

[2] D.Geldart, *Powder Technol.* 7 (1973) 285.

[3] Deiva Venkatesh R., Grmela M. and Chaouki J., *Powder Technol.* (1998).

[4] J.Chaouki, C.Chavarie, D.Klvana and G.Pajonk, *Powder Technol.* 43 (1985) 117.

[5] R.Deiva Venkatesh, *Master's thesis*, Ecole Polytechnique de Montréal, 1995.

[6] S.Mori, A.Yamamoto, T.Haruta, *Int. Chem. Eng.*, 31 (1991) 475.

[7] C.Lauga, J.Chaouki, D.Klvana and C.Chavarie, *Powder Technol.* 65 (1991) 461.

[8] R.Chirone, L.Massimilla and S.Russo, *Chem. Engr. Sci.* 48 (1993) 41.

[9] R.Deiva Venkatesh, J.Chaouki and D.Klvana, *Powder Technol.* 89 (1996) 179.

[10] Deiva Venkatesh R., Grmela M. and Chaouki J., *Powder Technol.* b (to be published).

[11] Brady J.F. and Bossis G., *Annu. Rev. Fluid Mech.*, 20 (1985) 111.

[12] Ichiki K. and Hayakawa H., *Phys. Rev. E*, 52-1 (1995) 658.

[13] Ichiki K. and Hayakawa H., *Phys. Rev. E*, 57-2 (1998) 1990.

[14] M.M.Mansour and F.Baras, *Physica A* 188 (1992) 253.

[15] R.D.Cadle, *Particle Size*, Reinhold Publishing Corporation, NewYork, 1965.

[16] E.R.A.Eccles, K.Erdesz and A.S.Mujumdar, *Fluidization VI* (1989) 219.

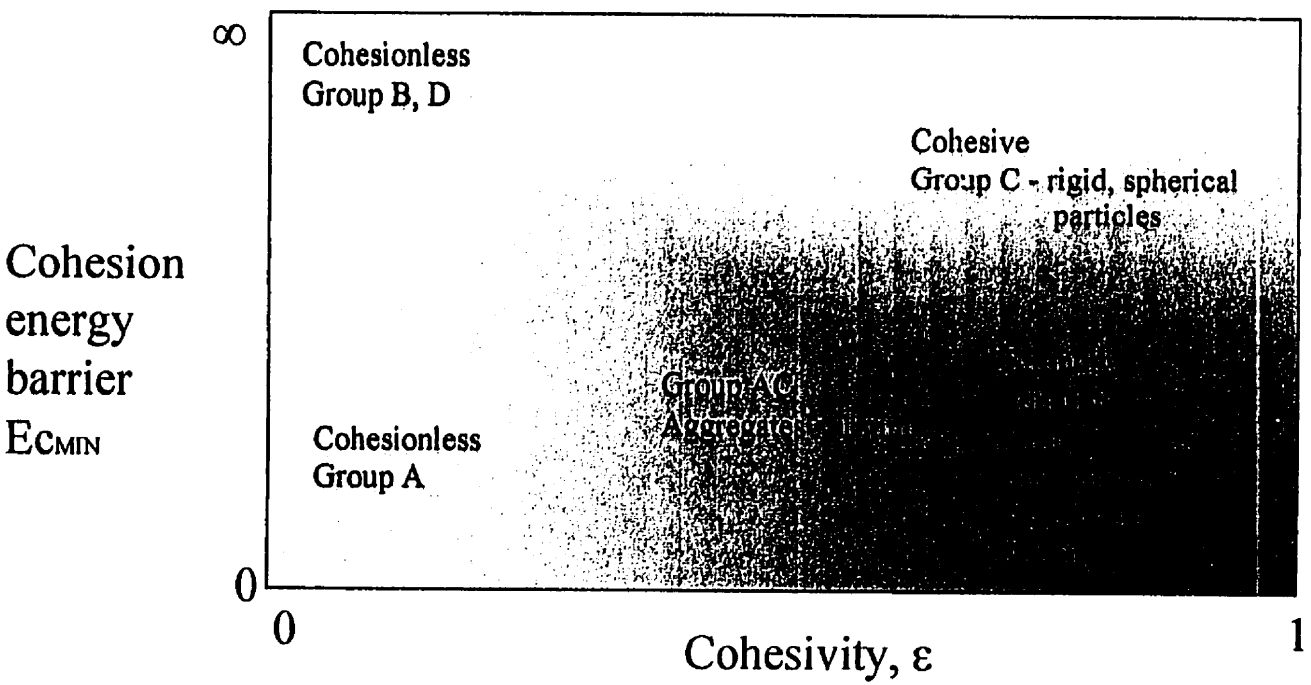

Figure 5.1 Relationship between model parameters and Geldart powder types

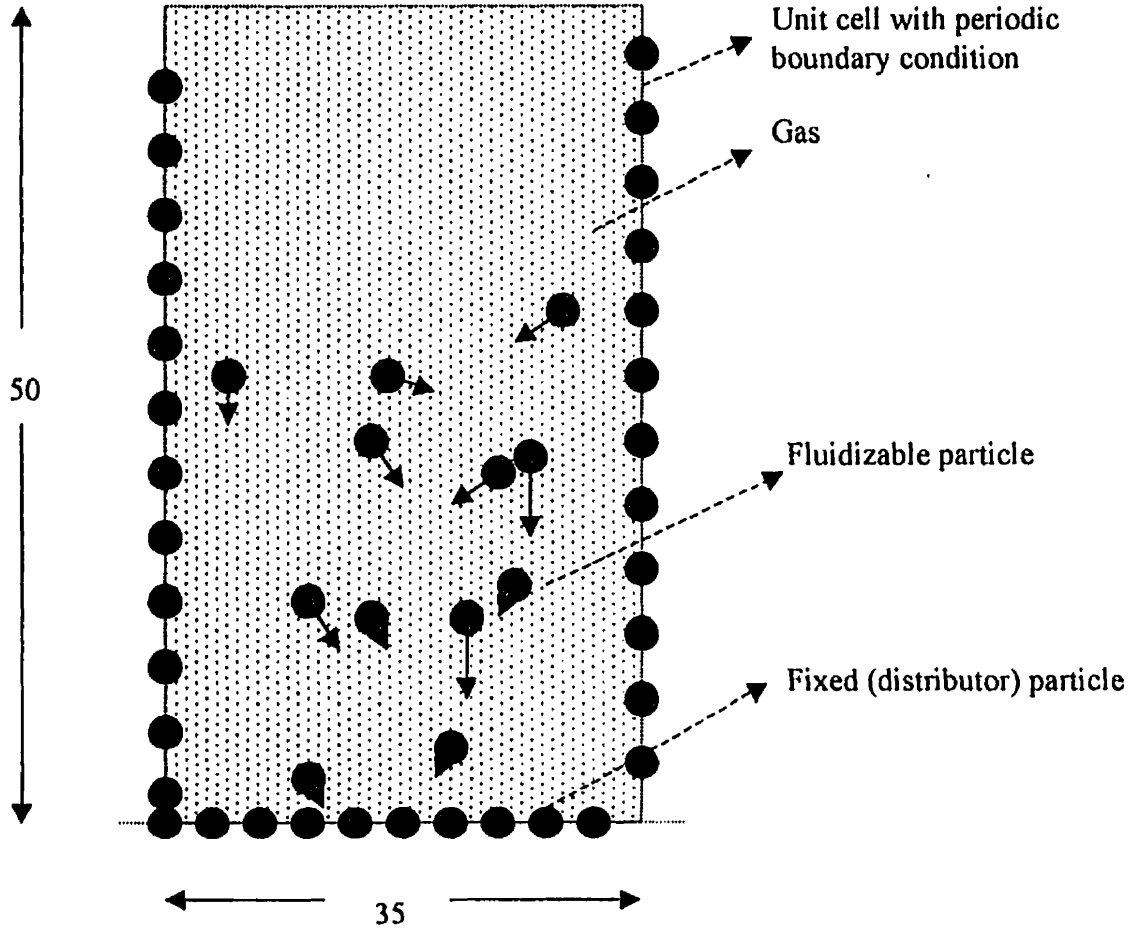

Figure 5.2 Unit cell with fluidized particles and rectangular wall

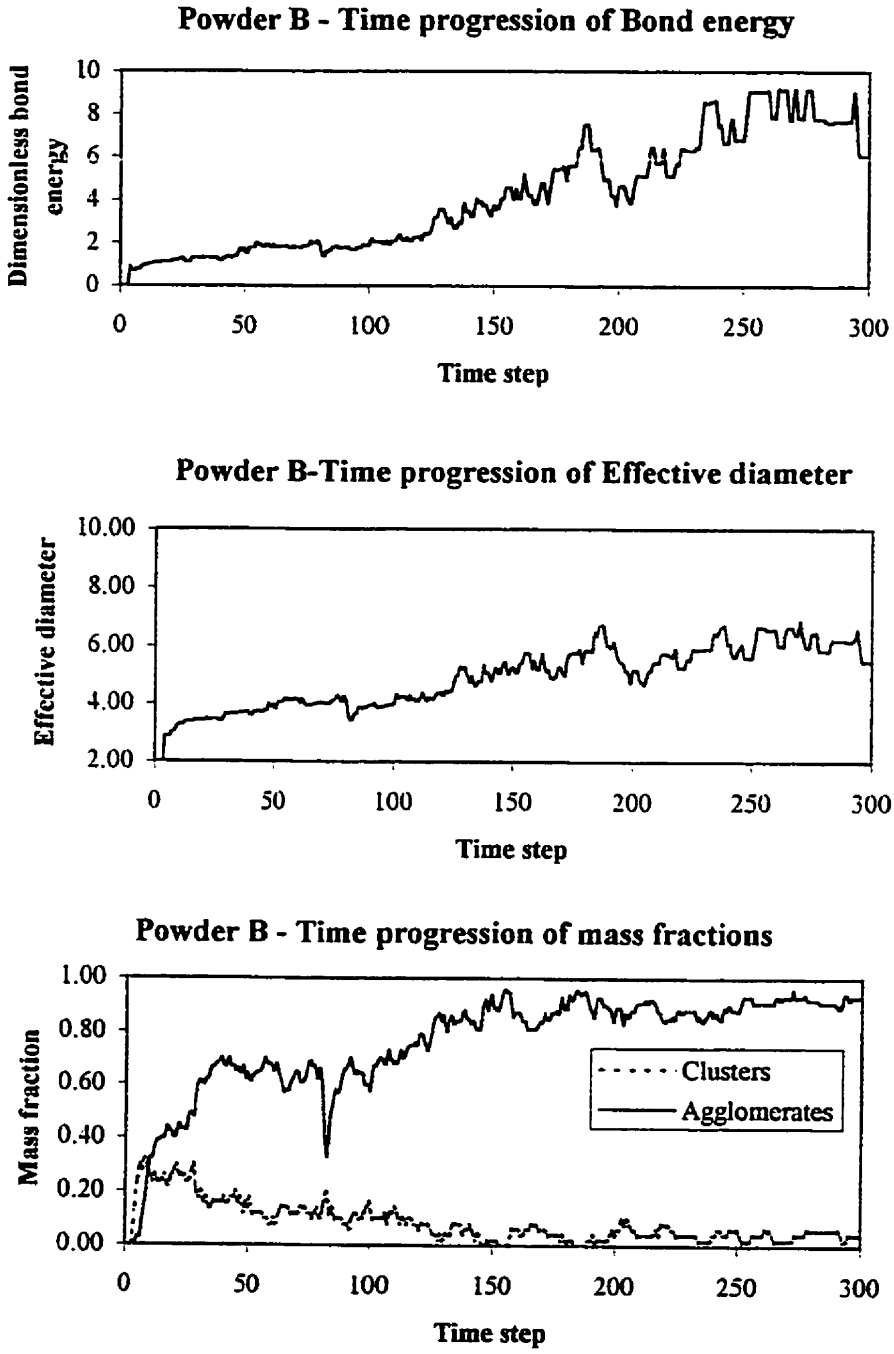

Figure 5.3 Bed characteristics of a strongly cohesive powder (basic case)

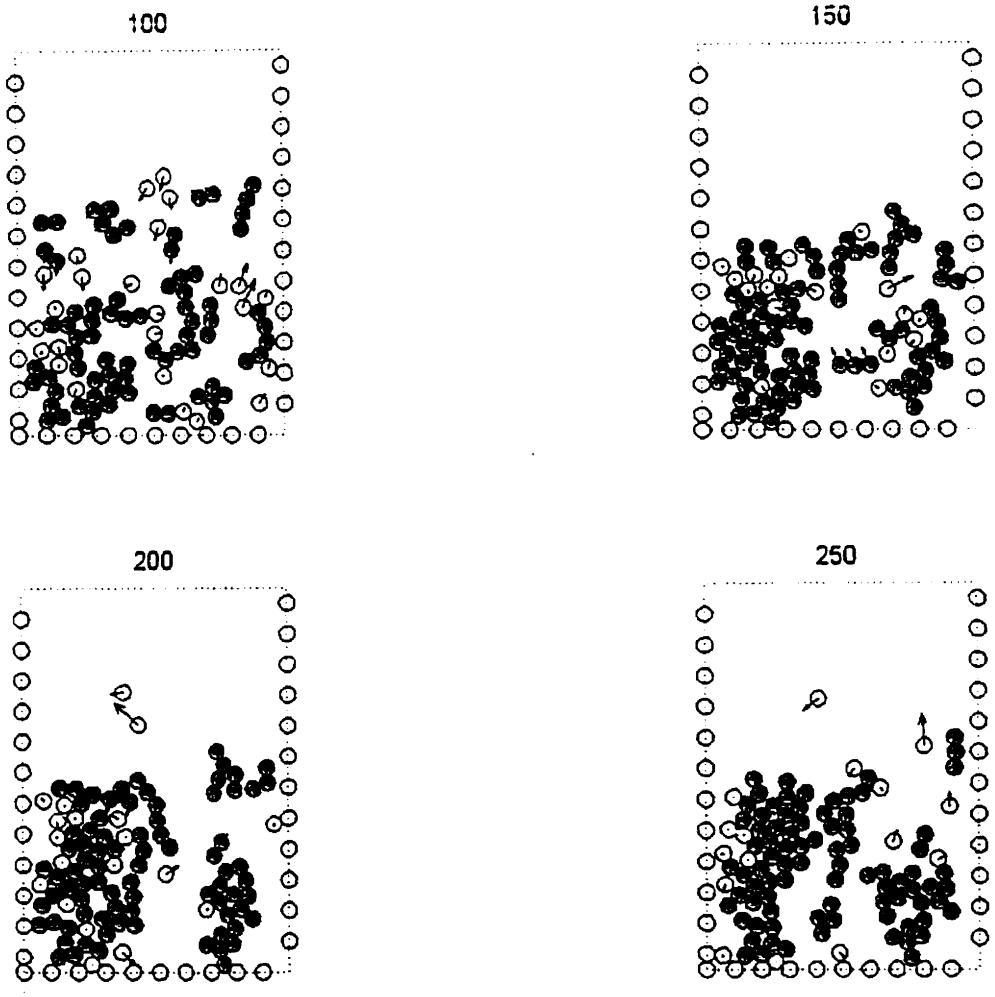

Figure 5.4 Defluidization of a strongly cohesive powder

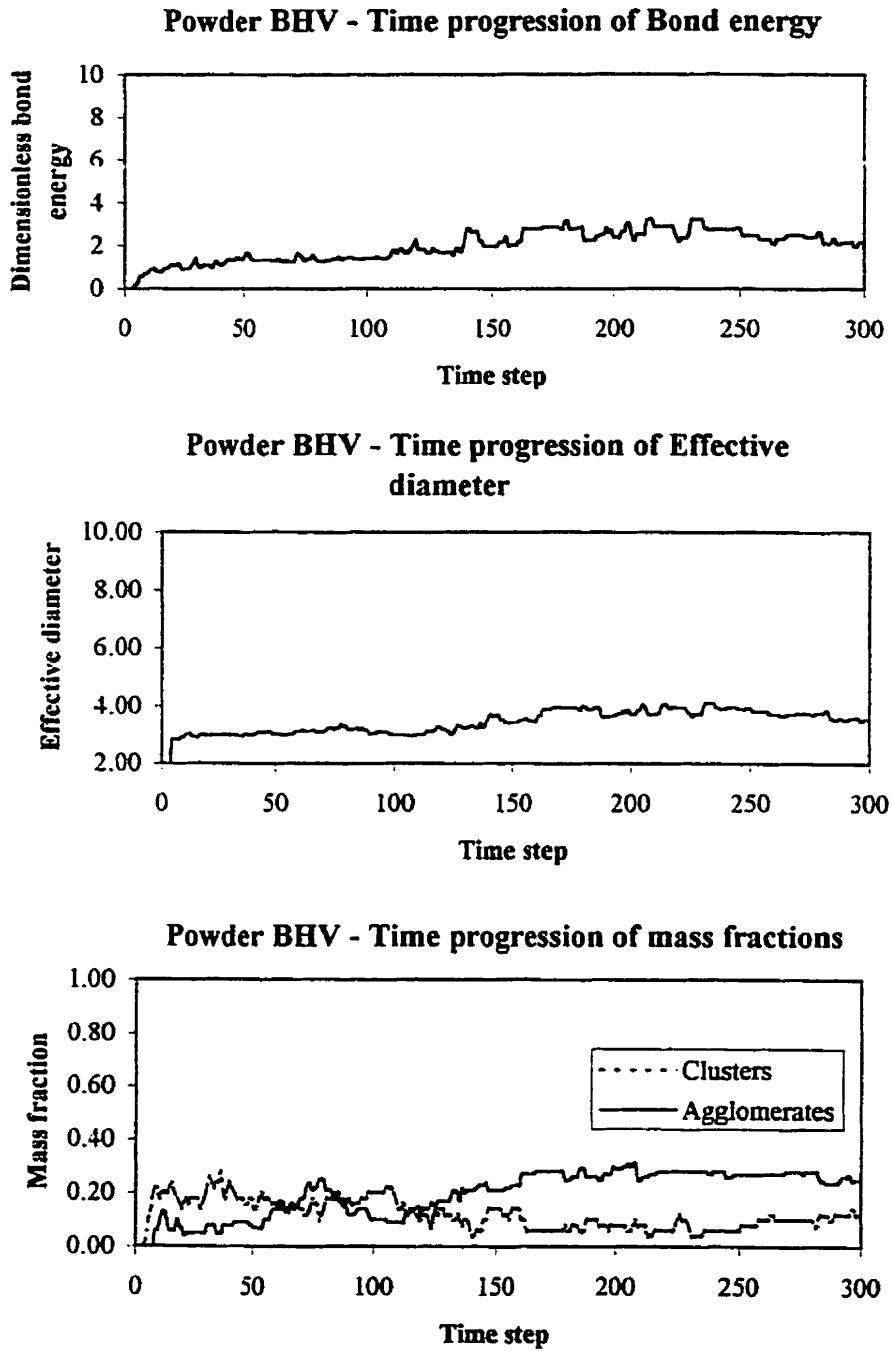

Figure 5.5 Bed characteristics at high velocity fluidization

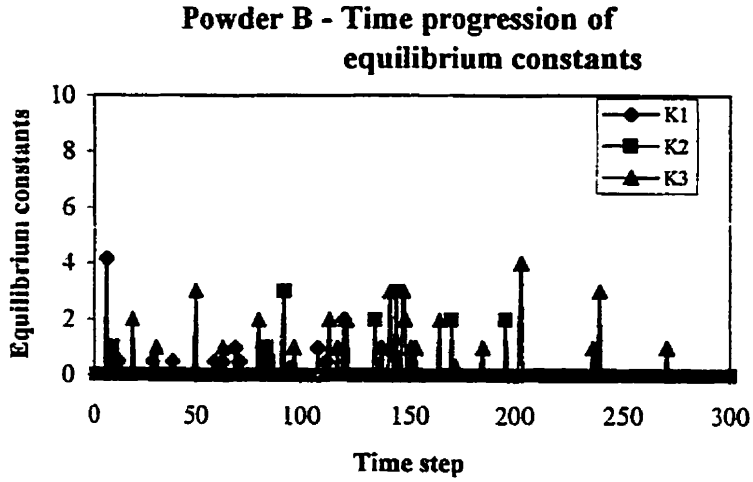

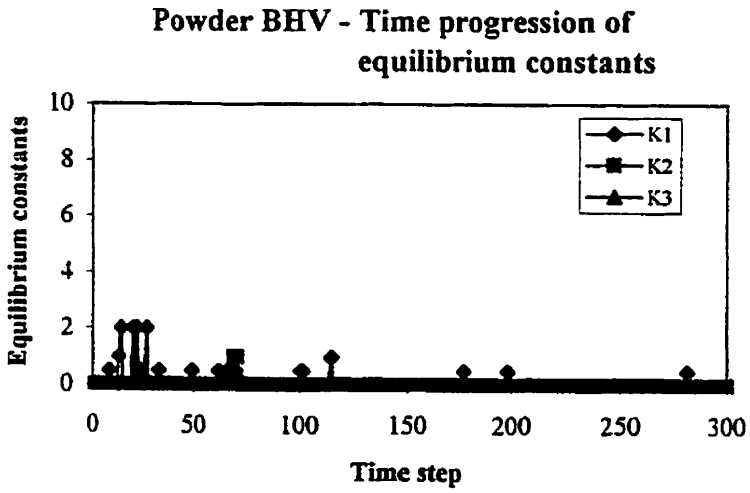

Figure 5.6 Effect of gas velocity on particle interactions

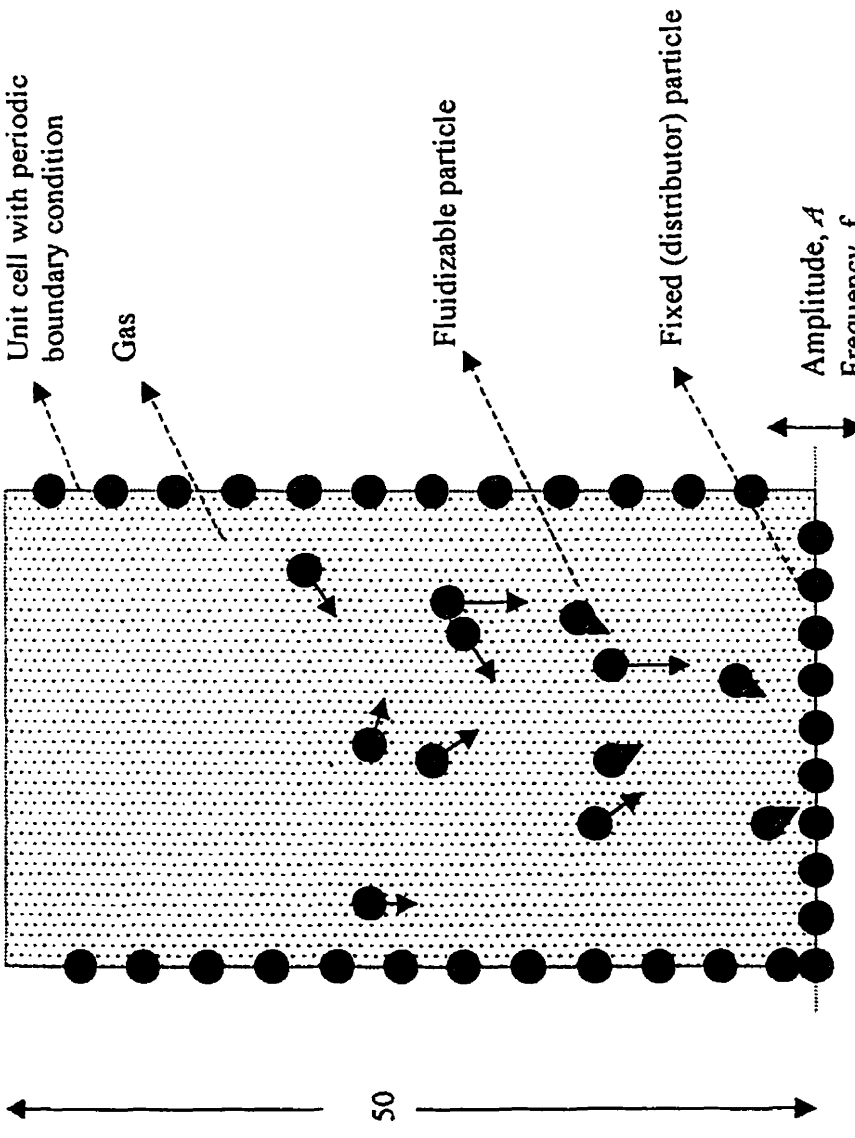

Figure 5.7 Vibration-assisted gas fluidization

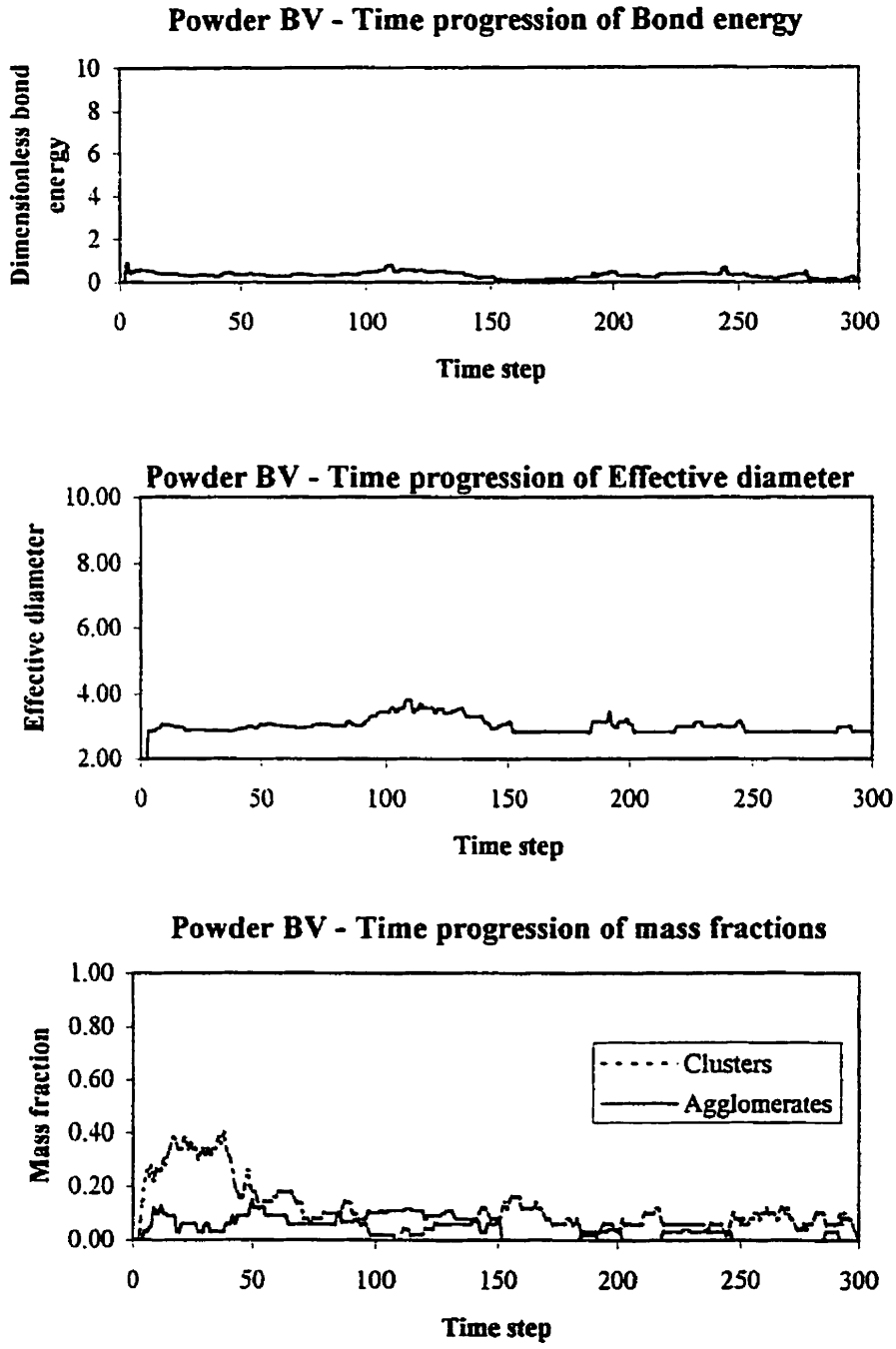

Figure 5.8 Influence of vibration on the hydrodynamics of a gas fluidized cohesive powder

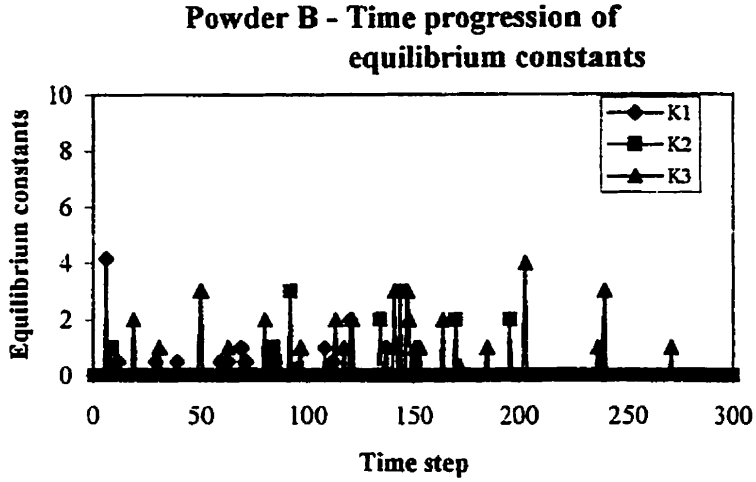

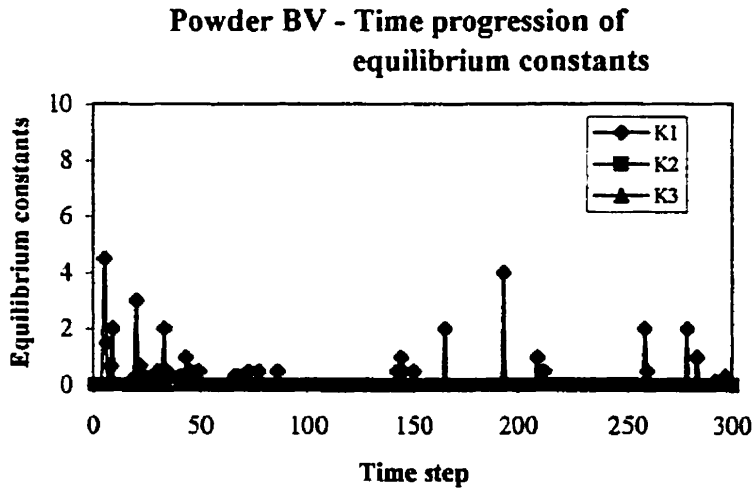

Figure 5.9 Effect of vibration on particle interactions

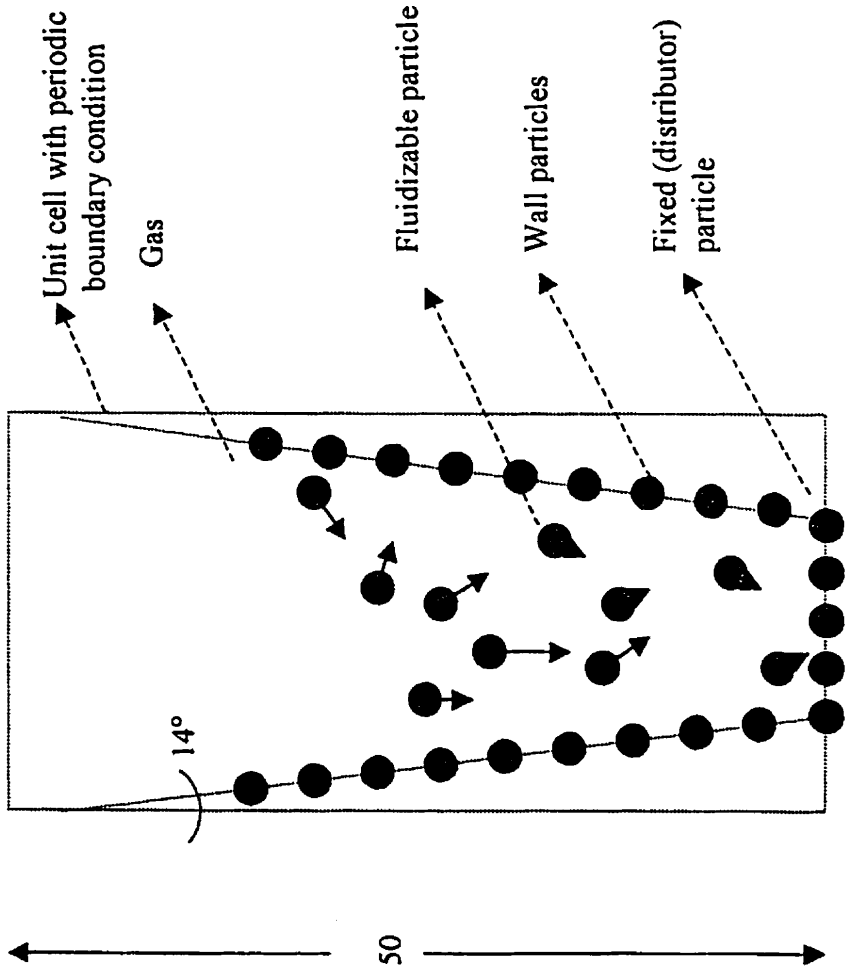

Figure 5.10 Tapered bed

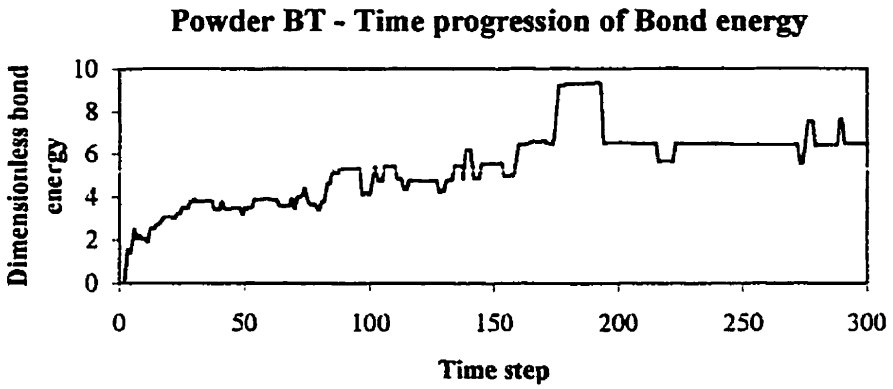

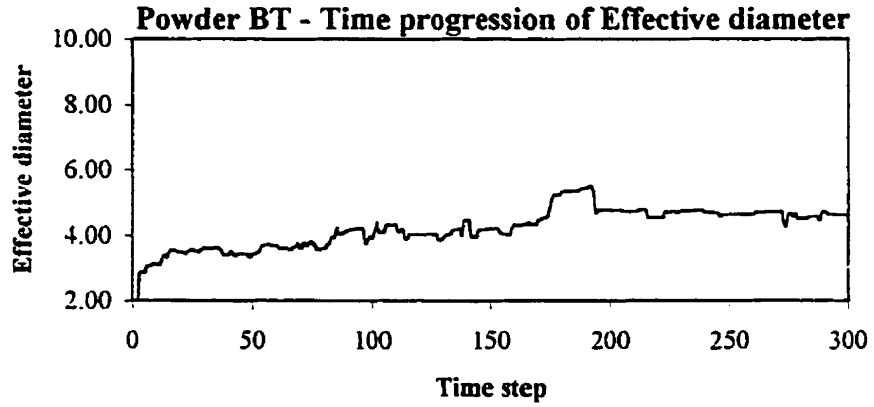

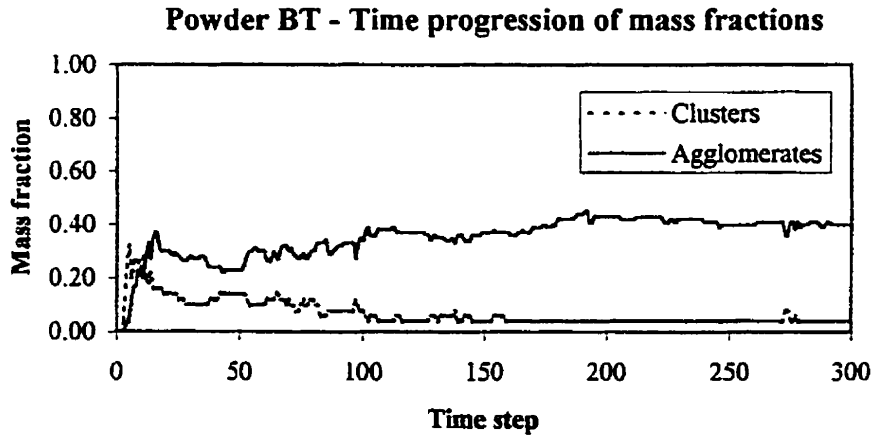

Figure 5.11 Tapered bed characteristics

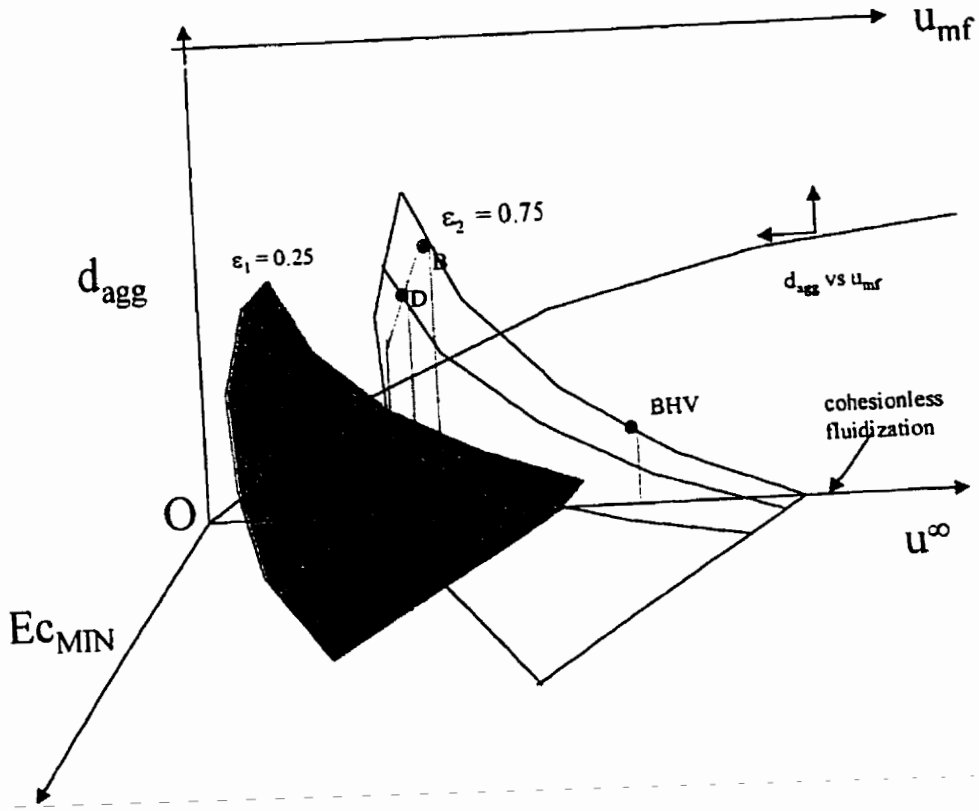

Figure 5.12 Cohesive powder diagram

CONCLUSIONS

A foundation for a simulation technique allowing to predict the macroscopic behaviour of vibrated and gas fluidized cohesive fine powders has been made. Firstly, we have simulated 300 spheres in a trapezoidal container vibrated vertically at an amplitude of 2.5 mm and a frequency of 20 Hz. Next, we have introduced a microscopic model of cohesion processes in powders (*powder chemistry*) and carried out the simulations involving agglomeration-deagglomeration. In theses simulations, the particles are allowed to form aggregates during collisions. The process is controlled by the energy barrier given by the model parameter Ec_{MIN}. The fraction of the collisional energy transformed into cohesive bond energy during such reactive (agglomerative or deagglomerative) collisions was represented by the second model parameter ε. Break-up of aggregates occurs when the collisional energy exceeds the strengths of 'weak' bonds in the colliding bodies. From the perspective of chemical reactions, the agglomeration-deagglomeration phenomena were considered to be reversible reactions with three types of interactions viz particle-particle (equilibrium constant K_1), particle-aggregate (equilibrium constant K_2), aggregate-aggregate (equilibrium constant K_3).

Vibrated beds:

Simulation of four cohesive powders I,III (weakly cohesive), II and IV (strongly cohesive) were carried out by varying both model parameters. Macroscopic results such as cohesive bond energies of aggregates, their effective diameters and circularities were

extracted from the microscopic simulation results viz positions and velocities of the particles and their various cohesive bond energies.

The macroscopic results indicate that in the case of the weakly cohesive powders, the aggregates are of constant minimum size (4 mm) called *clusters* having weak cohesive bond energies of the order of 10^0J and having no significant effect on the density or velocity distributions in the bed. Also, nearly 30 % of the bed mass had formed *clusters* which were formed mainly due to particle-particle interactions. In the case of strongly cohesive powders, besides 10% of the bed forming uniform-size *clusters*, more than 80% of the bed mass had formed larger *agglomerates* of size in the range 5-30 mm and whose cohesive bond energies were of the order of 10^3 J. Here, the formation of aggregates included all three types of interactions mentioned above. Simulation of powder I in a rectangular container exhibited vibromobilization only at the top and bottom of the bed.

In conclusion, the value of ε had a proportional control on the strength and size of the aggregates and their mass fractions while Ec_{MIN} determined mainly the starting time of agglomeration, t_a. Another interesting feature revealed by the simulation is that the first half of the vibratory cycle promotes agglomeration while the second half causes dominance of break-up of aggregates.

The conditions for satisfactory fluidization of fine powders would be low values of ε and high values of Ec_{MIN}. Larger values of Ec_{MIN} have to be used in simulations to observe significant influence on the cohesivity of the powder. How do we modify a fine powder to increase Ec_{MIN} and diminish ε ? These are questions of considerable practical significance.

Gas fluidized powders:

Preliminary simulations on FCC powder using the Stokesian Dynamics method yielded results which characterize the particle motion and the bed characteristics such as bubble size etc., which were then compared with experimental data arising from Radioactive Particle Tracking method (for comparing particle velocities) and the Fiber-optic method (for quantifying the characteristics of bubbling beds). The comparison with experiments showed acceptable agreement between simulation and experiment given the limitation on the size of the system that is simulated owing to the limitation on computing power by the available resources.

We then simulate the behaviour of cohesive fine powders in gas fluidized conditions by combining our powder chemistry model with the Stokesian Dynamics method. Initially, we simulate the cohesionless simulation of fine powders using 128 fluidizable particles of 20μm size with 10 fixed particles forming the distributor at the bottom of the bed. In this case, we considered particle collisions to be elastic and the gas velocity at 0.3. We

observe the finely fluidized state of the bed as well as the formation and destruction of bubbles as was observed in their work. The expanded bed porosity of this bed was in agreement with the Richardson and Zaki model of homogeneous fluidization.

Following simulations include the agglomeration and deagglomeration mechanims described by the powder chemistry model. The two model parameters were the (a) the minimum energy level Ec_{MIN} for collisions to be 'reactive', i.e., agglomerative or deagglomerative and (b) the cohesivity ε of the powder. Four powders A,C which are weakly cohesive and B,D which are strongly cohesive were studied. Powders A,B had no energy barrier for cohesion whereas C,D had $Ec_{MIN} = 0.5$. Macroscopic bed characteristics such as bond energies of the aggregates and their effective diameter and circularities were estimated from the microscopic simulation results.

Gas fluidization of weakly cohesive powders caused the formation of aggregates of uniform size of about 3.0 called 'clusters' here which formed 30% of the bed mass. Nearly 10% of the bed mass formed the large-sized 'agglomerates'. The instantaneous bond energies indicate aggregates held together by weak bonds characteristic of Group AC particles. Simulations of strongly cohesive powders indicate a gradual increase in the magnitude of the bond energy of the system. The effective diameter of the agglomerates reaches a maximum of 6.0. More than 90% of the bed had formed agglomerates in this case while the rest remained as weak clusters. This behaviour has been commonly observed in strongly cohesive powders such as cryogels. Another

interesting relation to experiments observed in the simulation of highly cohesive powders is the de-fluidization of the bed due to agglomeration leading to unstable channeling. The estimated u_{mf} values of the particles and the clusters were well below the fluid velocity unlike the u_{mf} of the agglomerates which was higher.

Considering the formation and destruction of agglomerates as reversible reactions, we find that particle-particle interactions in the case of weakly cohesive powders and particle-particle, interagglomerate interactions in the case of strongly cohesive powders play a decisive role in determining their behaviour under the given gas flow conditions. For a strongly cohesive powder, higher values of Ec_{MIN} reduces agglomeration and favours homogeneous fluidization of the powder.

Conclusively, low values of the cohesivity and high values of Ec_{MIN} have been found to improve the gas fluidizability of cohesive fine powders.

Our integration of the Stokesian Dynamics method with the powder chemistry model helps to extract the macroscopic properties of cohesive powders from microscopic simulation results. This simulation technique paves a way for further detailed studies on the behaviour of cohesive fine powders under gas fluidized conditions.

Following our earlier work on the simulation of fluidization of cohesive powders using the Stokesian Dynamics method and our agglomeration-deagglomeration model, we

have simulated three techniques of improving the fluidizability of fine powders which normally exhibit poor gas fluidization due to the influence of the interparticle forces.

The first technique that we used to improve the fluidization quality of Powder D is to operate the fluidized bed at high gas velocities at values much greater than the minimum fluidization velocity of the particles. The gas velocity used was 0.8. At this velocity we observed that fewer agglomerates were formed at a smaller size range (3.0 – 4.0). Unlike the basic case, the strength of the bonds were much reduced by nearly a factor of 10 and only 25% of the bed had formed agglomerates and clusters as opposed to the entire bed of Powder D which had agglomerated and defluidized at the air velocity of 0.3. At the higher gas velocity we also note that particle-particle interactions is the most dominant type. The disadvantage in this method is that the fine particles would be entrained by the gas at high flow rates which could also be limited by process requirements.

Simulations of Powder D when the 'fixed' particles forming the wall of the fluidized bed were vibrated at an amplitude of 0.5 and frequency of 0.1 revealed interesting results. Not only did the addition of the external vibratory force destroy the agglomerates, but the vibrated powder nearly reached a state of homogeneous fluidization. Only 10% of the bed had formed weak clusters.

Simulations of the cohesive powder D in a tapered bed (wall angle = 14°) whose cross-section increases with height at the same flow rate as in a rectangular bed showed a slight improvement in the fluidizability. However, at a higher air flow rate of 0.6, the powder formed few clusters and showed a better quality of fluidization. Experiments on cryogels in a conical fluidizer at high air velocities (twice the minimum fluidization velocity) markedly improved the fluidizability of the highly cohesive powders with intense particle circulation and homogeneous fluidization. However, the same experiments showed that at lower velocities near incipient fluidization, agglomerates formed at the core of the bed.

From the current simulations we conclude that a combination of high velocity gas fluidization assisted by vibration at the bottom of the bed can greatly improve the fluidizability of cohesive powders by destroying the agglomerates which are usually formed.

We also have presented a cohesive powder diagram which relates our experimental understanding of the behaviour of cohesive powder under fluidized conditions to the proposed model parameters for simulation and operating conditions. The diagram qualitatively allows to find suitable operating conditions for the satisfactory fluidization of a given cohesive powder.

RECOMMENDATIONS

Based on the limitations and lessons learned from the Molecular Dynamics simulations of vibrated beds and simulation of gas fluidized powders using the Stokesian Dynamics method, the following recommendations are suggested for future work:

1. Acceleration of the Stokesian Dynamics method, i.e., fast estimation of the resistance matrix: The matrix inverse is already speeded-up by a factor of two by using the Cholesky factorization technique for symmetric, positive-definite matrices compared to the classical LU decomposition. The speed can be further improved by matrix partitioning which is a must especially for large systems with thousands of particles to be simulated.

2. Modify the Stokesian Dynamics simulation package for multi-sized particle systems. This requires altering the Ewald-summed mobility matrix and the lubrication matrix.

3. Simulate larger fluidized bed systems (N>1000) using the accelerated Stokesian Dynamics package.

4. Model the relation between the cohesion model parameters and physical properties of fine powders.

5. Based on the above modeling, estimate value ranges of the model parameters for Group A, AC and C powders of Geldart's classification.

6. The author hopes that in the near future, rigorous modeling would be done to develop Navier-Stokes dynamics to simulate the gas fluidization of coarser powders which might involve estimation of a particle-interaction matrix which is also a function of the fluid velocity.

GENERAL BIBLIOGRAPHY

BEENAKKER, C.W.J. (1986). Ewald sum of the Rotne-Prager tensor. J. Chem. Phys., 50, 1581-1582.

BLOISE, Y. (1995). Applications de la dynamique moléculaire à la fluidisation des particules par vibration. Master's thesis, Ecole Polytechnique de Montreal, Canada.

BRADY, J.F. and BOSSIS, G. (1985). Stokesian Dynamics. Annu. Rev. Fluid Mech., 20, 111-133.

CADLE, R.D. (1965). Particle Size, Reinhold Publishing Corporation, 48-66.

CHAOUKI, J., CHAVARIE, C., KLVANA, D. and PAJONK, G. (1985). Effect of interparticle forces on the hydrodynamic behaviour of fluidized aerogels. Powder Technol., 43 , 117-121.

CHEREMISINOFF N.P. and CHEREMISINOFF, P.N. (1984). Hydrodynamics of Gas-Solids Fluidization, Gulf Publishing Co., 115-163

CHIRONE, R., MASSIMILLA, L. and RUSSO, S. (1993). Bubble-free fluidization of a cohesive powder in an acoustic field. Chem. Engr. Sci., 48, 41-45.

CLEMENT, E. and RAJCHENBACH, J. (1991). Fluidization of a bidimensional powder. Europhys. Lett., 16-2, 133-142.

DAVIDSON, J.F. and HARRISON, D. (1963). Fluidised Particles, Cambridge Univ. Press, 119-155.

DEIVA VENKATESH, R. (1995). Hydrogenation of toluene. Master's thesis, Ecole Polytechnique de Montréal, Canada.

DEIVA VENKATESH, R., CHAOUKI, J. and KLVANA, D. (1996). Fluidization of cryogels in a conical column. Powder Technol. 89, 179-184.

DEIVA VENKATESH, R., GRMELA, M. and CHAOUKI, J. (1998). Simulations of vibrated fine powders. Powder Technol., 1965-1969.

DEIVA VENKATESH, R., CHAOUKI, J., GRMELA, M. and MORTAZAVI, R. (to be published). Simulations and experiments on fine powder fluidization. Powder Technology (a).

DEIVA VENKATESH, R., GRMELA, M. and CHAOUKI, J. (to be published). Dynamic simulations of fine powder fluidization. Powder Technol. (b)

ECCLES, E.R.A., ERDESZ, K. and MUJUMDAR, A.S. (1989). Resonance phenomenon in aerated vibrated beds of particles. Fluidization VI, 219-224.

ENNIS, B.J., GREEN, J. and DAVIES, R. (1994). The Legacy of Neglect in the U.S. Chem. Eng. Prog., 32-38.

GALLAS, J.A.C., HERRMANN, H.J. and SOKOLOWSKI, S. (1992 a). Molecular dynamics simulation of powder fluidization in two dimensions. Physica A, 189, 437-442.

GALLAS, J.A.C, HERRMANN, H.J. and SOKOLOWSKI, S. (1992 b). Convection cells in vibrating granular media. Phys. Rev. Lett., 69, 1371-1375.

GELDART, D. (1973). Types of Gas Fluidization. Powder Technol., 7, 285-288.

ICHIKI, K. and HAYAKAWA, H. (1995). Dynamical simulation of fluidized beds: Hydrodynamically interacting granular particles. Phys. Rev. E, 52-1, 658-663.

ICHIKI, K. and HAYAKAWA, H. (1998). Analysis of statistical quantities in simulation of fluidized beds. Phys. Rev. E, 57-2, 1990-1996.

JAEGER, H.M. and NAGEL, S.R. (1992). Physiscs of the granular state. Science, 255 1523-1526.

JEFFREY, D.J. and ONISHI, Y.J. (1984). Calculation of the resistance and mobility functions for two unequal rigid spheres in low-Reynolds number flow. J. Fluid Mech., 139, 261-280.

KUNII, D. and LEVENSPIEL O. (1991). Fluidization Engineering, Second Edition, Butterworth-Heineman, New York.

LAN, Y. and ROSATO, A.D. (1995). Macroscopic behaviour of vibrating beds of smooth elastic spheres. Phys. Fluid A, 7, 1818-1825.

LARACHI, F., KENNEDY, G. and CHAOUKI, J. (1994). A γ-ray detection system for 3-D particle tracking in multiphase reactors. Nuclear Instruments and Methods in Physics Research A, 338, 568-576.

LARACHI, F., CASSANELLO, M., CHAOUKI, J. and GUY, C. (1996). Flow structure of the solids in a 3-D gas-liquid-solid fluidized bed. AIChE J., 42-9, 2439-2447.

LAUGA C., CHAOUKI, J., KLVANA, D. and CHAVARIE, C. (1991). Improvement of the fluidisability of Ni/SiO_2 aerogels by reducing interparticle forces. Powder Technol., 65, 461-466.

LEE, J. (1997). Time-dependent behaviour of granular material in a vibrating box. Physica A, 238, 129-136.

MANSOUR, M.M. and BARAS, F. (1992). Microscopic simulation of chemical systems. Physica A, 188, 253-269.

MEHTA, A. (1993). in Mehta, A. (ed.), Granular Matter: an Interdisciplinary Approach, Springer-Verlag, 213-250.

MORI, S., YAMAMOTO, A. and HARUTA, T. (1991). Vibrofluidization of very fine particles. Int. Chem. Eng., 31, 475-481.

MORRIS, J.F. and BRADY, J.F. (1998). Pressure-driven flow of a suspension: buoyancy effects. Int. J. Multiphase Flow, 24-1, 105-111 .

REH and LI. (1976). Circulating Fluidized Bed Technology III, eds: Basu P., Horio M. and Rowe, P.N. Chem. Eng. Sci., 31, 285-294.

THOMAS, B., LIU, Y.A., CHAN, R. and SQUIRES, A.M. (1987). Method for observing phase-dependent phenomena in cyclic-systems: Application to study of dynamics of vibrated beds of granular solids. Powder Technol., 52, 77-82.

THOMAS, B., MASON, M.O., LIU, Y.A. and SQUIRES, A.M. (1989). Identifying states in shallow vibrated beds. Powder Technol., 57, 267-271.

VISSER, J. (1989). An invited review: van der Waals and other cohesive forces affecting powder fluidization. Powder Technol., 58, 1-6.

WANG, Z., KWAUK, M. and LI, H. (1998). Fluidization of fine particles. Chem.Eng.Sci., 53-3, 377-395.

APPENDIX 1 Radioactive Particle Tracking method

The system used in this research employs NaI detectors. The mapping is carried out by Monte Carlo calculation with parameters such as the γ-ray linear attenuation coefficient adjusted to fit count-rates measured at a number of calibration positions. For particle tracking, the flow follower positions are calculated using a least-squares approach.

Radioactive tracer

The tracer particle is made up of a mixture of gold Au^{198} and epoxy resin. The amount of resin in the tracer is such that the hydrodynamics of the tracer is close to that of the bed particles whereas the minimum amount of gold in the tracer is restricted by the minimum amount that can be used in the nuclear reactor. The tracer is activated in the SLOWPOKE nuclear reactor of Ecole Polytechnique. The NaI detectors which detect the γ-rays saturate at about 10^5 counts/s.

Counting system

Each NaI(Tl) detector is connected to a non-NIM amplifier and bias supply workstation (EG & G ORTEC ACE Mate 925) which provides voltage distribution to the 10-stage PMT via a photomultiplier base (EG & G ORTEC PMB model 266) as well as signal amplification and discrimination (SCA mode). The discriminators are set to accept only pulses corresponding to full energy deposited in the detector. Thus γ-rays which Compton scatter in the reactor are rejected. The logic pulses from the discriminators are

sent to a personal computer which contains eight multichannel scaling boards (EG & G ORTEC ACE-MCS 4096 channels). Data are acquired simultaneously for the detectors. When the MCS buffers are full (after 4096 counting intervals of 30 ms each), the acquisition is momentarily interrupted and the data are transferred and stored in binary format on the PC RAM. It is retriggered after data transfer by a TTL signal sent in series to the input boards. After a tracking experiment, which lasts typically 6-12 hours, the acquired data are transferred to the PC hard disk and then converted to the ASCII format before being sent via an RS-232 interface to a fast computer (IBM RS/6000 370) where the tracer co-ordinates are reconstructed from the γ-ray counts.